UCID- 18592

Reactively Sputtered Thin Film Cu_xS/CdS Photovoltaic Devices

L. D. Partain
G. A. Armantrout
J. H. Yee
J. Y. Leong
D. Okubo

April 2, 1980

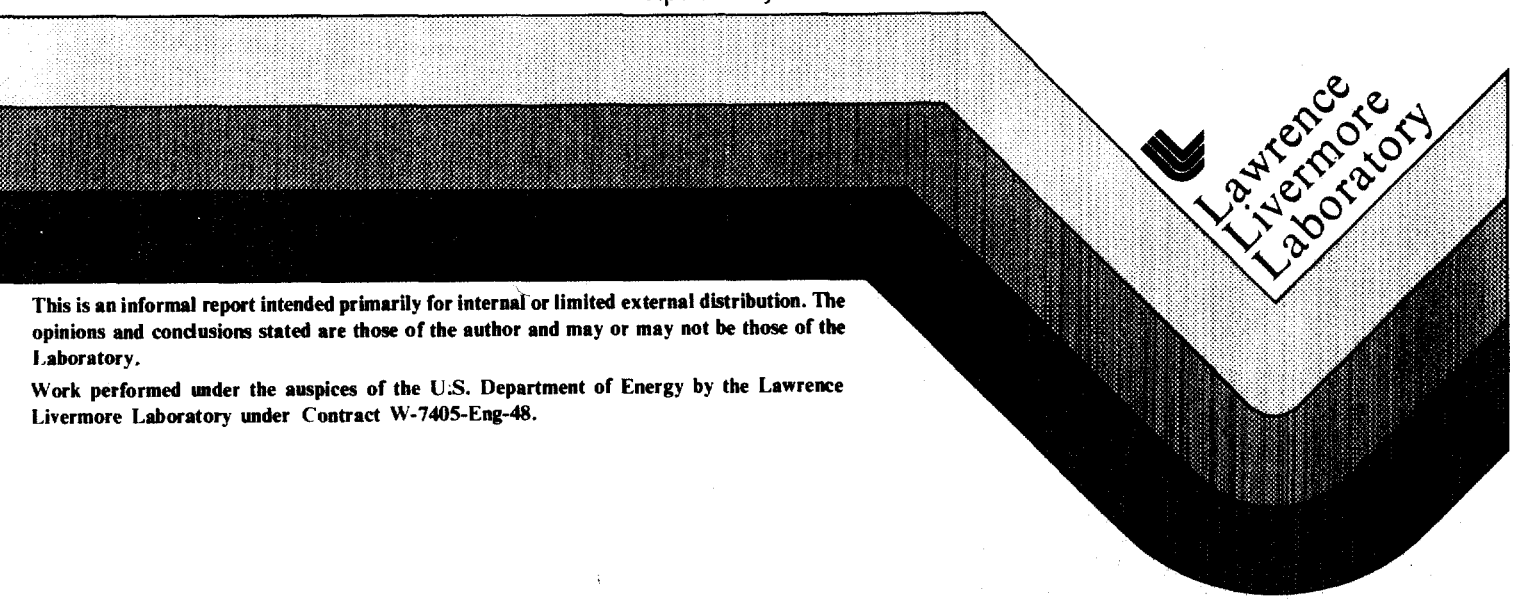

Work performed under the auspices of the U.S. Department of Energy by the Lawrence Livermore Laboratory under Contract W-7405-Eng-48.

Reactively Sputtered Thin Film Cu_xS/CdS Photovoltaic Devices

Final Progress Report

Covering the Period

October 1, 1978 to September 30, 1979

Contract No. DS-9-8103-1

L. D. Partain

G. A. Armantrout

J. H. Yee**

J. Y. Leong†

D. Okubo

Lawrence Livermore Laboratory

Livermore, California 94550

October 1979

**Yee's contributions came from continual consultations with the principal investigators but at no direct cost to this contract.

†Leong is U.C. Davis Ph.D. student whose thesis topic is Cu_xS/CdS but whose work was supported by sources external to this contract.

Table of Contents

	Page No.
I. Summary	1
II. Introduction	5
A. Controlling Mechanisms	5
B. Thin Film Characterizations	10
C. Junction Collection Efficiency	15
D. Sputtering Control of Cu_xS	18
E. Performance Potential	25
III. Detailed Studies Described in Technical Article Preprints and Reprints	26
A. SCL I Theoretical Modeling	27
1. "Space-Charge-Limited Current in Cu_xS/CdS Solar Cells," Journal of Electronic Materials, L. D. Partain, G. A. Armantrout, J. Leong, and P. Warter (in press).	27
2. "Space-Charge-Limited Current and Capacitance in Cu_xS/CdS Heterojunction Solar Cells," Physical Review B, R. Moorthy and L. Partain (submitted).	52
3. "Space-Charge-Limited Current and Capacitance in Cu_xS/CdS Solar Cells," International Electron Devices Meeting, Washington, DC, Dec. 1979, R. Moorthy, L. Partain, D. Okubo, and D. Henderson (accepted).	94
B. EBIC Studies	99
1. "Obtaining Accurate Values of Diffusion Length with the Scanning Electron Microscope," 2nd E. C. Photovoltaic Energy Conference, West Berlin, April 1979, p. 639, L. D. Partain and S. P. Shea.	100

Page No.

2. "Non-Destructive SEM Measurement of Minority Carrier Transport Parameters of Cu_xS/CdS Solar Cells as a Function of Heat Treatment," IEEE Trans. Electron Devices, Special Issue on Photovoltaics, April 1980, L. Partain, G. Armantrout and D. Okubo (submitted). 114

C. Hall Effect Measurements 150

"Hall Effect in Reactively Sputtered Cu_2S," Applied Physics Letters, 35, 601 (1979), J. Y. Leong and J. H. Yee. 150

IV. Conclusions 152

V. References 154

I. SUMMARY

Analytical and theoretical advances over the past year have provided the first determinations of several crucial transport parameters for sputtered Cu_xS/CdS solar cells that indicate that device behavior is dominated by entirely different physical mechanisms than previously considered and that further efforts to control and improve performance should focus in new directions. The characterization capabilities extended to measure sputtered film properties have shown that several anticipated variations do not take place and that important unanticipated effects play primary roles. This has first order implications for the fundamental problems of fabrication reproducibility and device stability. This work can be summarized with nine key questions listed below and by the indicated brief answers that directly follow. These answers are of varying degrees of completeness. The details are given in the body of the report.

KEY QUESTIONS:

1. What materials properties and physical mechanisms control the behavior of sputtered Cu_xS/CdS solar cells?

   Answer: Strong preliminary evidence indicates that the behavior of Cu_xS/CdS formed by sputtering and by other techniques is dominated by space-charge-limited current mechanisms through trapping phenomena that are entirely different than processes that control ordinary p-n junction performance. The results further show that losses due to the imperfect junction region reduce the magnitude of the light generated current.

2. How can the important transport properties of sputtered Cu_xS/CdS devices be determined?

   Answer: Extension of SEM EBIC techniques allowed the first direct measurement of the minority carrier transport parameters in polycrystalline, thin film Cu_xS/CdS devices. These samples had their Cu_xS/CdS layer formed by sputtering. This characterization included diffusion lengths, surface recombination velocity, and junction collection efficiency. Sputtered free standing polycrystalline Cu_xS films on glass permitted Hall measurements of majority carrier properties.

3. What values do the important transport properties of sputtered Cu_xS films have and how are these values influenced by heat treatment?

   Answer: The minority carrier transport parameters of sputtered Cu_xS formed on polycrystalline CdS are essentially the same as those previously reported for films topotaxially formed on single crystal CdS. The majority carrier properties of the sputtered Cu_xS films are among the best that have been reported for polycrystalline material. These parameters are not strongly influenced by air or reducing heat treatments except for variations in the Cu_xS hole concentration.

4. How can the optical properties of polycrystalline sputtered Cu_xS films be determined?

   Answer: Free standing sputtered films on glass have allowed the first clear determinations of the optical properties of polycrystalline Cu_xS without the ambiguity encountered in layered Cu_xS/CdS structures.

5. What are the optical properties of sputtered Cu_xS films?

   Answer: The optical properties found with high quality, sputtered Cu_xS films are essentially the same as reported by Mulder for single crystal material. However the optical absorption constant is strongly affected by post fabrication heat treatment.

6. Does something peculiar occur at the sputtered Cu_xS/CdS interface?

   Answer: A primary characteristic of Cu_xS/CdS devices formed by sputtering and by other techniques is the loss of minority carrier current due to an imperfect junction region. This loss is strongly affected by heat treatment with loss values ranging from 50 to 80 percent for specific sputtered device cases. Two possible responsible mechanisms are direct recombination through interface states and/or losses caused by photocurrent suppression because of poor transport in the junction region.

7. Are the properties of sputtered and topotaxial Cu_xS films similar?

   Answer: Comparisons among single crystal Cu_xS material and Cu_xS films formed topotaxially and by sputtering onto poly and single crystal CdS indicate that the minority carrier and optical properties among all these materials are highly correlated. Good correlation is also expected for the majority carrier properties of polycrystalline Cu_xS formed either by topotaxy or by sputtering.

8. Does reactive sputtering provide a promising technique for Cu_xS/CdS device fabrication?

   Answer: Reactive sputtering provides polycrystalline samples in

forms uniquely suited for studies of the controlling mechanisms operating in Cu_xS/CdS that must be understood if full potential is to be reached. Justification of this more complex technique as a large scale process would require that some performance advantage over alternate techniques be identified. So far such identification has not been accomplished.

9. What approaches would most likely lead to further improvement in Cu_xS/CdS behavior?

   Answer: The solutions to major problems encountered in obtaining fabrication reproducibility and in understanding stability limitations would likely be found by careful monitoring and control of the trap structures involved in Cu_xS/CdS devices.

II INTRODUCTION

This section provides an overview of the major results achieved, evaluates them in terms of device development, and relates them to the prior work in the area. It is shown that the gross I-V properties not explained by standard theory is well modeled by space-charge-limited current (SCL I) analysis. Extension of the SEM EBIC techniques coupled with the unique material fabrications obtained with sputtering have allowed rather complete characterizations of thin film devices for the first time. These measurements included the minority and majority carrier transport parameters and the optical properties and indicated that unanticipated parameters determine performance and control repeatability and should establish device stability limits. The junction region losses of minority carrier current are identified as a dominant effect of heat treatment and actual junction collection efficiency values are quantified using a new analysis technique. Sputtering provided unique advantages that allowed free standing, polycrystalline Cu_xS films to be formed on glass for clear determinations of charge transport and optical properties in addition to providing a highly planar geometry on the CdS substrates required for the SEM studies. The benefits of sputtered device fabrication is assessed. Following this overview, more extensive discussions of the individual efforts are contained in the reprints and preprints of technicle articles contained in Section III of this report.

A. Controlling Mechanisms

Until recently there were no theoretical models capable of quantitatively explaining the gross electrical properties of Cu_xS/CdS solar cells such as the I-V's dark-light crossover, the non-exponential I-V, and the temperature-independent slopes of the I-V. The best agreement

has been achieved with the recently developed, SCL I model (see Sect. III A) controlled by new processes. This has strong implications for achieving fabrication repeatability and device stability and for the establishment of ultimate device performance.

The match this SCL I approach gives to the I-V cross-over is shown in Fig. 1 for a wet dip, topotaxial cell fabricated by the University of Delaware and is explained in Sect. III A.3. The characteristic, non-exponential I-V of SCL I is shown by the experimental data in Fig. 2 over 4 to 6 orders of magnitude in current for an LLL sample whose Cu_xS was sputtered onto vacuum deposited CdS (for the theory see Sect. III A.1). Since this approach has its behavior controlled by entirely different physical mechanisms than found in standard solar cell theory, the question immediately arises as to what mechanisms actually control the performance of these solar cells. If this new model is true, then entirely different material parameters need to be monitored, controlled, and optimized. For instance the change in the current-voltage characteristics with a two trap SCL I model, implied by a change in the deeper trap's density in CdS (located at $E_c-E_t=.44$ eV) is shown in Fig. 3. The data points shown are the light exposed values also given in Fig. 1. For the 17 mA/cm^2 short circuit current, the open circuit voltage would drop from 0.5 V down to 0.4 V and to 0.27 V as shown as the deeper traps density decreases from $5.1(10^{14})$ through $3.6(10^{14})$ to $1.8(10^{14})cm^{-3}$. The other parameters utilized for these curves are identified and their magnitudes specified in Sect. III A.3 where this model is described in detail. Such variation in CdS trap density with heating and other treatments is well known (1-5). Changes in characteristics like those shown are often observed for sputtered Cu_xS/CdS cells during heat treatment.

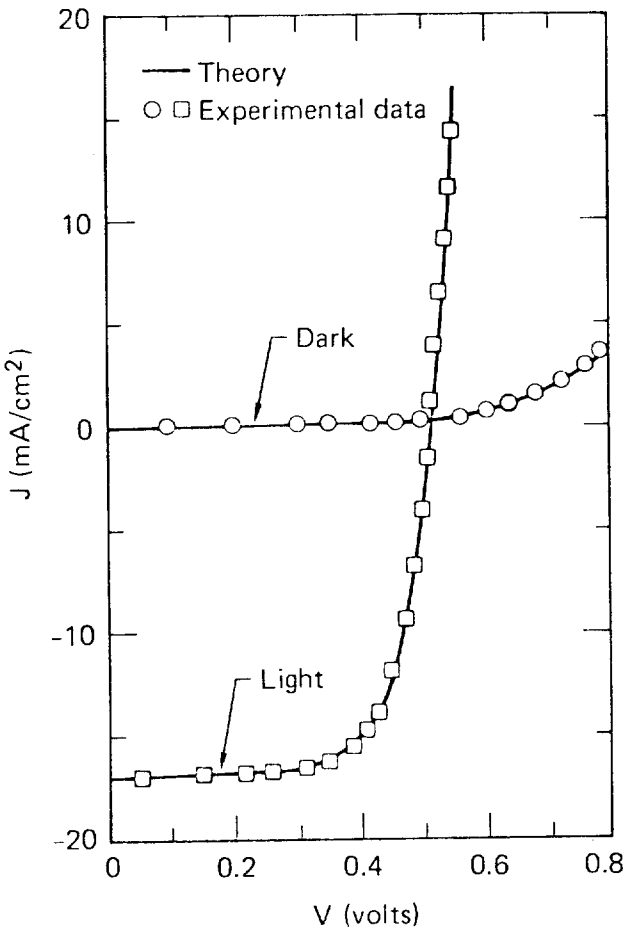

Fig. 1. The theoretical fit of the dark and light J-V characteristics of a "wet dip", thin film, Cu_xS/CdS cell of 6.1% efficiency (AM1) obtained using a SCL I model.

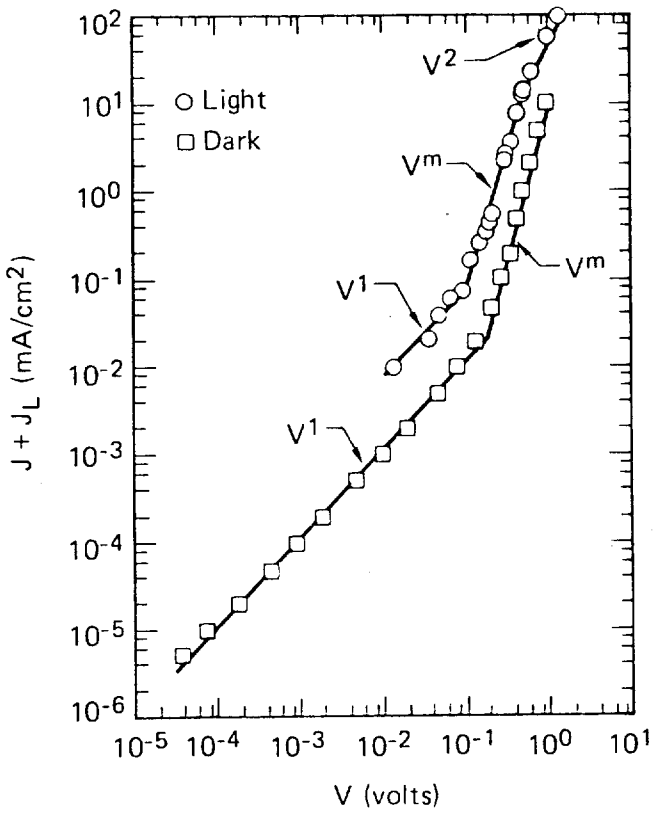

Fig. 2 The logarithmic variation of the light (AM1) and dark J-V characteristics of a reactively sputtered, thin film Cu_xS/CdS cell that demonstrates the characteristic SCL I behavior of Ohmic, V^m, and V^2 dependence over 4 to 6 orders of magnitude in current density. The short circuit current density J_L has been added to the light data so current is zero when V is zero.

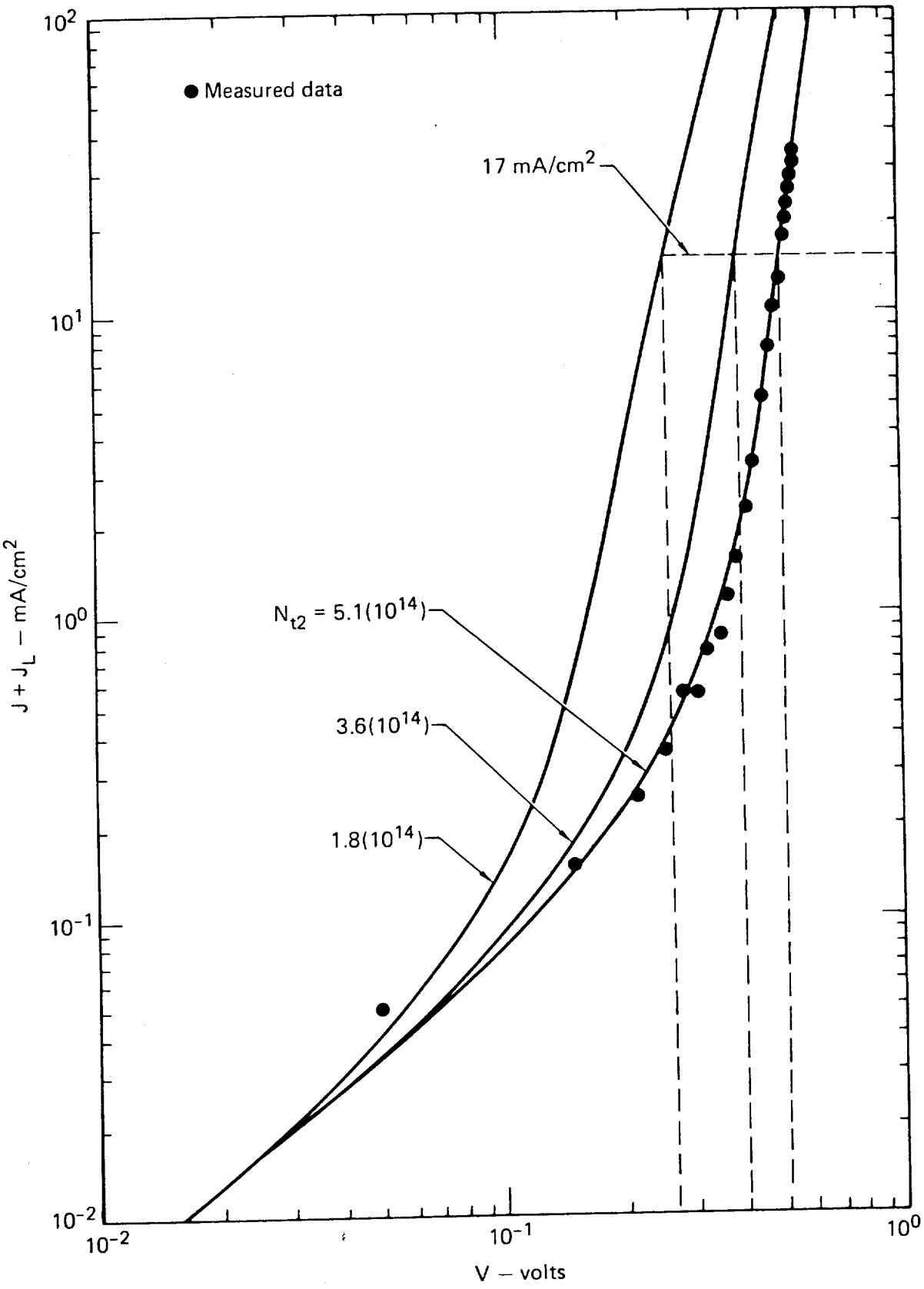

Fig. 3 The two trap, SCL I model of the variation of the J-V properties as a function of the density of the deeper trap which indicates how the open circuit voltage would vary with a constant short circuit current density of 17 mA/cm^2. The light exposed, experimental data of Fig. 1 is shown for reference.

This has strong relevance for a major experimental problem - device repeatability. Rather random fluctuations of device performance have often been seen between sputtered device, fabrication runs even though all known parameters of importance (according to standard theories) have been monitored and controlled. Since the trap structure controlling SCL I has never been carefully monitored during cell fabrication, it is a prime suspect as the cause of the unpredictable changes that plague current experimental studies and impede commercial exploitation. This SCL I model also impacts questions of stability since light and heat and ambient induced changes of traps with time are widely reported (1-5). Thus there is sufficienct evidence now to justify a determination of how CdS trap parameters influence device behavior with the possible payoff in greatly increased consistency in device fabrications and in improved control of stability.

B. Thin Film Characterizations

Extending the SEM EBIC techniques allowed polycrystalline Cu_xS/CdS samples of planar geometry to be measured in terms of their minority carrier transport parameters. Reactive sputtering provided the planar shapes and also gave free standing Cu_xS films that allowed characterization of the majority carrier properties. These transport properties were found to not vary appreciably with air or reducing heat treatment except for the Cu_xS hole concentration.

The minority carrier diffusion length values were found to lie in the 0.20 to 0.26 μm range for the sputtered Cu_xS and in the 0.41 and 0.46 μm range for vacuum deposited CdS (see Sect. III B.2) which bracket the

highest accuracy values measured on devices with a "wet dip" Cu_xS layer (see Sect. III B.1). These sputtered Cu_xS values are 20 to 50 percent higher than those found by Westinghouse with a "dry process" single crystal CdS sample measured with a laser scan technique(6).

This past year's development at LLL of the non-destructive technique to accurately measure these values on ordinary, polycrystalline cells whose top layer is less than a diffusion length wide represents a major advance in characterization technology applicable to a wide range of thin film devices. The results are obtained from analyzing the slopes of EBIC (electron-beam-induced current) data as a function of high energy electron beam penetration into the sample as described in Section III B.2. Typical EBIC data curves are shown in Fig. 4 as a function of heat treatment at 180°C in hydrogen-argon for a sample with vacuum deposited CdS and sputtered Cu_xS. The unchanging shapes indicate constant diffusion lengths and also constant values of Cu_xS surface recombination velocity equal to the diffusion velocity. Comparing this to similar studies of "wet dip" single crystal devices heat treated in air(7) indicates that unchanging magnitudes of these quantities are obtained for devices with epitaxially sputtered(8) and topotaxially reacted Cu_xS layers on polycrystalline and single crystal CdS substrates and heated in either air or hydrogen-argon ambients.

LLL's reactive sputtering allowed free standing films of Cu_xS to be formed on glass substrates simultaneously with device fabrication. This allowed the Hall effect measurements (by Yee and Leong) of the majority carrier properties to be obtained as described in Sect. III C. As fabricated, a typical film showed a hole mobility of 5.5 cm^2/V-sec and

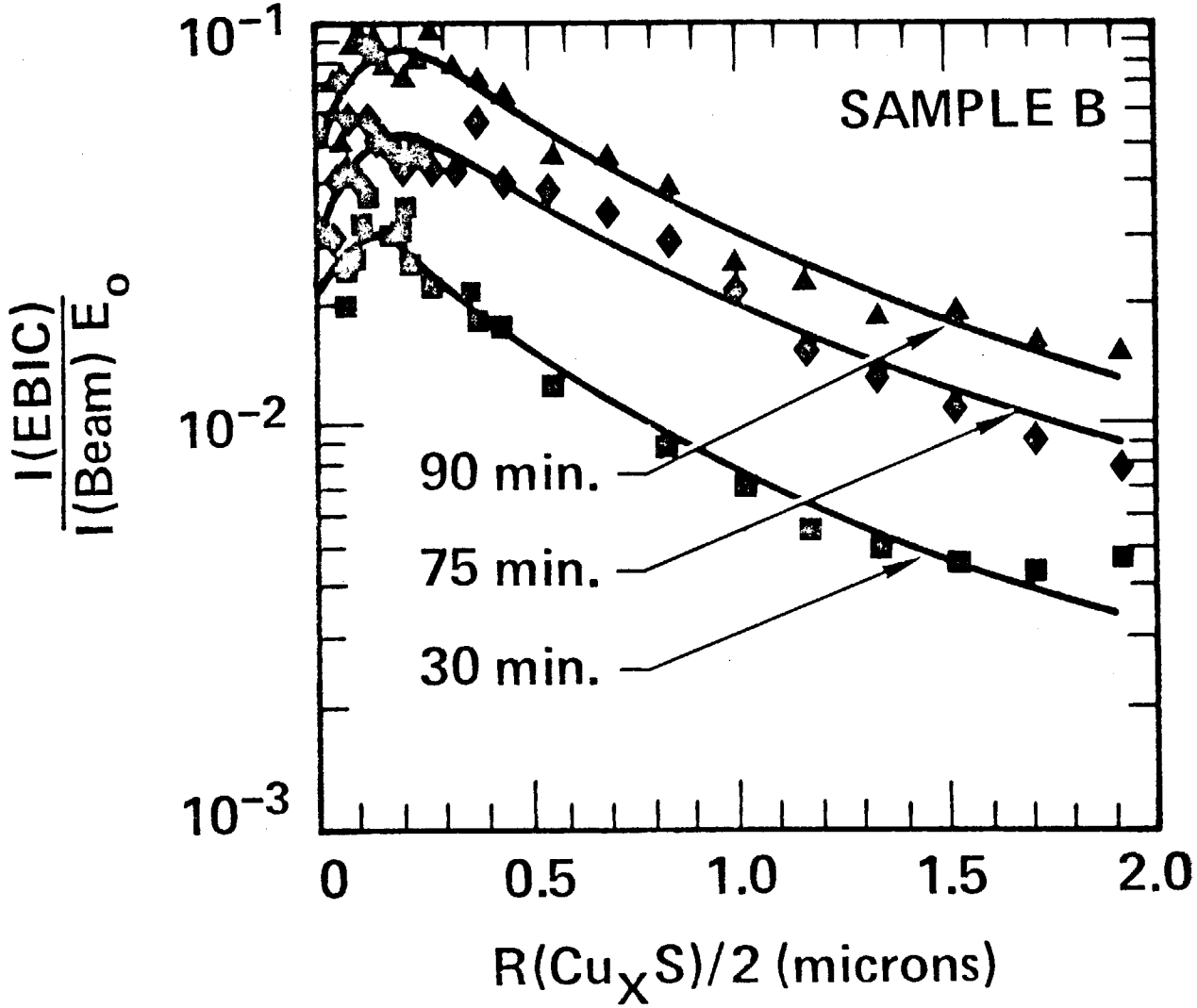

Fig. 4 Electron-beam-induced current data measured as a function of the high energy electron beam penetration into a thin film, polycrystalline Cu_XS/CdS sample heat treated in hydrogen-argon gas at 180°C for the indicated time intervals.

a hole concentration of $2(10^{19})cm^{-3}$ corresponding to 0.06 ohm-cm resistivity at room temperature. Subsequent heat treatment in air and hydrogen-argon showed no large variations in this mobility but strong changes in hole concentration.

To the extent that such carrier concentration excursions with heating represent changes in the Cu_xS stoichiometry and its defect density, it has been postulated that parallel changes could also be occurring in mobility and thus in diffusion lengths(9-11). However the temperature dependence of the Cu_xS mobility investigated in the LLL studies as shown in Fig. 5 (and discussed in Sect. III C), shows that the high quality film had its mobility determined by the intrinsic lattice scattering mechanism of optical phonons at room temperature and not by extrinsic crystal defects. Thus no mobility improvements (nor related diffusion length improvements) should be expected in such films with stoichiometry changes induced by heating or by other means. This is certainly consistent with the unvarying diffusion lengths reported above. Such a lack of a diffusion length change with heating was recently supported by the experimental measurements of the Westinghouse group(6) taken on a single crystal sample heated in a nitrogen ambient at 200°C.

The measured room temperature mobility mentioned above compares well to previously reported polycrystalline, Cu_xS values ranging from 5 cm^2/V-sec (12) to 12 cm^2/V-sec(13) and is at the lower end of the reported single crystal range from 4 cm^2/V-sec(14), 25 cm^2/V-sec(15), up to 90 cm^2/V-sec(11) Thus one can see that the minority and majority carrier transport parameters of sputtered Cu_xS films are among the best reported for polycrystalline

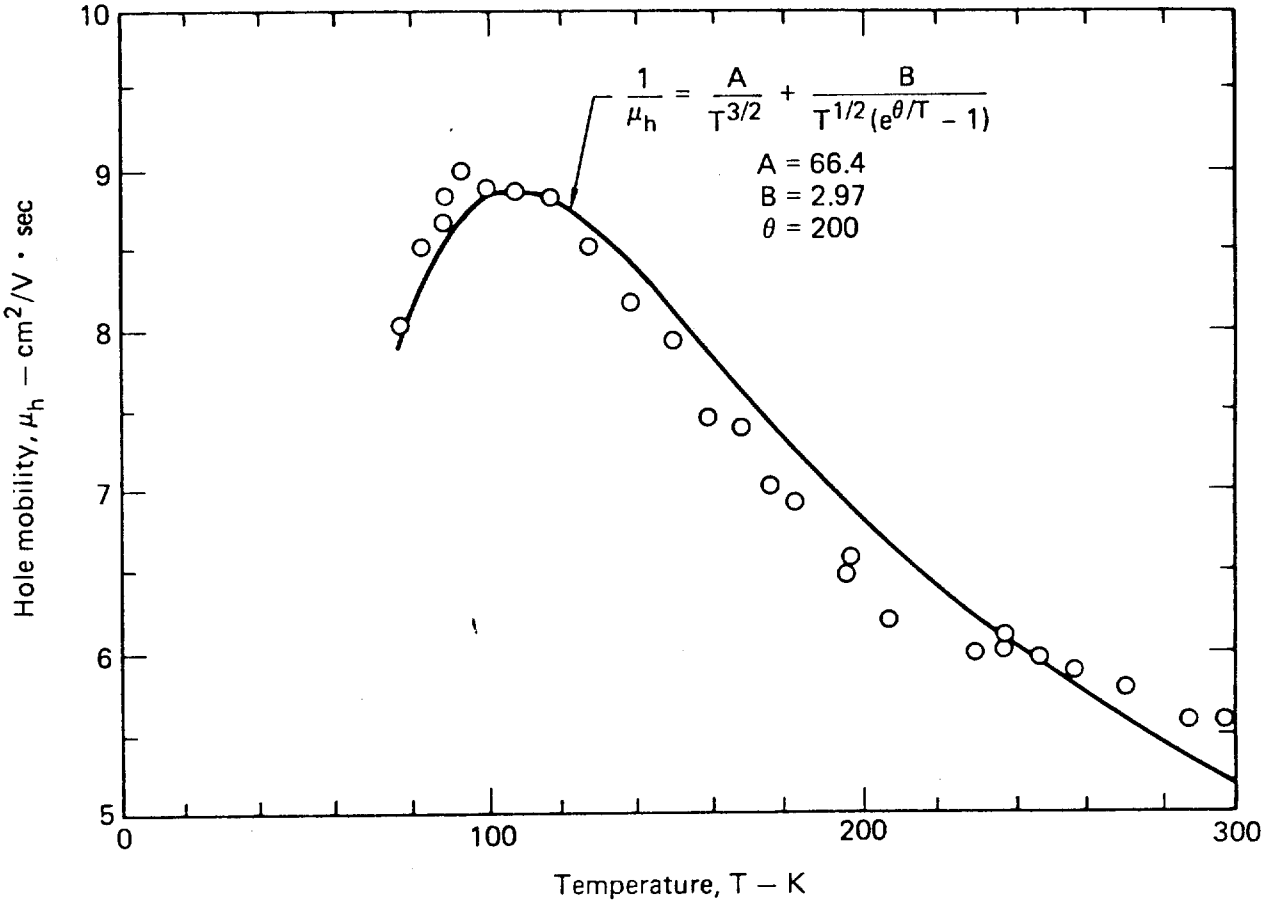

Fig. 5 The temperature dependence of the hole mobility in thin film Cu_xS reactively sputtered onto a glass substrate.

films and do not change with heat treatment except for hole concentration. With these important eliminations, the important question arises as to what is changing during heat treatment.

C. Junction Collection Efficiency

If most of the proposed mechanisms for changing device performance are rejected, then a burden is imposed to find what basic mechanisms are responsible for the large observed variations in device behavior. A prime prospect is the loss of photogenerated carriers due to the heterojunction interface region. Two possible responsible mechanisms have been proposed: 1) the loss of minority carriers through interface states at the heterojunction as suggested by Oldham and Milnes(16) and utilized by Rothwarf et al (9,17,19) and the Indian Group (18) and 2) the suppression of minority carrier current due to poor transport characteristics of the junction region as described by Rhoderick (20) and by Crowell et al (21,22) for Schottky barriers and extended to heterojunctions by Partain and Shea (23). Indeed the finding of the LLL studies has been than changes in the efficiency with which minority carriers are collected by the junction region are a major effect of heat treatment with sputtered samples. Half the minority carriers (generated in the dark by an electron beam) were found to be lost because of the junction region. The higher efficiencies required for high performance may be produced either by photoenhancement of by other means that improve junction transport.

The vertical shifts of the EBIC curves with heating as shown in Fig. 4 are direct indications of changes in the junction collection efficiency

as explained in Sect. III B.2. A major advance of the last year at LLL has been the extension of the EBIC technique to allow absolute values of junction collection efficiency to be determined in terms of the photocurrent suppression mechanism mentioned above (see Sect. III B.2). Figure 6 shows the typical variations in this junction efficiency with heat treatment at 180°C in hydrogen-argon for minority carriers originating in one of three regions (the low field Cu_xS region, the low field CdS region, or the junction space-charge-region) for a sputtered, polycrystalline device. Such results indicate that junction efficiency variations are a dominant effect of heating. Recently this loss of photocurrent due to the junction region and its change with heating has been verified by the laser measurements at Westinghouse(6).

Note that Fig. 6 indicates that about half the carriers generated outside the space-charge-region are lost in the junction region even at the peak of the curves. Since this EBIC data was obtained in the dark, these low values may be due to the lack of photoenhancement. This possibility will be clarified when the planned EBIC experiments in light are carried out. Another possibility is that there may be more interface losses with the LLL expitaxially grown Cu_xS than occurs with the buried interface of a topotaxially formed junction. Future measurements on topotaxially formed devices will answer this question. The prior topotaxial EBIC data only determined relative variations in junction collection efficiency (7).

The interface recombination velocity studies by Rothwarf et al also indicated significant loss of carriers in the interface (17). Use of

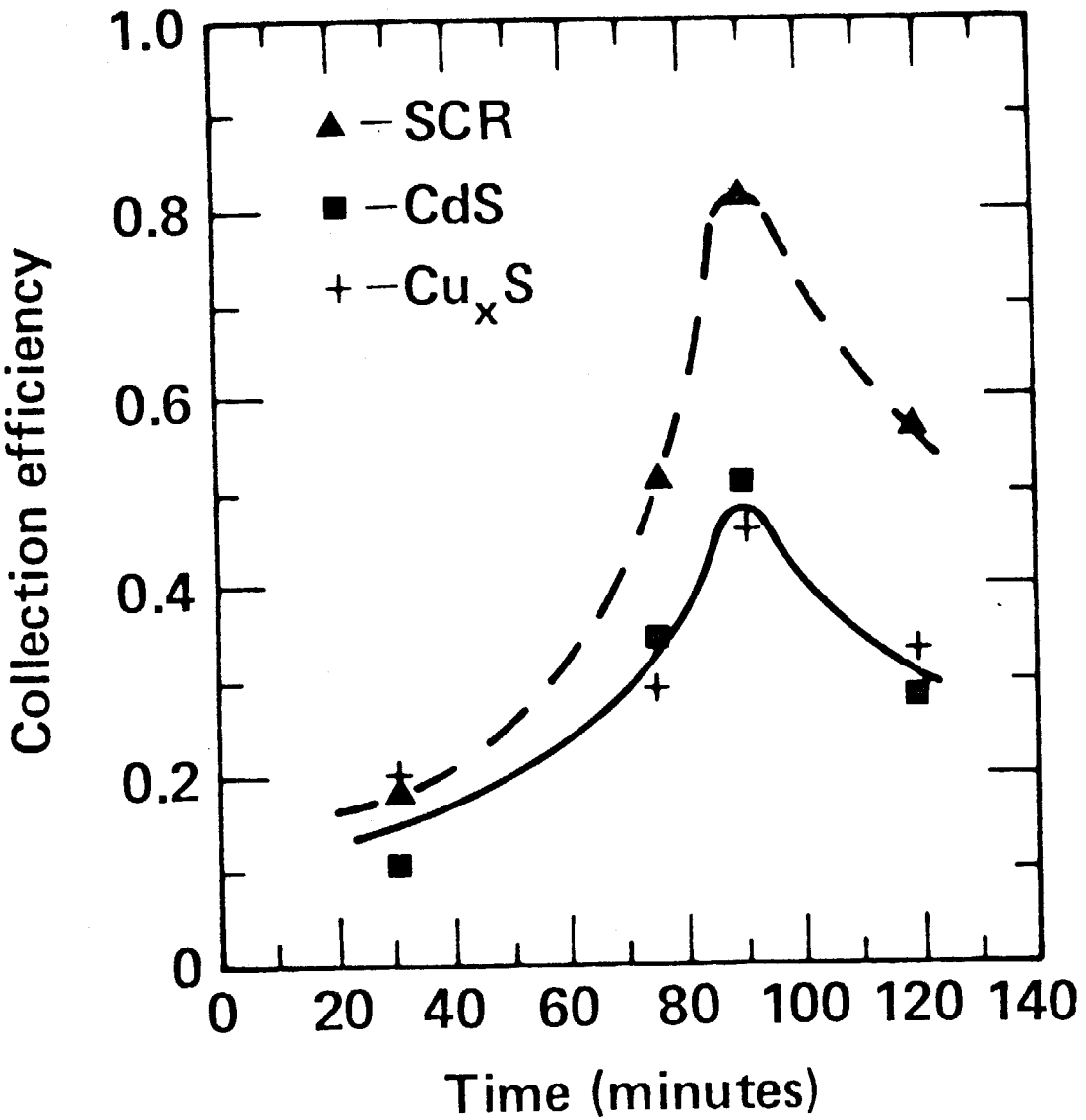

Fig. 6 The junction collection efficiency measured on a reactively sputtered, thin film, Cu_xS/CdS device as a function of heat treatment in hydrogen-argon at 180°C for minority carriers originating in the low field Cu_xS or CdS regions, or the high field, space charge region.

this approach in the light by the Indian group (18) indicates a junction efficiency of 50 percent in agreement with the LLL dark values given above. The interface recombination parameters reported in the Delaware publication (from measurements taken in the light) also specify a 50 percent collection efficiency (see Table 1 of Ref. 17) even though their data was not presented in a manner to show this magnitude. The point is that growing evidence points to significant junction region losses in samples formed by sputtering and by other techniques. An earlier Delaware report has reported interface collection efficiencies of up to 96 percent (19) indicating a possible range for this parameter's variation.

D. Sputtering Control of Cu_xS

Reactive sputtering allows a wider variation of thin film properties of Cu_xS to be obtained than with other fabrication processes. A discontinuous jump of resistivity of four orders of magnitude, to higher values than achieved topotaxially, is reproducibly seen with the sputtering. The optical properties were unambiguously determined because the free standing polycrystalline Cu_xS films could be produced. This showed that optical constants approaching single crystal values could be achieved but that they vary strongly with subsequent heat treatment. The high resistivity films were quite unstable, showed no clearly identifiable advantages and may be undesirable.

As the pressure of the reactive gas (4.4% H_2S, 95.6% argon) is lowered, the polycrystalline films exhibit a sudden four orders of magnitude jump as shown by the resistivity plot in Fig. 7. Such a transistion was

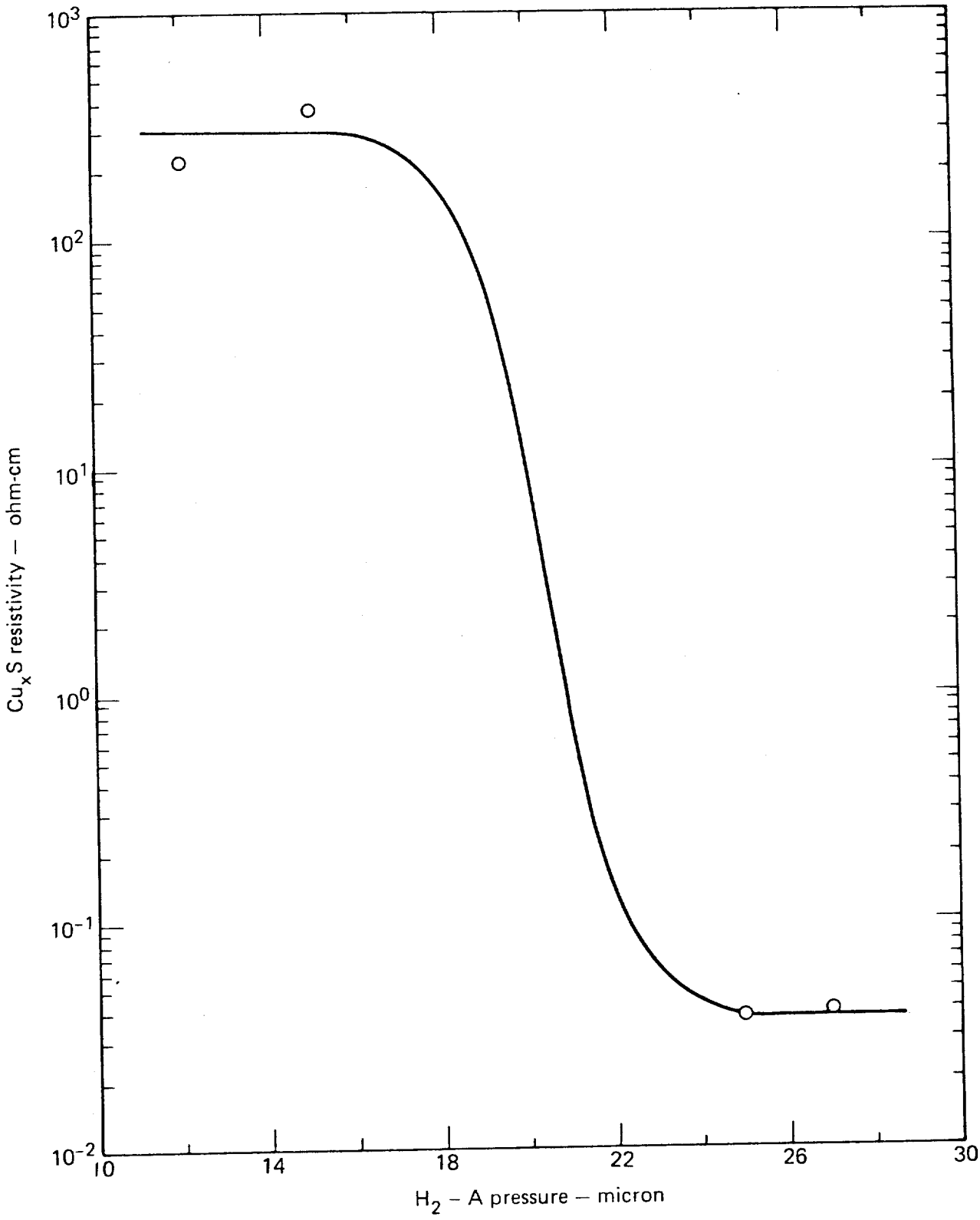

Fig. 7 The four order of magnitude change in the resistivity of Cu_xS films formed by reactive sputtering as the reactive gas pressure is varied.

earlier reported for the LLL approach (8) and it has been confirmed in Lockheed's reactive sputtering work (24). Low resistivities in the hundreths of an ohm-cm are consistent with the highest Cu_xS sheet resistivities reported for "wet dip" layers by Burton and Windawi (25) and by the French group for their single crystal samples (14). Apparently, reactive sputtering is one of the few techniques capable of producing Cu_xS in the 10^2 ohm-cm ranges. The polycrystalline nature of the Cu_xS films sputtered unto glass was established by x-ray diffraction. Spectrophotometer determinations of the optical absorption properties of low resistivity, sputtered film (0.06 ohm-cm) has essentially the same values as reported by Mulder on single crystal chalcocite. This is shown in Fig. 8 and indicates the high optical quality of such films as was also reported by Lockheed (24). This absorption constant varies significantly with heat treatment.

The high resistivity, sputtered films are highly unstable and are characterized by the presence of elemental copper nodules identified by x-ray analysis in a scanning electron microscope (8). Attempts at taking Hall effect measurements on such films result in Hall voltages so unstable in time as to preclude meaningful measurements. Immediately following heat treatment of these initially high resistivity films at 180°C in hydrogen-argon (for as little as 15 minutes), the resistivity immediately drops to the 10^{-2} ohm-cm range. EBIC measurements made to see if increased diffusion lengths predicted (9,10) for high resistivity, stoichiometric samples is actually achieved, gave inconclusive results. Heat treatment was required to make the devices rectifying enough for EBIC measurements. Such measurements then gave the same

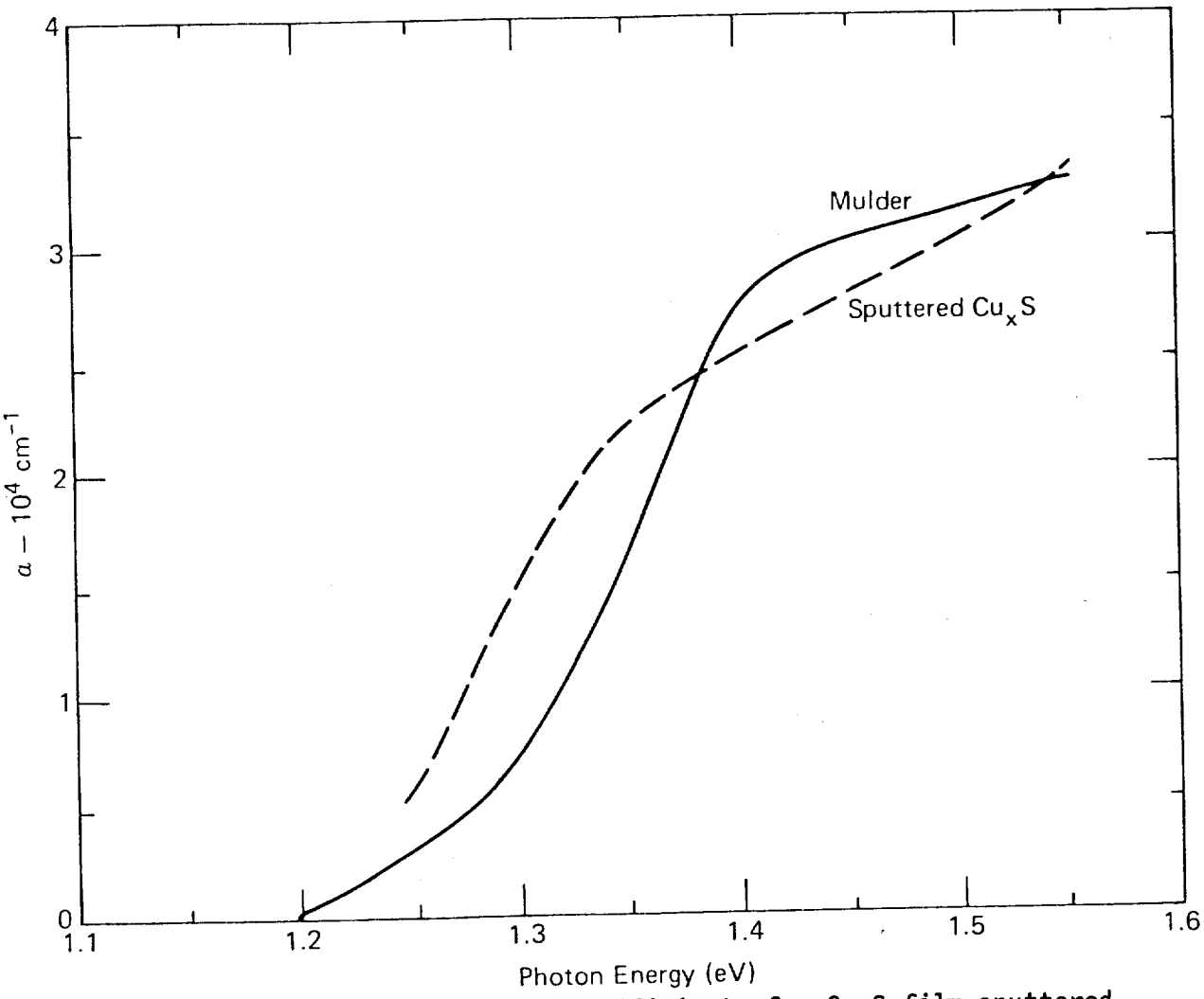

Fig. 8 The optical absorption coefficient of a Cu_xS film sputtered onto glass in comparison to Mulder's single crystal values.

diffusion length values as found with the Cu_xS films of intially lower (0.01 ohm-cm) resistivity. Unfortunately this heat treatment lowered the initially high Cu_xS resistivity down into the low range. Such unstable electrical properties were also found by Kramer (26) when he sulfurized ultra pure copper films into unusually high resistivity states using sulfur vapor in an ultra-high vacuum system and by Okamoto and Kawai (27) in stoichiometric Cu_xS at elevated temperatures.

At this point, the most that can be said is that anticipated advantages for high resistivity Cu_xS layer devices have not yet been observed. A large number of devices with very low efficienty have been formed that, before the first heat treatment, had a hundred ohm-cm Cu_xS layers with copper nodules. There is the distinct possibility that the highest resistivity forms are undesirable. However good devices and Cu_xS films with the desired optical properties and electrical properties are obtained in the low resistivity forms with reactive sputtering. These results show the wider variation of the Cu_xS properties is obtained with sputtering compared to other reported techniques.

E. Performance Potential

The potential efficiency of reactively sputtered devices is as good as for any other fabrication process based on the minority transport parameters and the optical properties. Actual achievement of this potential depends on two things. Equivalent light trapping and equivalent junction collection efficiency to the other techniques must be achieved. The theoretical calculations of achievable cell current with a planar structure agree well with experimental data. The highest demonstrated

efficiency for sputtered cells (4%) is being limited either by a lack of sufficient light trapping or by inferior junction collection. A differentiation between these two will be obtained in proposed experiments. A typical light I-V for one of the higher efficiency sputtered devices is shown in Sect. III B.2, Fig. 2. For the more complex fabrication techniques, like reactive sputtering, to be cost competitive with simpler processes for large scale fabrication, a significant performance advantage for the sputtered cells needs to be identified. Such identification has not been accomplished to the present time.

Reactive sputtering produces a relatively uniform thickness layer of Cu_xS similar to "dry processed" cells without the large light trapping, grain boundary instrusions of the "wet dip" process as identified by Shirland (28). The limitations that a highly planar geometry places on short circuit current as a function of the Cu_xS minority carrier diffusion length are shown in Fig. 9 assuming AM2 light (83 mW/cm^2) and at most two passes of light through the Cu_xS layer. Since the diffusion length has been found to equal 0.25 microns in both polycrystalline and single crystal devices (see Sect. III B), the following conclusions can be drawn. With a single light pass (front wall) and a 20% front surface reflection loss (no AR coating) 12 mA/cm^2 is indicated by the lower dashed curve. With a highly reflecting back surface giving a second pass, a 20 percent increase would be indicated up to 14.5 mA/cm^2 (this case has not been shown in Fig. 9). This agrees quite well with the 13 mA/cm^2 recently reported by Delaware for dry processed cells on a smooth substrate and no AR coating (see Ref. 29, Fig. 1). With an AR coating and 70% back surface reflection, the upper dashed line of Fig. 9 specifies a short circuit current of about 18 mA/cm^2 compared to the 17 mA/cm^2

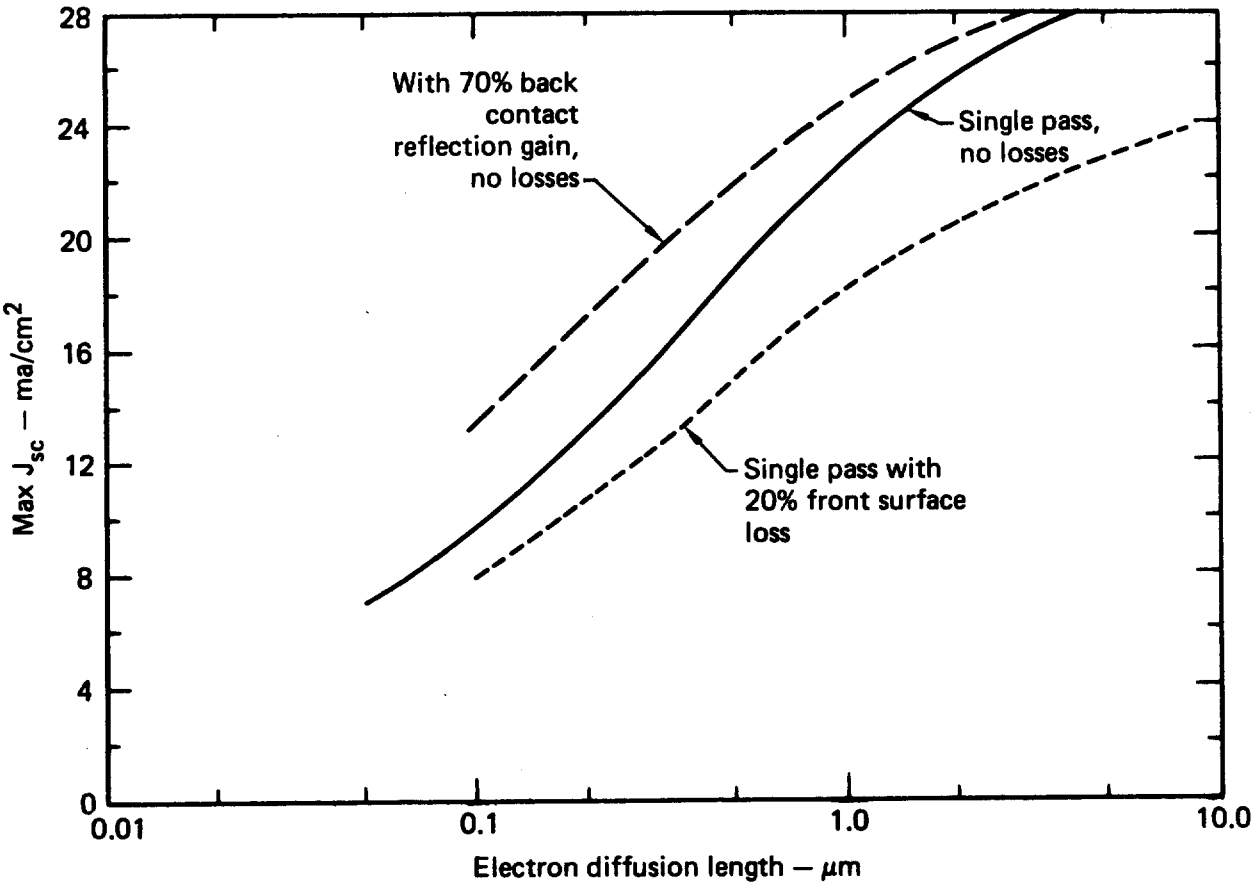

Fig. 9 The calculated maximum achievable current densities versus diffusion length for light absorption in a planar, Cu_xS layer assuming Mulder's absorption constant values (E ⊥ C axis), zero surface recombination loss, optimum choice of Cu_xS layer thickness, AM2 light intensity (83 mW/cm^2), and perfect minority carrier collection at the layer's back surface; a) for a single light pass with 20% front surface reflection, b) for single pass and no front reflection, and c) for no front surface reflection with 70% back surface reflection for a second light pass through the Cu_xS.

found for an AR coated device in the Delaware Progress report. These limitations on achievable current with a highly planar geometry are consistent with the reflected photon losses recently discussed by Bragagnolo (30). Increased currents therefore depend on roughened substrate or top surfaces or equivalent techniques to achieve light trapping such as suggested by Bragagnolo.

So far junction collection efficiencies of 50 percent and less have been reported for cells with both topotaxially and epitaxially (reactive sputtered) formed Cu_xS layers as discussed in the preceding section. However the high performance 9.15% cells (31) must have had much higher collection factors. For high performance, the sputtered devices need to demonstrate their capability for achieving this same performance. Comparative EBIC studies of epitaxial and topotaxial devices should clarify if there is any inherent difference between them. So far such comparison experiments have not been carried out but they are proposed. Significant performance advantages for sputtered cells compared to other techniques have not yet been found.

III. DETAILED STUDIES DESCRIBED IN TECHNICAL ARTICLE PREPRINTS AND REPRINTS

A. SCL I MODELING

Section III A.1

SPACE-CHARGE-LIMITED CURRENT IN Cu_xS/CdS SOLAR CELLS*

L. D. Partain

G. A. Armantrout

J. Leong

Lawrence Livermore Laboratory

Livermore, California 94550

and

Peter Warter

University of Delaware

Newark, Delaware 19711

This paper was Prepared for Submittal to

the Journal of Electronic Materials**

---

*Work performed under the auspices of the U.S. Department of Energy by the Lawrence Livermore Laboratory under contract number W-7405-ENG-48.

ABSTRACT

A space-charge-limited current model has been used to consistently and quantitatively model the gross electrical properties of Cu_xS/CdS heterojunctions not explained by standard p-n junction theory. Quantitative fits were obtained for the dark and light crossover of the I-V curves, the evolution of I-V from near Ohmic to rectifying during heat treatment, the high forward voltage drop in the dark, the non-exponential dependence of I on V, and the temperature independent slope of the I-V curves. These were found for CdS trap densities in the 10^{13} to 10^{15} cm^{-3} range, polycrystalline CdS mobilities in the 1 to 10 cm^2/V-sec range, and conduction electron concentrations in the 10^8 to 10^{10} cm^{-3} range in the thin Cu compensated region of CdS produced during cell fabrication heat treatments as monitored by zero bias capacitance. These results imply that entirely different physical mechanisms than those used to described standard p-n junctions control the dark and light I-V characteristics and the conversion efficiency of these solar cells.

I. INTRODUCTION

The gross electrical properties of Cu_xS/CdS solar cells have long presented unusual characteristics that have been difficult to explain with a consistent and quantitative, theoretical model based on reasonable parameter values. These properties include the dramatic crossover of the dark and light I-V curves (1-5), the non-exponential dependence (5) of current on voltage with a temperature independent slope (3,6,7), the evolution of the I-V properties with heat treatment from near Ohmic to rectifying (8-11), the high forward voltage drops in the dark (1-5,9), and a soft breakdown (4,9,10) under reverse bias. Existing models have either concentrated on just the illuminated characteristics (12) or just dark characteristics (6,13) or have given only qualatative descriptions for the observed behavior (8, 14-18). The quantitative theories have not made direct comparison to experimental results (19) or have been restricted to limited ranges of current and voltage (5,13,20) or have limited their treatments to specialized phenomena not easily related to both current and voltage (3,21-24).

Several workers (12,14,25) have suggested modeling the dark I-V properties using space-charge-limited current (SCL I), but no detailed studies were made. One early investigator (16) developed a detailed SCL I theory. However, it was for two carrier injection which is not physically justifiable in a rectifying device (26) such as Cu_xS/CdS which has a high barrier to hole injection (27). In this paper the gross electrical

properties are analyzed in terms of a single carrier injection SCL I. An approximate multi-trap theory is presented in addition to an exact, single trap analysis. It is shown that the observed experimental data can be consistently explained using these approaches.

II. THEORY

The general behavior of the I-V curves when SCL I conditions are present (26) is illustrated by the solid line curve in Fig. 1. An Ohmic region occurs at low currents. With increasing current an $I \propto V^2$ region appears next if shallow traps are present. Further current increases finally give a $I \propto V^m$ $(m > 2)$ region followed by $I \propto V^2$. For reference, Pizzarello's actual experimental data (28) for SCL I in vacuum deposited, polycrystalline CdS with two Ohmic contacts are shown in this figure. A sufficiently high resistivity is required in a material before SCL phenomena can be observed (26,29). The diffusion of Cu from the Cu_xS layer into the CdS to form such a compensated, high resistance region in the CdS during the cell fabrication heat treatment is well established (30,31).

The $I \propto V^m$ region is referred to as the trap filled limit (TFL). The intersection of the Ohmic line with the V^m line (see the dashed lines in Fig. 1) can be used to define a threshold for the TFL. Simple, first order approximations give this voltage threshold as (26)

$$V_{TFL} = \frac{qL^2}{\epsilon} p_{to} \qquad (1)$$

where q is the electronic charge, L is the width of the Cu compensated CdS high resistance region, p_{to} is the equilibrium concentration of holes in traps, and ϵ is the CdS dielectric constant. From Ohm's law

$$J = \frac{n_o\, q\, \mu V}{L} \quad \text{for } V < V_{TFL} \tag{2}$$

where n_o is the equilibrium concentration of conduction electrons and μ is the electron mobility. In the adjacent region

$$J \propto V^m \text{ for } V > V_{TFL} \tag{3}$$

where $m > 2$ but m takes on its smaller values when multiple traps are present (26,29). These Eqs. 1-3 will be referred to as the approximate, multi-trap model.

For the special case of a single trap, an analytic solution has been found of the form (26)

$$V = \frac{n_o q\, L^2}{\epsilon}\, \frac{y}{w^2} \tag{4}$$

$$J = \frac{n_o^{\,2}\, q^2\, \mu L}{\epsilon}\, \frac{1}{w} \tag{5}$$

where

$$y(u) = -\frac{C}{2G}u^2 - \left[\frac{C+1}{G+1} + \frac{G-C}{G^2(G+1)}\right]u - \frac{C+1}{G+1}\log(1-u)$$

$$+ \frac{G-C}{G^3(G+1)} \log(1+Gu) \tag{6}$$

$$w(u) = -\frac{C}{G}u - \frac{1+C}{1+G}\log(1-u) + \frac{G-C}{G^2(G+1)}\log(1+Gu) \tag{7}$$

and

$$B = N_t/n_o \tag{8}$$

$$C = \frac{2}{n_o}\left(\frac{2\pi m^* kT}{h^2}\right)^{3/2} \exp\left[-(E_c-E_t)/kT\right] \tag{9}$$

$$G = C + \frac{BC}{1+C} \tag{10}$$

$$u = n_o/n(L). \tag{11}$$

Here N_t is the concentration of the single trap spaced an energy (E_c-E_t) below the conduction band edge. The m^* is the density-of-states effective mass, k is Boltzmann's constant, T is absolute temperature, h is Planck's constant and n(L) is the non-equilibrium concentration of conduction electrons at the edge of the compensated, high resistance region opposite the electron injecting, cathode contact. The above

expressions are characterized in many cases by a near vertical rise of J with V for voltage values approaching the V_{TFL} of the simpler, approximate theory.

A condition for observing single carrier, SCL I is Ohmic, electron injecting contacts (for an n-type material) to the high resistance region. If an Ohmic and a blocking contact are made to the material, SCL I can still be observed but only for forward bias of the blocking contact so that electrons are injected through the Ohmic contact. For the opposite bias, rectification (rather than SCL I) is seen. In the two SCL I theories given above, the simplest conditions have been considered with a uniformly doped, Cu compensated CdS layer at the heterojunction interface. More complicated, position dependent profiles were not used since they would greatly complicate the analysis and require numerical integration calculations. The insight and understanding of the parameter interrelationships given by the analytical expressions would then have been lost.

III. RESULTS

The polycrystalline samples were fabricated by vacuum depositing 20 to 30 microns of n-CdS, with resistivity in the 1 to 10 ohm-cm range and a carrier density of about $10^{17}/cm^3$, onto a metal layer substrate that acts as an Ohmic contact. The opposite surface was etched for a few seconds in hot HCl. The polycrystalline sample #1 had its Cu_xS layer formed by reactively sputtering a copper target onto the etched CdS

surface in a H_2S atmosphere. Polycrystalline sample #2 was fabricated by the Institute of Energy Conversion, University of Delaware by dipping the etched CdS into a 90°C CuCl bath solution for several seconds. Single crystal sample A was fabricated on a single crystal slice of n-type CdS cut from an ultra-high-purity (no intentional dopant other than excess Cd) boule with resistivity in the 1 to 10 ohm-cm range and a carrier concentration in the 10^{15} to 10^{16} cm^{-3} range. This boule was purchased from the Eagle-Pitcher Corporation. After the hot HCl etch, sample A's Cu_xS layer was formed by reactive sputtering and its Ohmic contact to the CdS was obtained by pressed-on indium contacts. The Ohmic contact to the Cu_xS layer was gold for the polycrystalline samples and an indium-tin-gallium amalgam for the single crystal sample. Sample #1 was subjected to a 200°C air heat treatment for two minutes. Sample #2 was exposed to a 16 hour treatment in hydrogen-argon at 170°C and 0.5 hour in vacuum at 190°C. Single crystal sample A was given only the heat treatments described below.

After a 150 minute heat treatment in hydrogen-argon (14% H_2) at 180°C, single crystal sample A had the J-V characteristics shown in Fig. 2a. This log-log plot clearly shows that forward bias gives an Ohmic region that sharply breaks into a V^m region at a V_{TFL} of a few tenths of a volts. Reverse bias gives the characteristic "soft" breakdown. For comparison Fig. 2b shows the SCL I measured by Dresner and Shallcross(32) on vacuum deposited CdS to which an Ohmic gold contact and a blocking

tellurium contact had been attached. Its current density was estimated here by dividing its total current by the area of its dot contact. Note that for forward bias, its V_{TFL} is also a few tenths of a volt and its m value is similar to that of sample A. Under reverse bias it also has soft breakdown. Both Fig. 2 plots for forward bias demonstrate the standard SCL I features illustrated in Fig. 1. Similar SCL I J-V properties have been reported by other workers on vacuum deposited CdS with an Ohmic and a blocking contact (33,34).

The evolution of single crystal sample A's J-V characteristics is shown in Fig. 3 from initial fabrication (0 minute heat treatment) to treatment intervals up to 270 minutes total in hydrogen-argon at 180°C. Throughout this evolution the forward bias data, given by the upper lines and data points, maintain the characteristic SCL I form and the reverse bias results, of the lower curves and data points, give the soft breakdown. Note that after 270 minutes, the forward voltage drop exceeds one volt at a current density of 10 ma/cm^2. Analysis of these forward bias curves with the approximate, multitrap theory of Eqs. 1-3, gave the p_{to} values as a function of heat treatement time shown in Fig. 4. These values were determined from Eq. 1 using a CdS relative dielectric constant of 10 and using observed V_{TFL} values with L specified by the measured zero bias capacitance C(0) using the SCL I capacitance relation(26)

$$L = \frac{3 \epsilon A}{2C(0)} \qquad (12)$$

where A is the junction area of the device. These measured C(0)/A values and calculated L values are shown in Table I. No corrections were made in the flat projected value for A to account for surface roughness. The resulting trapped hole concentrations in the 10^{13} to $10^{15}/cm^3$ range is on the same order of magnitude as the values other workers have reported for SCL current in CdS (35,36). The Table I L values vary approximately as $L^2 = D(t-t_o)$ with a copper diffusion constant in CdS of $D = 4.6(10^{-12})$ $cm^2/V\text{-sec}$ where t is time and t_o = 18 min. accounts for the initial copper profile produced during device fabrication. This 180°C value for D lies in the range reported in the literature with agreement with Woodbury's extrapolated D value (37) and lying two orders of magnitude above and below Sullivan's (31) and Purohit's (30) values respectively.

Similar determinations of p_{to} for the polycrystalline sample #2, as it was taken from the dark into simulated 100 mW/cm^2 AM1 light, gives the similar order of magnitude values of p_{to} (dark) = 5.0 (10^{14}) cm^{-3} and p_{to} (light) = 3.9 (10^{14}) cm^{-3}. The J-V data used to determine these values using the measured C(0)/A of 10 nf/cm^2 are shown by the data points in Fig. 5. The approximate, multitrap model fit of this cross-over data is shown by the solid line curves for empirically determined values of m(dark) = 5.6 and m(light) = 9.0 and for a μ(dark) = 10 $cm^2/V\text{-sec}$ and μ(light) = 30 $cm^2/V\text{-sec}$. Such a factor of 3 increase in μ with light was reported by Wu and Bube (38) from thermoelectric measurements on Cu doped CdS formed by vacuum deposition. The dark value of m

compares well to the 5 to 7 range founded by McGarthy and Yee (39) in Cu doped single crystal CdS in which SCL I was observed. The increase in m with light suggests optical filling of shallow traps (with electrons) so that the voltage dependence of current more closely approaches the vertical behavior of a single (empty) trap condition. Such optical modification of the hole populations of traps is consistent with the hole trapping dynamics described by Fahrenbruch and Bube (22). Furthermore the 0.44 eV trapping level of the present work is identifical to the activation energy they found for optical degradation and the SCL I model is in agreement with their major conclusion that current transport is controlled by the Cu compensated CdS layer next to the Cu_xS/CdS interface. The major difference is in their use of a thermionic-emission-over-a-barrier model that differs markedly from SCL I theory. Note that the polycrystalline sample #2 had a 0.51 V open circuit voltage, a 17 ma/cm^2 short circuit current, a 0.70 fill factor, and a 6.1% conversion efficiency in the simulated AM1 light intensity.

If the sample A data of Fig. 3 is redrawn on a linear plot with a current scale low enough to clearly show the lowest current break (see the 90 minute heat treatment curve) between the Ohmic and TFL region, the previously reported form (9) of the evolving J-V becomes evident. At 0 minutes heat treatment, the J-V seems Ohmic because the current levels are so high. After 270 minutes, the high forward voltage drop becomes

quite evident. From the above one can note that the approximate, multi-trap SCL I theory consistently models the J-V evolution with heat treatment, the non-exponential J dependence on V, the dark-light cross over, and the high forward voltage drop in the dark.

Next we consider the temperature influence on the J-V curve. If temperature dependent sample #1 data are plotted on log-log scales, the resulting graph has the form shown by the data points in Fig. 6. To study such temperature variations, the preciseness of the exact single trap theory is required. The fit that Eqs. 4 and 5 give for these measurements are shown by the solid line curves obtained with the parameter values shown in Table II. This match is obtained again with trap densities in the same 10^{14} to $10^{15} cm^{-3}$ range and reasonable mobilities in the 1 to 10 $cm^2/V\text{-sec}$ range. The equilibrium conduction electron concentrations n_o are in the range reported in high resistivity, polycrystalline CdS in which SCL current has been observed (32,40). The identification of different E_c-E_t levels at each temperature results from the single trap theory giving the "effective" trap density within a few kT of the Fermi level as it retreats from the conduction band edge at higher T as explained in more detail by Bube et al (41). The L value was given by zero bias capacitance. Notice how well this temperature independent slope is modeled by SCL current. Also note the near vertical rise of the single trap theory at higher J values. The Table II trap energy levels agree within 15 percent to those obtained for CdS native defects by Grill et al (42) using deep level transient spectroscopy and they have the same

order of magnitude densities. The role of the deeper, Cu compensating levels, was to lower the Fermi level well below the conduction band edge so that rising temperatures sweep the Fermi level through progressively deeper traps (41,42).

IV. SUMMARY

A SCL current theory using reasonable parameter values has provided a quantitative model for the gross electrical properties of Cu_xS/CdS solar cells unexplained by standard p-n junction theory. These properties include the dark-light crossover of the I-V, the non-exponential dependence of I on V, the evolution of I-V with heat treatment, the high forward bias voltage drop in the dark and the temperature independent slope of the I-V characteristics. The soft breakdown is not included in standard SCL I theory. However similar breakdown has been widely observed in other polycrystalline CdS devices in which SCL I was observed and to which an Ohmic and blocking contact have been attached (32-34). These results imply that physical mechanisms entirely different from those described in earlier models control the dark and light I-V properties and thus the conversion efficiency of these Cu_xS/CdS devices. Similar SCL I behavior has also been identified for another heterojunction, solar cell structure comprised of n-ZnSe/p-GaAs (43).

ACKNOWLEDGEMENT

Significant credit is due D. Okubo and H. Brown for sample fabrication and for measurement assistance. Thanks are due J. D. Meakin and A.

Rothwarf for arranging for sample #2's fabrication and measurement and for very useful discussions. Primary credit is due R. Moorthy whose Master's thesis study provided the present workers with the initial evidence of SCL I in Cu_xS/CdS and on whose results, the present work is built. Very helpful discussions on SCL I were held with A. Rose. A valuable tool repeatably used to find relevant references was the report Cadmium Sulfide (JPL Public. 78-77, July 1978) Vols. I and II by A. G. Stanley.

TABLE I. Measured C(0)/A values and calculated L values for single crystal sample A as a function of 180°C heat treatment in hydrogen-argon.

Heat Treatment Time (min)	C(0)/A (nf/cm^2)	Calculated L(micron)
0	18.8	.71
30	12.2	1.1
60	8.8	1.5
90	7.5	1.8
150	6.0	2.2
270	4.8	2.8

TABLE II. Parameter values used in the exact, single trap, SCL current theory to fit the temperature dependent J-V data measured on polycrystalline sample #1.

T(°K)	$n_o(cm^{-3})$	$\mu(cm^2/V\text{-}sec)$	$N_t(cm^{-3})$	$E_c-E_t(eV)$
99	$2.0(10^8)$	10.0	$5.0(10^{14})$	.17
190	$6.5(10^9)$	2.0	$1.1(10^{15})$	.31
294	$2.0(10^{10})$	1.6	$6.0(10^{14})$	.44

Parameters held constant:

$L = 1.33(10^{-4})cm$

$\epsilon/\epsilon_o = 10$

$m_n^*/m_o = 0.2$

FIGURE CAPTIONS

Fig. 1. Functional form for the typical variation of I with V for standard space-charge-limited current theory. Data points were measured by Pizzarello(28) on polycrystalline CdS film formed by vacuum deposition.

Fig. 2. Log-log plot of the forward and reverse bias J-V properties of CdS devices. Plot a) is for Cu_xS/CdS single crystal sample A after 150 minutes of 180°C hydrogen-argon heat treatment. Plot b) is Dresner and Shallcross's (32) data on vacuum deposited, polycrystalline CdS to which an Ohmic gold contact and a blocking tellurium contact had been applied.

Fig. 3. The evolution of the forward and reverse bias J-V properties of single crystal Cu_xS/CdS sample A as a function of 180°C heat treatment time in hydrogen-argon. Upper curves and data are forward bias. Lower curves and data are for reverse bias.

Fig. 4. The equilibrium concentration of holes in traps as a function of 180°C, hydrogen-argon heat treatment time as determined for single crystal sample A using the approximate, multi-trap theory and the Fig. 3 forward bias data.

Fig. 5. The approximate, multi-trap model fit of the dark-light cross over characteristics of polycrystalline sample #2. Solid curves are theory and data points are measured values.

Fig. 6. The exact, single trap model fit for the temperature dependent J-V characteristics of polycrystalline sample #1. Solid curves give the theory and data points are the measured values.

REFERENCES

1. A. E. Middleton, D. A. Gorski, and F. A. Shirland, Progr. Astronaut. Rocketry 3, 275 (1961).

2. F. A. Shirland, Advanced Energy Conversion 6, 201 (1966).

3. W. D. Gill and R. H. Bube, J. Appl. Phys. 41, 3731 (1970).

4. M. Sayed and L. Partain, Energy Conversion 14, 61 (1975).

5. A. Rothwarf and K. W. Boer, Progr. Solid-State Chem. 10, 71 (1975).

6. S. Martinuzzi and O. Mallem, Phys. Stat. Sol. (A) 16, 339 (1973).

7. S. R. Das, A. Banerjee, and K. L. Chopra, Solid State Electr. 22, 533 (1979).

8. T. S. Te Velde, Solid State Electronics 16, 1305 (1973).

9. L. D. Partain and S. P. Shea, IEEE Intern. Electron Devices Meeting, Tech. Digest, Washington, DC, Dec. 1978, p. 239.

10. K. W. Boer, Phys. Rev. B 13, 5373 (1976).

11. A. Rothwarf, 2nd E. C. Photovoltaic Solar Energy Conf. Proc. (D. Reidel Publ. Co, Dororech, Holland, 1979) p. 370.

12. A. Rothwarf, International Conf. Solar Energy, Toulouse, France, March 1976.

13. A. Amith, J. Appl. Phys. 50, 1160 (1979).

14. L. R. Shiozawa, F. Augustine, G. A. Sullivan, J. M. Smith III and W. R. Cook, Aerospace Res. Lab Report #ARL-0155, Clevite Corp., Oct. 1969.

15. L. R. Shiozawa, G. A. Sullivan, and F. Augustine in Solar Cells, C. E. Backus, Ed. (IEEE Press, NY 1976) p. 231.

16. P. N. Keating, J. Phys. Chem. Solids 24, 1101 (1963).

17. A. E. van Aerschodt, J. J. Capart, K. H. David, M. Fabbricotti, K. H. Heffels, J. J. Loferski, and K. K. Reinhartz, IEEE Trans. Electron Devices ED-18, 471 (1971).

18. P. Massicot, Phys. Stat. Sol. All, 531 (1972).

19. A. Rothwarf, Intern. Workship on Cadmium Sulfide Solar Cells and Other Abrupt Heterojunctions, Newark, DE, April 1975, p. 9.

20. K. W. Boer, J. Appl. Phys. 50, 5356 (1979).

21. R. J. Mytton, Brit. J. Appl. Phys. D 1, 721 (1968).

22. A. L. Fahrenbruch and R. H. Bube, J. Appl., Phys. 45, 1264 (1974).

23. B. G. Caswell, G. J. Russell, and J. Woods, J. Phys. D, Appl. Phys. 8, 1889 (1975).

24. A. Rothwarf, J. Phillips, and N. C. Wyeth, 13th IEEE Photovoltaic Spec. Conf. Record, Washington, DC, June 1978, p. 399.

25. R. R. Bockemuehl, J. E. Kauppila, and D. S. Eddy, J. Appl. Phys. 32, 1324 (1961).

26. M. A. Lampert and P. Mark, Current Injection in Solids (Academic Press, NY, 1970).

27. A. G. Milnes and D. L. Feucht, Heterojunction and Metal-Semiconductor Junctions (Academic Press, NY 1972).

28. F. A. Pizzarello, J. Appl. Phys. 35, 2730 (1964).

29. A. Rose, Concepts in Photoconductivity and Allied Problems (Wiley, NY 1963).

30. R. K. Purohit, B. L. Sharma, and A. K. Sreedar, J. Appl. Phys. 40, 4677 (1969).

31. G. A. Sullivan, Phys. Rev. 184, 796 (1969).

32. J. Dresner and F. V. Shallcross, Solid State Electronics 5, 205 (1962).

33. R. Zuleeg, Solid State Electronics 6, 645 (1963).

34. G. T. Wright, Proc. IEEE 51, 1642 (1963).

35. M. A. Lampert, A. Rose and R. W. Smith, J. Phys. Chem. Solids 8, 464 (1959).

36. G. A. Marlor and J. Woods, Brit. J. Appl. Phys. 16, 1449 (1965).

37. H. H. Woodbury, J. Appl. Phys. 36, 2287 (1965).

38. C. Wu and R. H. Bube, J. Appl. Phys. 45, 648 (1974).

39. S. J. McGarthy and S.S. Yee, Solid State Electronics 17, 485 (1974).

40. K. V. Shalimova, L. P. Pavlov and R. R. Rezuyi, Soviet Physics - Solid State 6, 1749 (1965).

41. R. H. Bube, G. A. Dussel, C. T. Ho, and L. D. Miller, J. Appl. Phys. 37, 21 (1966).

42. C. Grill, G. Bastide, G. Sagnes, and M. Rouseype, J. Appl. Phys. 50, 1375 (1979).

43. J. W. Balch and W. W. Anderson, Phys. Stat. Sol. A9, 567 (1972).

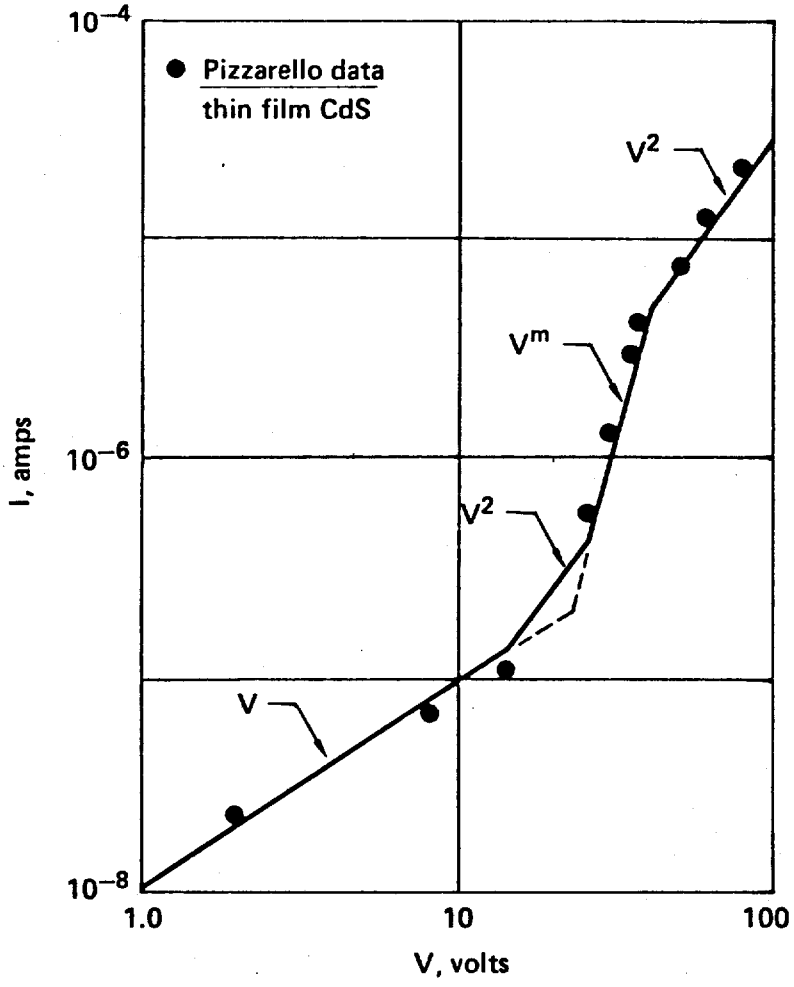

Fig. 1. Functional form for the typical variation of I with V for standard space-charge-limited current theory. Data points were measured by Pizzarello(28) on polycrystalline CdS film formed by vacuum deposition.

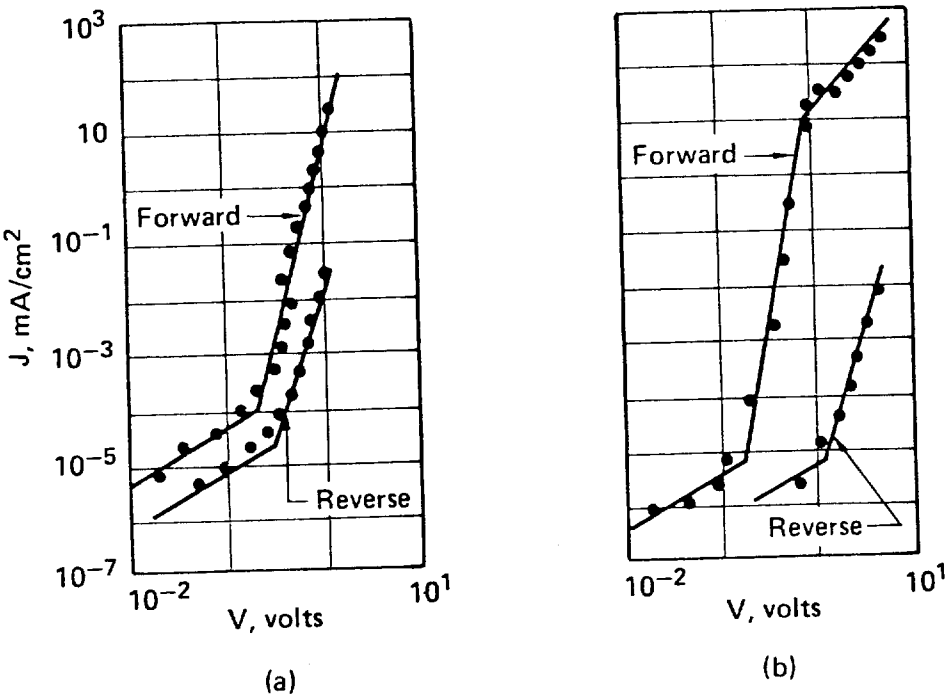

Fig. 2. Log-log plot of the forward and reverse bias J-V properties of CdS devices. Plot a) is for Cu_xS/CdS single crystal sample A after 150 minutes of 180°C hydrogen-argon heat treatment. Plot b) is Dresner and Shallcross's (32) data on vacuum deposited, polycrystalline CdS to which an Ohmic gold contact and a blocking tellurium contact had been applied.

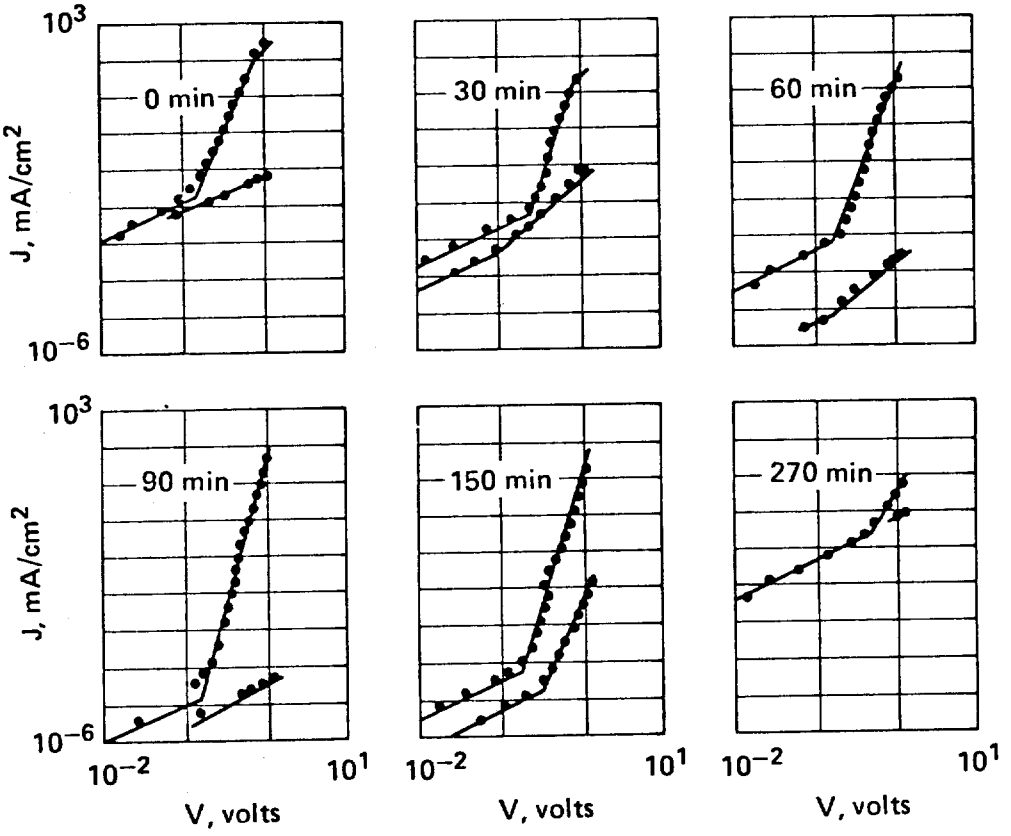

Fig. 3. The evolution of the forward and reverse bias J-V properties of single crystal Cu_xS/CdS sample A as a function of 180°C heat treatment time in hydrogen-argon. Upper curves and data are forward bias. Lower curves and data are for reverse bias.

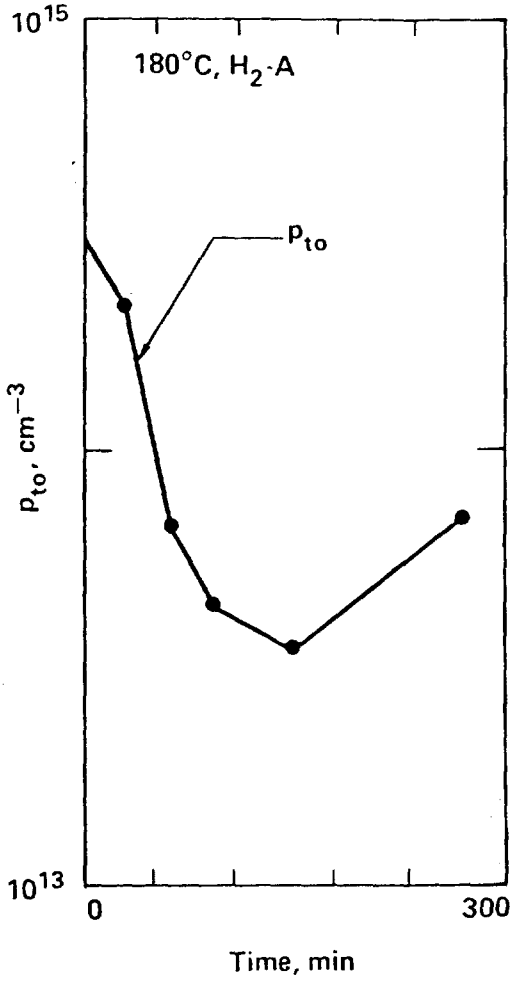

Fig. 4. The equilibrium concentration of holes in traps as a function of 180°C, hydrogen-argon heat treatment time as determined for single crystal sample A using the approximate, multi-trap theory and the Fig. 3 forward bias data.

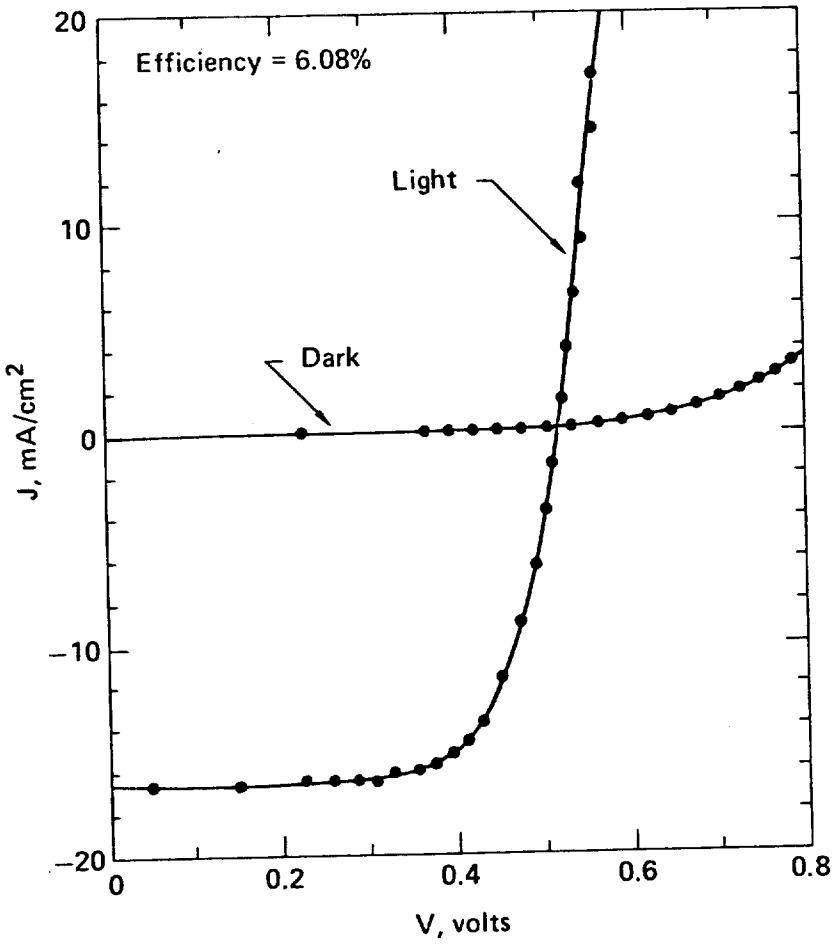

Fig. 5. The approximate, multi-trap model fit of the dark-light cross over characteristics of polycrystalline sample #2. Solid curves are theory and data points are measured values.

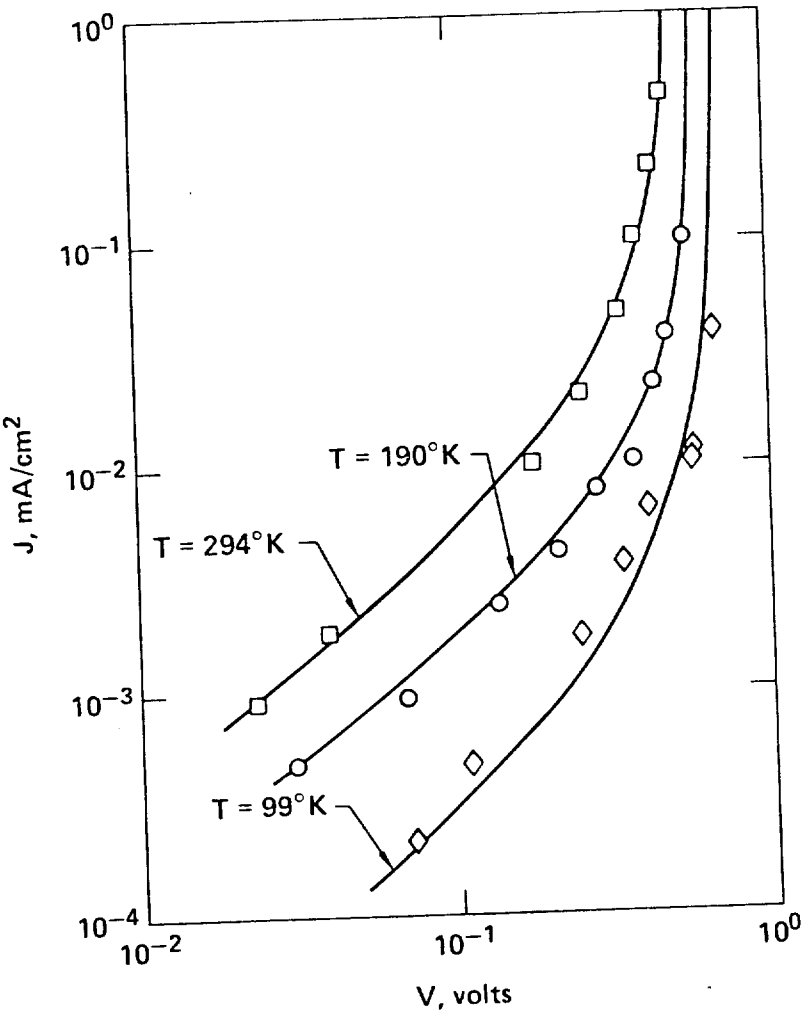

Fig. 6. The exact, single trap model fit for the temperature dependent J-V characteristics of polycrystalline sample #1. Solid curves give the theory and data points are the measured values.

Section III A.2

SPACE CHARGE LIMITED CURRENT AND CAPACITANCE IN Cu_xS/CdS HETEROJUNCTION SOLAR CELLS*

Ravi Moorthy**
Electrical Engineering Department
University of Delaware
Newark, Delaware 19711

and

Larry Partain
Lawrence Livermore Laboratory
Livermore, California 94550

This Paper was Prepared for Submittal to
the Physical Review B†

---

*Work performed in part under the auspices of the U.S. Department of Energy by the Lawrence Livermore Laboratory under contract number W-7405-ENG-48.

**Presently with W. L. Gore and Associates Inc. Newark, Delaware 19711

Abstract

A quantitative treatment is given for charge transport in P-N heterojunctions that is controlled by mechanisms and relationships different from those widely used to describe such junction behavior. The model, based on space-charge-limited (SCL) current, has been used to provide the first quantitative explanation for the gross electrical properties of thin film, polycrystalline Cu_xS/CdS heterojunction solar cells which are characterized by non-exponential J-V properties and by cross over of their dark and light J-V curves. Fitting parameter values of $6(10^{14})/cm^3$ trap density located at 0.442 eV below the conduction band in a Cu compensated region of CdS $1.33(10^{-4})$ cm thick for free electron concentrations in the $6(10^9)$ to $2(10^{10})/cm^3$ range and mobilities in the 10 to 30 cm^2/V-sec range are consistent with other reported values SCL current in polycrystalline CdS. A transient technique allowed small signal capacitance to be measured in high forward bias near the trap-filled-limit where anticipated capacitance variations were found to agree with prior measurements of SCL current in CdS.

I. INTRODUCTION

The Cu_xS/CdS heterojunction solar cell was first reported about 25 years ago (1). The subsequent development of low cost fabrication processes for thin-film, polycrystalline forms of this device (2,3) coupled with recently demonstrated conversion efficiencies exceeding 9 percent for polycrystalline cells (4) demonstrate the strong potential this structure has for large scale conversion of sunlight into electricity (5). Despite this long period of attention, consistent quantitative models have not yet been developed to describe some of the gross electrical properties of these devices. In particular, the non-exponential dependence of current on voltage and the cross-over (2) of the dark and light I-V curves have proven quite difficult to explain. The models proposed so far have either concentrated on just the illuminated characteristics (6) or just the dark characteristics (7,8) or have presented only qualitative descriptions of the observed behavior (9-14). The more quantitative theories have not made direct comparisons to experimental data (15) or have been restricted to limited ranges of current and voltage (13,16,17) or have limited themselves to basic phenomena like quantum efficiency (18), photocapacitance (19), short circuit current (20), spectral response (21) or interface recombination (22) that are not easily related to both current and voltage. The recent

tunneling model (8) does quantitatively fit current-voltage data in the dark as a function of temperature for a limited voltage range. Unfortunately it is still qualitative to the extent that the critical transport coefficients are only empirically determined without being related to known material properties through existing detailed models such as Crowell and Rideout's thermionic field emission theory (23). When such analysis is applied to single step tunneling processes, the magnitude of the tunneling current is found to be too small to make significant contributions to total heterojunction current (24). Multi-step tunneling analysis of Cu_xS/CdS cells has given qualitative agreement but only over limited voltage ranges and only in the dark (7).

Several workers have briefly mentioned that space-charge-limited (SCL) current could be involved in the dark I-V properties of these solar cells (6,9,25). The purpose of this paper is to explore the usefulness of modeling the dark and light exposed electrical properties of Cu_xS/CdS heterojunctions with a SCL current model. The theoretical model of the present work is an elaboration and extension of the SCL analysis initiated by Warter (26). SCL currents are well known in high resistivity CdS (27). The diffusion of copper from the Cu_xS layer into the CdS during heat treatment to form a high resistance layer is also well known (28,29). Heat treatment is a necessary step in the fabri-

cation of high efficiency, polycrystalline cells (2,3,6-10). In Section II, the known theory for the voltage dependence of SCL current and capacitance is reviewed. Capacitance is included because C-V techniques are well known for their ability to probe the degree of compensation of the space-charge-region (SCR) of P-N heterojunctions which can be modeled by standard junction theory (30). Section III presents a comparison between the SCL theory and experimental data on a polycrystalline, thin-film Cu_xS/CdS solar cell. Comparisons to other relevant experimental results are also made. An evaluation of this approach is summarized in Section IV.

II. THEORY

In this section, a rigorous analytical model of SCL phenomena is given for the single trapping level case and approximate expressions are given for multiple trapping level cases. Also a technique is described that allows small-signal capacitance measurements at high forward bias voltages.

Lampert and Mark (31) have given closed form expressions for the voltage (V) dependence of the current density (J) through a homogeneous planar slab of semiconducting material of width L containing densities n_o and N_t respectively of equilibrium conduction electron concentration and trap

concentration where the N_t are located an energy $E_c - E_t$ away from the conduction band. With electron injecting, Ohmic contacts attached at each side of the slab, this is given in parametric form as

$$V = \frac{n_o e L^2}{\epsilon} \frac{y(u)}{w^2(u)} \tag{1}$$

$$J = \frac{n_o^2 e^2 \mu L}{\epsilon} \frac{1}{w(u)} \tag{2}$$

where

$$y(u) = -\frac{C}{2G} u^2 - \left[\frac{C+1}{G+1} + \frac{G-C}{G^2(G+1)}\right] u - \frac{C+1}{G+1} \log(1-u) + \frac{G-C}{G^3(G+1)} \log(1+Gu) \tag{3}$$

$$w(u) = -\frac{C}{G} u - \frac{1+C}{1+G} \log(1-u) + \frac{G-C}{G^2(G+1)} \log(1+Gu) \tag{4}$$

and

$$B = N_t/n_o \tag{5}$$

$$C = \frac{2}{n_o} \left(\frac{2\Pi m^* KT}{h^2}\right)^{3/2} e^{-\frac{E_c - E_t}{KT}} \tag{6}$$

$$G = C + \frac{BC}{1+C} \tag{7}$$

$$u = n_o/n(L). \tag{8}$$

Here e is the electronic charge, ϵ is the dielectric constant, μ is the electron drift mobility, and n(L) is the non-equilibrium conduction electron concentration at the side of the slab opposite the electron injecting, cathode contact. The K is Boltzmann's constant, T is the absolute temperature, m* is the density of states effective mass, and h is Planck's constant. This solution involves the standard SCL current theory assumptions of negligible diffusion current, field independent mobility and a negligible separation distance between the zero electric field point (the virtual cathode) and the actual cathode.

For the single-trap case, the theory predicts that at voltage values approaching a magnitude termed the trap-filled limit (TFL), the current will rise essentially vertically toward the trap-free insulator values (31). If multiple trap levels or a distribution of trap levels is involved, the rate of rise is decreased (27,31) to less than infinity but at a steep rate empirically observed to be approximated by

$$J \propto V^m \qquad (9)$$

where $m > 2$ and where the transition voltage V_{TFL} from Ohmic to TFL is approximately specified by (31)

$$V_{TFL} \cong \frac{eL^2}{\epsilon} p_{to} \tag{10}$$

where p_{to} is the equilibrium concentration of holes in the electron traps. Of course, at the low voltage values in the Ohmic region

$$J = \frac{n_o e \mu V}{L} . \tag{11}$$

These Eqs. 9-11 will be referred to as the simplified, multi-trap model. No exact, closed-form, analytic expressions have been found for the multi-trap case.

Under SCL current conditions, the small-signal a.c. capacitance C is given by (31)

$$C = \frac{3\epsilon A}{2L} \tag{12}$$

for regions where J is proportional to V^2 and where A is the cross-sectional area of the device. In regions where J rises much more steeply with V than square law, no analytic expressions for C have been derived. In such steep regions, the traps become filled (32) so that incremental increases in current result in little incremental storage of charge in the traps so that very little increase in terminal voltage

is observed. Under such trap-filled-limit conditions, it is reasonable to expect C to differ in value from Eq. 12.

With forward biased diodes, the in-phase current is so large compared to the quadrature (capacitive) current that ac techniques no longer give accurate capacitance values. For this forward bias condition of interest in this study, the following alternate technique is proposed for small signal capacitance determination. The standard small signal equivalent circuit for the capacitance C of a reversed biased junction is generalized to forward bias by the addition of the shorting resistance R_N as shown in Fig. 1. For generality let R_N be non-linear and consider both C and R_N to be single valued functions of the applied voltage V. To account for the transient effects well known in SCL current conditions (31), time dependence is also included to give C(V,t) and $R_N(V,t)$. Different dc bias conditions are obtained by connecting the device in series with a variable dc bias voltage V_B and variable bias resistance R_B like in Fig. 1a. If this bias is applied for a sufficiently long time, a constant, steady state current of I(0-) will flow through the device. At time t equal 0, the switch S is opened with no instantaneous change in the voltage V_o measured across the device relative to ground but with a current $I_o(0+)$

flowing to discharge C as shown in Fig. 1b. Since R_N is a single valued function of V, the current immediately preceding the switch opening I(0-) must equal that immediately following the switch opening. Observing the transient decay of $V_o(t)$ then allows the small signal C to be determined by

$$C = \left| \frac{I(0+)}{dV_o/dt\big|_{t=0}} \right| = \left| \frac{I(0-)}{dV_o/dt\big|_{t=0}} \right| \qquad (13)$$

as long as dV_o/dt is measured over small voltage excursions and small time periods compared to any transient time constants so that all the elements of the circuit can be approximated with linear, time-invariant values. Since $V_o(t)$ and I(0-) are directly observable, this provides a useful measurement technique whose accuracy is undeminished by large current values. As long as the series resistance remains low, this equivalent circuit treatment is general enough to handle the capacitance behavior of a standard P-N junction depletion region or the charge storage behavior of a space-charge-limited current region.

III. RESULTS AND DISCUSSION

The experimental sample was fabricated by the Institute of Energy Conversion, University of Delaware by vacuum depositing approximately 25 microns of n-type CdS unto a zinc

plated, copper substrate to form a polycrystalline CdS layer. The sample was etched in HCl and then dipped for a few seconds into a 90°C CuCl solution to form a p-type Cu_xS layer on the order of 1000-2000 angstroms thick. A 15 hour heat treatment at 170° C in hydrogen-argon gas followed. The sample was cut into a square of 3.80 cm^2 area and a gold-plated copper grid and mylar plastic cover were attached to the Cu_xS with epoxy by clamping the sandwich of materials into a vacuum hydraulic press for 0.5 hour at 190° C. A final treatment for one hour at 170° C in hydrogen-argon produced a cell whose dark and light I-V properties are as shown by the data points in Fig. 2. In a simulated, air-mass-one intensity of 100 mW/cm^2, the light exposed measurements gave an open circuit voltage of 0.512 V, a fill factor of 0.699, a short-circuit current density of 17.0 mA/cm^2, and a conversion efficiency of 6.08 percent. The light entering through the Cu_xS is strongly attenuated before reaching the CdS because of the high Cu_xS absorption constant (33). The current density and capacitance per unit area were obtained by dividing actual current and capacitance by the 3.80 cm^2 square area with no correction for surface roughness that makes the actual cell area larger than its projected 3.80 cm^2 value. The J-V data was obtained with an

X-Y plotter and representative values are given by the Fig. 2 data points.

The transient capacitance measurements were all made in the dark with the circuit of Fig. 3 using the electronic switch of Fig. 4. A square wave input voltage waveform of 400 Hz repetition rate caused the switch to open for the positive part of the applied input voltage. The desired current values were obtained by adjusting the applied dc voltage. The current I(0-) was obtained by measuring the amplitude of the voltage across a test resistor R_T during the "on" condition. The transient voltage V_o (t) and the voltage across R_T was processed by a Tektronix Model 5A22N differential amplifier with variable dc voltage offset before being fed into a Princeton Applied Research Model 162, box-car averager and then into a Hewlett-Packard Model 7044A X-Y recorder. This circuit was used for both forward and reverse bias measurements. Comparative reverse bias capacitance values were obtained with a Hewlett-Packard Model 4270A automatic capacitance bridge that utilized a 100 KHz sinusoidal test voltage. Repeatability was improved for the forward bias, transient capacitance measurements by leaving the square wave signal applied to the sample at the highest value of forward bias "on" voltage of interest for 24 hours before data was taken. Measurement at d.c. bias voltages below

this maximum were then obtained at approximate 10 minute intervals for monotonically decreasing bias values into the reverse bias region.

If the J-V data of Fig. 2 are replotted on a log-log scale, the dependence shown in Fig. 5 is obtained. For convenience, the light generated, short circuit current density J_L has been added to the light data to make it pass through zero when V equals 0. The fit of this data by the analytic, single trap theory of Eqs. 1 and 2 for the parameter values given in Table I are shown by the solid line curves assuming that the light generated, short circuit current J_L is superimposed on the SCL limited current. The L value was obtained using Eq. 12 and the measured value (given below) of device capacitance in the dark at a forward bias of 0.276 volts assuming a high resistivity CdS layer formed by Cu diffusion. The increase of mobility and carrier concentration with exposure to 100 mW/cm^2 white light indicated in Table I compares well to the absolute values of the increase in μ of from 1.0 to 10 $cm^2/V\text{-sec}$ and to the factor of three relative increase in n_o of from $3(10^{15})$ to $10^{16}/cm^3$ after exposure to 50 mW/cm^2 white light reported by Wu and Bube(34) for copper compensated, polycrystalline CdS formed by vacuum deposition.

Such an increase in μ with light has been widely reported for copper doped CdS formed by vacuum evaporation (35,36). The trap density and electron mobility values reported here also compare well to the $2.5(10^{14})$ traps/cm^3 and 18 cm^2/V-sec respectively reported by Pizzarello (37) for SCL current in high resistivity polycrystalline CdS films formed by vacuum deposition. These polycrystalline trap densities are about an order of magnitude higher than those reported by Marlor and Woods (38) and by Bube (39) for single crystal CdS. The energy location of the traps in the band gap is consistent with the 0.4 and 0.5 eV range reported for CdS single crystals (38,39). The dark resistivity in the 10^8 ohm-cm range specified by n_o and μ are typical of the higher values reported in polycrystalline CdS films in which SCL current has been observed (40,41). This fit indicates that the cross-over phenomena is well modeled by light causing a factor of three increase in the conduction electron concentration at low voltages (in the Ohmic region) and by a similar increase in electron mobility through these parameters' influence on V_{TFL} as described by Eqs. 1 and 2. Presumably the light removes some charge from scattering centers or modifies the barrier height around the grain boundaries (35,36,42) so that mobility is increased. To the best of our knowledge this is the first theoretical model that quantitatively fits the dark and light J-V characteristics of Cu_xS/CdS solar cells for reasonable parameter values.

From Fig. 5, note that current rises rapidly for the higher V values. The slopes approach straight lines with high m values but with lower magnitudes than specified by the near vertical dependence of the solid line curves of the single trap theory. The fit of these data with the approximate theory of Eqs. 9-11 and the parameter values of Table II are shown by the solid line curves in Fig. 2. Again the light generated current was assumed to superimpose on the SCL current. The V_{TFL} values were obtained by the intersection of two straight lines in log-log plots like Fig. 5. One line is determined by the high voltage data asymptotically approaching a straight line. The other line had unity log-log slope and passes through the lowest voltage data point assumed to lie in the Ohmic region. The L value was taken from measured capacitance as described above. The mobility values were taken from Table I so that n_o values could be obtained from Eq. 11 using the lowest voltage data point assumed to lie in the Ohmic range. The p_{to} values are consistent with the Table I results, since they are less than the N_t concentration. The approximate multi-trap n_o values are on the same order of magnitude as the single level theory values of Table I. The rate of current rise with voltage implied by the m values are consistent with the rises observed experimentally in polycrystalline and single crystal CdS samples that exhibit SCL current (32,39,41). Note the agreement with the m values of 5 to 7 reported by McGarthy and Yee for Cu compensated, single crystal CdS in the dark (43).

A typical transient voltage waveform $V_o(t)$ used to determine C values is shown in Fig. 6 for the case of "on" voltage of 0.276 V forward bias and I(0-) of 0.633 mA. After about 0.5 microsecond of switching transient following the switch opening at about 3 microseconds, the curve settles into a well behaved decay transient with a $dV/dt\Big|_{t=0}$ value of $1.55(10^4)$ V/sec as indicated by the broken straight line which specifies a capacitance per unit area of 10.7 nf/cm^2. Since heat treatment is an important fabrication step, the transient capacitance values were taken as a function of heat treatment in addition to the fabrication heat treatment described earlier. This additional heating was performed in air at 180°C. The Fig. 6 data is for zero additional treatment. The measured variation of capacitance with the dc bias "on" voltage is shown in Figs. 7 and 8 as a function of additional heat treatments of from 0 to 170 minutes. Note that a relatively constant value is found until dc bias voltages in the 0.3 to 0.4 forward range are reached. At that point a persistent drop with increasing voltage is seen that goes through a maximum after 40 minutes of additonal air heat treatment. Such a decrease in capacitance with increasing bias voltage is not consistent with standard P-N junction models of junction capacitance (30). However, a capacitance anomaly is anticipated for SCL current at bias voltages

approaching the TFL in the 0.3 volt range such as indicated by the dark data in Fig. 5. A similar drop in capacitance with increasing forward bias has been reported by Dresner and Shallcross (40) in vacuum deposited, polycrystalline CdS of high resistivity to which a Te Schottky barrier contact and an Au Ohmic contact had been applied. They apparently also used some type of square-wave modulation measuring technique but of an unspecified form. As with the present data, their drop corresponded to the part of the J-V curve where the observed SCL current approached the TFL. These results are also consistent with the experimental data of Ruppel (44) on high resistivity CdS single crystals that showed the rate of change of charge storage in the samples goes through a minimum at voltages where the J-V curve approaches the trap filled limit. Since $C \propto dQ/dV$, a sharp drop in small signal capacitance is thus also indicated. Calculating an L value from Sullivan's data (29) for the diffusion constant D(T) of substitutional copper in CdS as a function of temperature T specifies

$$L^2 \simeq \sum_i D(T_i)\Delta t_i \qquad (14)$$

where Δt_i is the heat treatment time spent at temperature T_i. For the original fabrication heat treatments (no additional air heat treatment), this gives an L value of $4(10^{-5})$ cm within a factor of three of the L value obtained from

the measured C values as listed in Tables I and II.

For consistency, the reverse bias capacitance was also measured using a sinusoidal voltage capacitance bridge after 30 and 170 minutes of additional air heat treatment as shown by the solid lines and square data points in Fig. 9. For comparison, the transient measured values are shown as the diamond shaped data points. Under reverse bias, the a.c. bridge has the higher accuracy. The transient data scatter about this a.c. data gives a measure of the experimental error for the transient technique of less than 20 percent.

For the reverse biased case, the efficient electron-injecting contact required for space-charge-limited current (31) is of course no longer present so that standard p-n junction capacitance behavior occurs as has been well established experimentally (45-47). Plotting the a.c. data of Fig. 9 as $1/C^2$ versus voltages shows a slight slope to the data that specifies a CdS carrier concentration (the Cu_xS is degenerate) of about $10^{17}/cm^3$. Using this with Wu and Bube's mobility values (34) then gives resistivities in the 1 to 10 ohm-cm range typically measured on the CdS films.

IV. SUMMARY AND CONCLUSIONS

The purpose of this study was to evaluate SCL current theory

as a model of the gross electrical behavior of Cu_xS/CdS heterojunctions. An analytic, single trap theory gives a reasonable fit for the logarithmic variation of J and V using parameter values well known to be characteristic of SCL current in CdS. The cross-over is quantitatively explained by a three-fold increase in conduction electron concentration and mobility upon exposure to light as widely reported in the literature for evaporated CdS films. The non-infinite slopes of log J - log V past the TFL indicated multiple traps are present. A simplified, multi-trap theory provided an excellent fit of the linear J-V data in the dark and in the light with parameter values consistent with the single trap theory results. This provides the first theory to quantitatively model the dark and light cross-over phenomena and the non-exponential dependence of J on V for reasonable parameter values to the best of our knowledge. These results are consistent with the non-exponential J-V properties reported by Riben and Feucht for another heterojunction structure (24).

The development of a transient technique allowed capacitance to be measured at high forward biases. Anticipated changes in capacitance were found at forward bias voltages approaching the TFL and of a form consistent with prior measurements in CdS. Time intervals of microseconds and voltage excursions

of hundredths of a volt appeared to be small enough so that the linear, time invariant expressions for capacitance gave useful results. The J-V properties of Cu_xS/CdS heterojunctions have been known for years (2,3). It was the unique behavior of the forward bias capacitance as reported here for the first time that provided new evidence of the inadequacy of standard P-N junction models and that motivated the pursuit of the alternate SCL current model. The analytic, single trap expressions for J and V were found to be very useful for modeling the observed behavior. Because of their parametric form, some care had to be exercised in selecting the $n(L)/n_o$ parameter values. Figure 10 shows how J varied with the rather non-obvious range of $n(L)/n_o$ values used to provide the fit of the light exposed J-V data in Fig. 5. Perhaps it is this difficulty in specifying this parameter range that led Lampert and Mark (31) to describe these analytic expressions as "unwieldy and of correspondingly limited practical significance."

The superposition of the light generated, short-circuit current J_L on the SCL current provided a surprisingly good fit of the data. Such superposition had not been anticipated because of the complex mechanisms proposed for minority carrier collection at Cu_xS/CdS junction regions (48,49,50) However, such superposition of light generated current on

dark current is routinely observed in simpler heterojunctions and homojunctions (30). Apparently, the heat treatment process drives copper from the Cu_xS into the CdS to form a high resistance layer that lowers the forward current tending to short out the light generated reverse current at forward bias voltages. By processes that have yet to be explained, this insulating region does not appear to seriously reduce the minority carrier collection. This effect, if verified by further studies, would be similar to the beneficial influence claimed for the insulating region in MIS solar cells (51,52). The voltage dependence of capacitance reported here has some similarity to that reported on MIS devices (53).

Current rectification with Ohmic contacts to an insulating SCL current region is not expected (27,31). However, the rectifying properties of Cu_xS/CdS devices with SCL current for forward bias, is similar to that widely reported for a Schottky barrier and an Ohmic contact to polycrystalline, thin-film (40,54,55) and to single crystal CdS (56).

This study indicates that the transport in heat treated, Cu_xS/CdS heterojunctions is dominated by space-charge-limited current mechanisms and relationships that differ sharply from the thermionic-emission-over-a-barrier, the

tunneling mechanisms, or the diffusion-limited transport typically used to describe such heterojunctions(30). Furthermore SCL current behavior has been reported for a P-N heterojunction formed on n-type ZnSe with either a GaAs (57) or a Ge (58) p-type layer. The high resistance ZnSe layer next to the junction in these devices gave the characteristic logarithmic dependence of current on voltage rather than exponential behavior. Exposure to light for the GaAs sample gave a photovoltaic effect with obvious cross-over (48) like reported here for Cu_xS/CdS as shown in Fig. 2. This ZnSe work was not described by a quantitative theory such as Eqs. 1 and 2 and thus did not give direct comparisons of theory to experiment nor specify the energy band location of the traps as given by the present work.

ACKNOWLEDGMENTS

This work was part of a thesis submitted by R. Moorthy to the University of Delaware in partial fulfillment of the requirements for the Master of Electrical Engineering Degree in 1979. Helpful interactions with A. Rose and G. Warfield on the concepts of SCL current are gratefully recognized. Arrangements through J. D. Meakin for the sample fabrication and the current-voltage measurements by the Institute of Energy Conversion is acknowledged. Assistance with the ac

capacitance measurements by C. Wyeth and G. Storti was greatly appreciated. Discussion with J. Kramer on Cu diffusion were most helpful. Use of unpublished confirming data measured by G. Armantrout on Cu_xS/CdS was of crucial assistance. Discussion of various transport processes with J. Yee was very useful. Help with the electronic switch design by C.Ih was greatly appreciated.

Table I The parameter values used in the analytic, single trap theory to fit the experiment data as shown in Fig. 5

n_o (Dark)	$6(10^9)/cm^3$
(Light)	$2(10^{10})/cm^3$
μ(Dark)	10 cm^2/V-sec
(Light)	30 cm^2/V-sec
N_t	$6(10^{14})/cm^3$
E_c-E_t	0.442 eV
L	$1.33(10^{-4})$ cm
ϵ/ϵ_o	10
m^*/m_o	0.2
T	294°K

Table II The parameter values used in the approximate, multi-trap theory to fit the experimental data as shown in Fig 2.

	Dark	Light
$V_{TFL}(V)$	.43	.33
$p_{to}(cm^{-3})$	$1.03(10^{14})$	$1.34(10^{14})$
m	5.6	9.0
$n_o(cm^{-3})$	$2.32(10^{10})$	$2.77(10^{10})$
$\mu(cm^2/V\text{-}sec)$	10	30
L(cm)	$1.33(10^{-4})$	$1.33(10^{-4})$
ϵ/ϵ_o	10	10

REFERENCES

1. D. C. Reynolds, G. Leies, L. L. Antes, and R. E. Marburger, Phys. Rev. 96, 533 (1954).

2. A. E. Middleton, D. A. Gorski, and F. A. Shirland in Energy Conversion for Space Power, Progress in Astronautics and Rocketry, N. W. Snyder Ed. (Academic Press, New York, 1961) p. 275.

3. F. A. Shirland, Advanced Energy Conversion 6, 201 (1966).

4. A. M. Barnett, J. A. Bragagnolo, R. B. Hall, J. E. Phillips, and J. D. Meakin, 13th IEEE Photovoltaic Specialists Conference Record, Washington, D.C., June 1978, p. 419.

5. L. D. Partain and M. M. Sayed, in Hydrogen Energy, T. N. Veziroglu, Ed. (Plenum, New York, 1975), Part A, p. 45.

6. A. Rothwarf, International Conference on Solar Energy, Toulouse, France, March 1976.

7. S. Martinuzzi and O. Mallem, Phys. Stat. Sol. (A) 16, 339 (1973).

8. A. Amith, J. Appl. Phys. 50, 1160 (1979).

9. L. R. Shiozawa, F. Augustine, G. A. Sullivan, J. M. Smith III and W. R. Cook, Aerospace Research Laboratories Report No. ARL 69-0155, Clevite Corporation, October 1969.

10. L. R. Shiozawa, G. A. Sullivan, and F. Augustine, 7th IEEE Photovoltaic Specialists Conf., Nov. 1968, p. 39, also appears in Solar Cells, C. E. Backus, Ed. (IEEE Press, NY, 1976), p. 231.

11. A. E. van Aerschodt, J. J. Capart, K. H. David, M. Fabbricotti, K. H. Heffels, J. J. Loferski, and K. K. Reinhartz, IEEE Trans. Electron Devices ED-18, 471 (1971).

12. T. S. Te Velde, Solid-State Electronics 16, 1305 (1973).

13. P. N. Keating, J. Phys. Chem. Solids 24, 1101 (1963).

14. P. Massicot, Phys. Stat. Sol. A11, 531 (1972).

15. A. Rothwarf, Intern. Workshop on Cadmium Sulfide Solar Cells and Other Abrupt Heterojunctions, Newark, DE, April 1975, p. 9.

16. A. Rothwarf and R. W. Boer, Progress in Solid-State Chemistry 10, Part 2, 71 (1975).

17. K. W. Boer, J. Appl. Phys. 50, 5356, (1979).

18. R. J. Mytton, Brit. J. Appl. Phys. D, 1, 721 (1968).

19. W. D. Gill and R. H. Bube, J. Appl. Phys. 41, 3731 (1970).

20. A. L. Fahrenbruch and R. H. Bube, J. Appl. Phys. 45, 1264 (1974).

21. B. G. Caswell, G. J. Russell, and J. Woods, J. Phys. D, Appl. Phys. 8, 1889 (1975).

22. A. Rothwarf, J. Phillips, and N. C. Wyeth, 13th IEEE Photovoltaic Specialists Conference Record, Washington, D.C., June 1978, p. 399.

23. C. R. Crowell and V. L. Rideout, Solid-State Electronics 12, 89 (1969).

24. A. R. Riben and D. L. Feucht, Solid-State Electronics 9, 1055 (1966).

25. R. R. Bockemuehl, J. E. Kauppila, and D. S. Eddy, J. Appl. Phys. 32, 1324 (1961).

26. P. J. Warter, S. P. Shea and L. D. Partain, Bulletin American Physical Soc. 24, 273 (1979).

27. A. Rose, Concepts in Photoconductivity and Allied Problems (Wiley, New York, 1963).

28. R. K. Purohit, B. L. Sharma, and A. K. Sreedhar, J. Appl. Phys. 40, 4677 (1969).

29. G. A. Sullivan, Phys. Rev. 184, 796 (1969).

30. A. G. Milnes and D. L. Feucht, Heterojunctions and Metal-Semiconductor Junctions (Academic Press, New York, 1972).

31. M. A. Lampert and P. Mark, Current Injection in Solids (Academic Press, New York, 1970).

32. M. A. Lampert, A. Rose, and R. W. Smith, J. Phys. Chem. Solids 8, 464 (1959).

33. B. J. Mulder, Phys. Stat. Sol. A18, 633 (1973).

34. C. Wu and R. H. Bube, J. App. Phys. 45, 648 (1974).

35. I. A. Karpovich and B. N. Zvonkov, Soviet Physics - Solid State 6, 2714 (1965).

36. J. Dresner and F. V. Shallcross, J. Appl. Phys. 34, 2390 (1963).

37. F. A. Pizzarello, J. Appl. Phys. 35, 2730 (1964).

38. G. A. Marlor and J. Woods, Brit. J. Appl. Phys. 16, 1449 (1965).

39. R. H. Bube, J. Appl. Phys. 33, 1733 (1962).

40. J. Dresner and F. V. Shallcross, Solid-State Electronics 5, 205 (1962).

41. K. V. Shalimova, L. P. Pavlov, and R. R. Rezuyi, Soviet Physics - Solid State 6, 1749 (1965).

42. R. H. Bube and H. E. MacDonald, Phys. Rev. 121, 473 (1961).

43. S. J. McGarthy and S. S. Yee, Solid State Electronics 17, 485 (1974).

44. W. Ruppel, J. Phys. Chem. Solids 22, 199 (1961).

45. H. W. Brandhorst, Jr., 7th IEEE Photovoltaic Specialists Conf. Record, Pasadena, Nov. 1968, p. 33.

46. J. Lindmayer and A. G. Revesz, Solid-State Electronics 14, 647 (1971).

47. S. R. Das, A. Banerjee, and K. L. Chopra, Solid-State Electronics 22, 533 (1979).

48. A. Rothwarf, 13th IEEE Photovoltaic Specialists Conference Record, Washington, D.C., June 1978, p. 1312.

49. F. A. Lindholm, J. G. Fossum, and E. L. Burgess, IEEE Trans. Electron Devices ED-26, 165 (1979).

50. L. D. Partain and S. P. Shea, International Electron Devices Meeting Technical Digest, Washington, D.C., December 1978, p. 239.

51. R. J. Stirn and Y. M. Yeh, 11th IEEE Photovoltaic Specialists Conference Record, Scottsdale, Ariz., May 1975, p. 437.

52. H. C. Card and E. S. Yang, Appl. Phys. Lett. 29, 51 (1976).

53. S. Kar and W. E. Dahlke, Solid-State Electronics 15, 221 (1972).

54. R. Zuleeg, Solid State Electronics 6, 645 (1963).

55. G. T. Wright, Proc. IEEE 51, 1642 (1963).

56. R. S. Muller, J. Appl. Phys. 34, 2401 (1963).

57. J. W. Balch and W. W. Anderson, Phys. Stat. Sol. A9, 567 (1972).

58. H. J. Hovel and A. G. Milnes, Int. J. Electronics 25, 201 (1968).

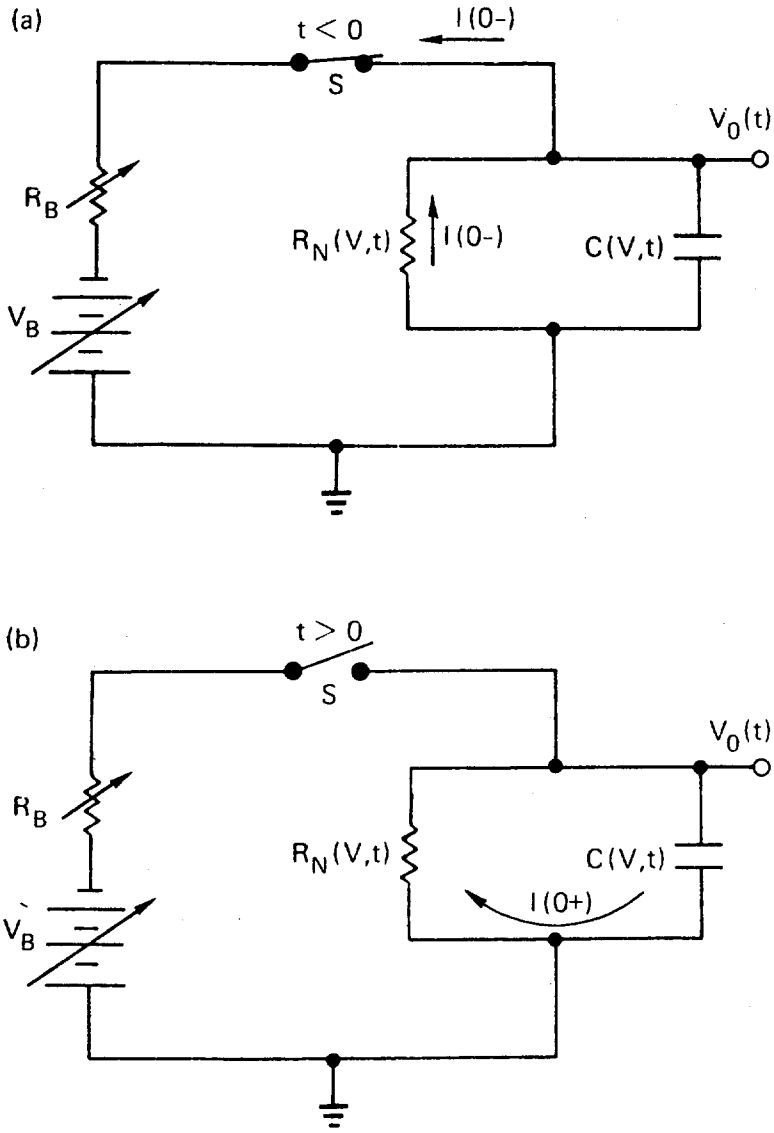

Fig. 1 Equivalent circuit for the transient capacitance measurement for a) the switch closed for $t < 0$ and b) the switch open for $t > 0$.

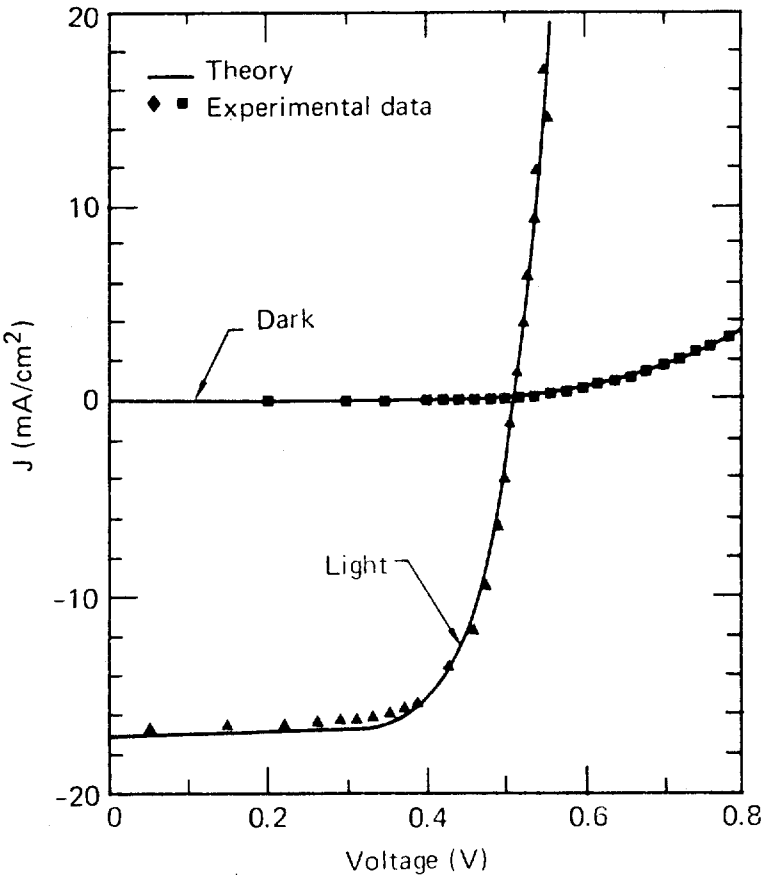

Fig. 2. The current density as a function of voltage for a dark and light exposed device. Data points are experimentally measured. Solid curves are the approximate, multi-trap theory.

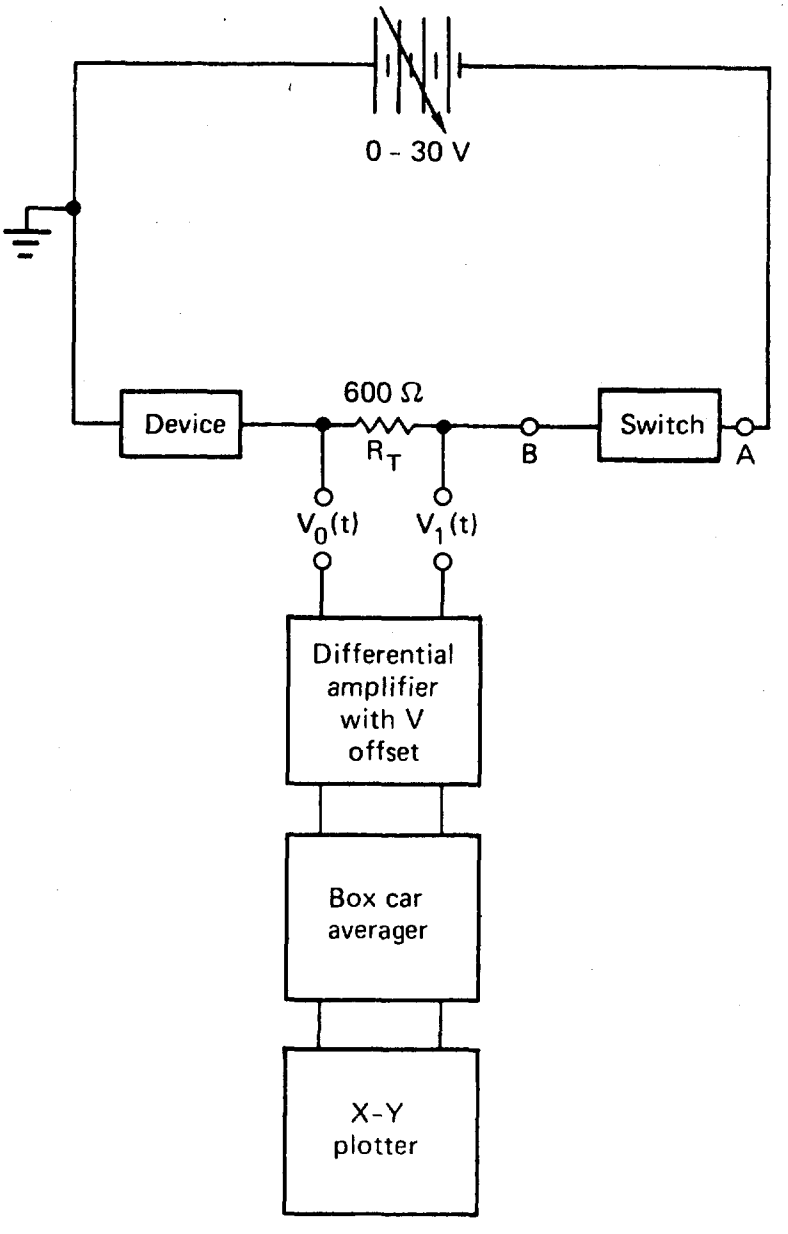

Fig. 3. Circuit diagram for the components used to make the transient measurements of capacitance.

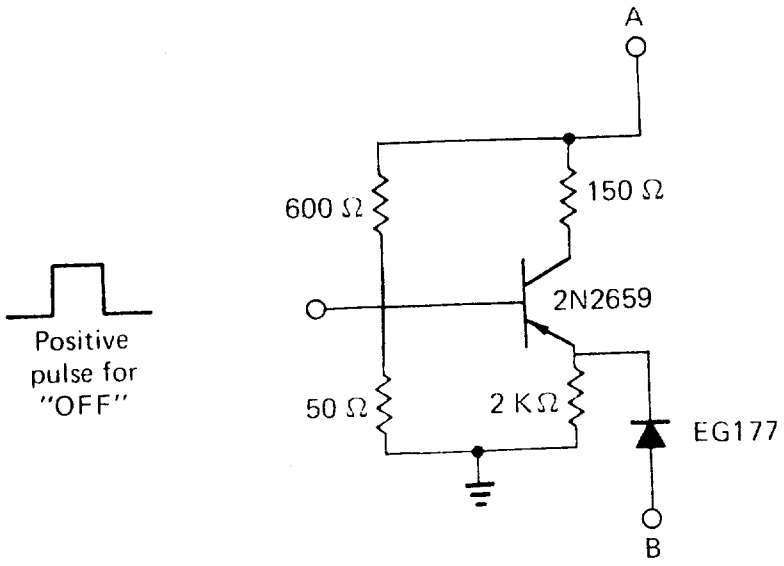

Fig. 4. Electronic switch used to open and close the circuit for the transient measurement of capacitance.

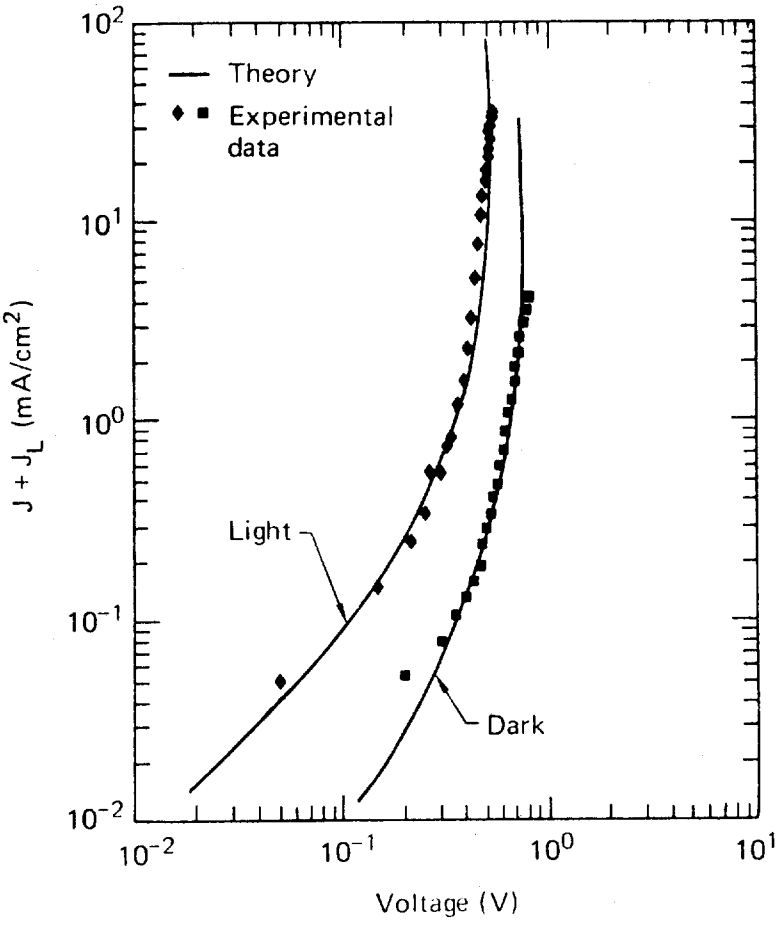

Fig. 5. Logaritmic plot of the current density-voltage characteristics. Data points were experimentally measured. Solid curves are from the analytic, single trap theory.

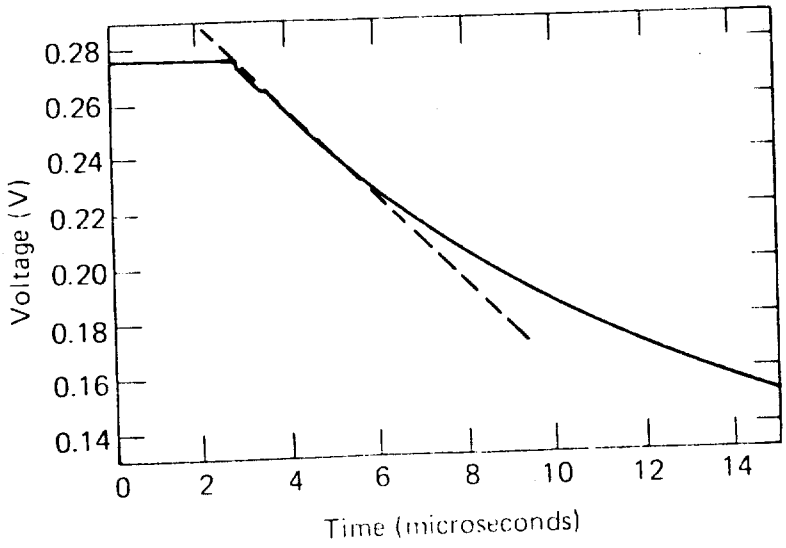

Fig. 6. Typical transient voltage waveform used to determine capacitance. This data was obtained for I(0-) = 0.633 mA, "on" voltage of 0.276 V, and 0 additional air heat treatment. The dashed line indicates the slope used for calculations.

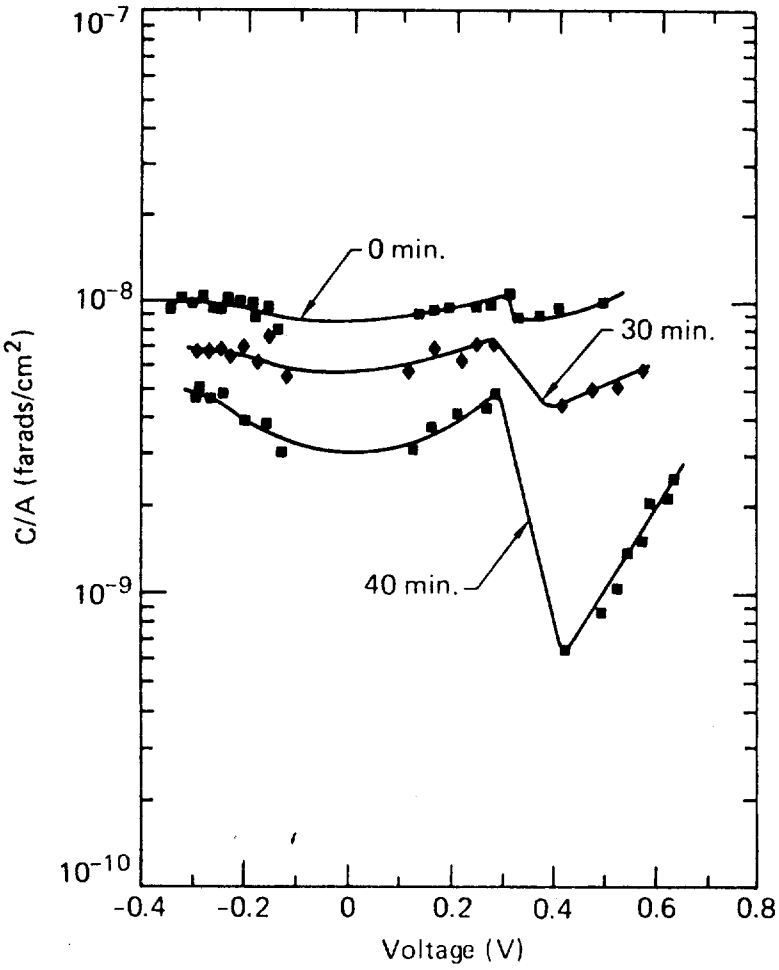

Fig. 7. Small signal capacitance per unit area as a function of the dc bias "on" voltage for additional air heat treatments of from 0 to 40 minutes at 180°C.

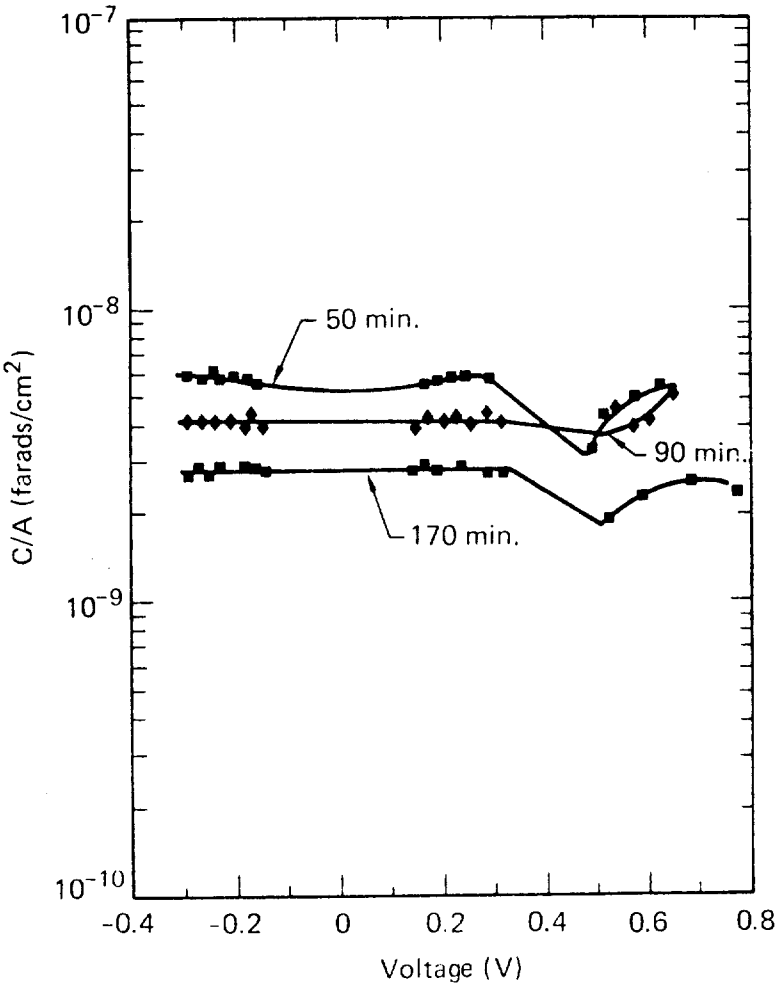

Fig. 8. Small signal capacitance per unit area as a function of the dc bias "on" voltage for additional air heat treatments of from 50 to 170 minutes at 180°C.

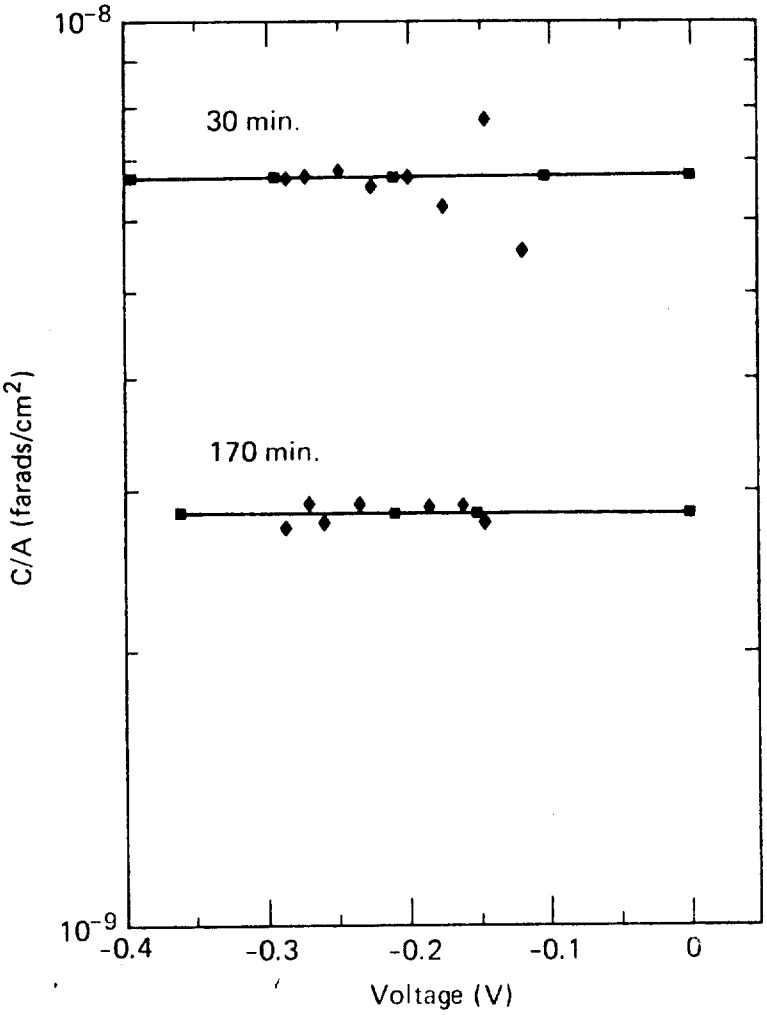

Fig. 9. Comparison of reverse bias capacitance values as a function of dc bias voltage obtained with an ac bridge (solid lines and square data points) and with the transient technique (diamond data points).

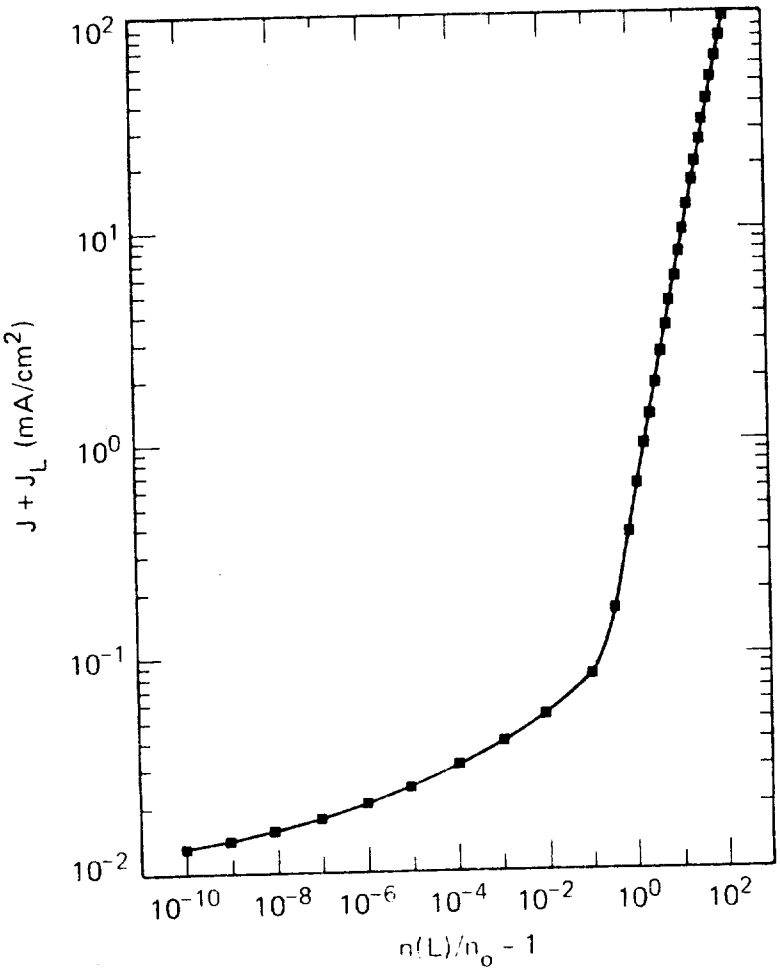

Fig. 10. Plot of the Eq. 2 expression for current density as a function of $n(L)n_o$ for the Table I parameter values with light exposure.

Section III A.3

SPACE-CHARGE LIMITED CURRENT AND CAPACITANCE IN Cu_xS/CdS SOLAR CELLS

R. Moorthy

L. D. Partain

D. Okubo

and

D. Henderson

Paper prepared for

International Electron Devices

Washington, D.C.

December 3-5, 1979*

SPACE-CHARGE-LIMITED CURRENT AND CAPACITANCE IN Cu_xS/CdS SOLAR CELLS*

Ravi Moorthy**
Electrical Engineering Dept., Univ. of Delaware
Newark, Delaware 19711

Larry Partain, Dan Okubo, and Debra Henderson***
Lawrence Livermore Laboratory
Livermore, California 94550

ABSTRACT

The unusual behavior of Cu_xS/CdS solar cells is better described with space-charge-limited current (SCL I) than with standard junction models. The SCL I theory provides the first quantitative explanation of these devices' I-V characteristics including their non-exponential form, the dark-light crossover, the temperature independent slope in addition to qualitatively modeling the voltage variation of capacitance. This is accomplished with trapping parameter values well known to be characteristic of Cu compensated CdS. It indicates that the voltage dependence of current is controlled by mechanisms entirely different than previously proposed with important implications for device fabrication and optimization and ultimate device performance.

INTRODUCTION

The unusual electrical properties of Cu_xS/CdS solar cells have long presented characteristics that have been difficult to model quantitatively. Gross behavior such as the dark-light crossover of the I-V, the non-exponential dependence of I on V, and the temperature independent slope of the I-V (1-5) have not been adequately explained. Analysis of this paper shows that such behavior is well described by a space-charge-limited current (SCL I) model that is controlled by physical mechanisms that are distinctly different from those involved in standard models (4-7).

THEORY

SCL I models have distinctive voltage and temperature dependences unlike that of standard theories. Qualitatively SCL I has a voltage dependence that sequentially shows I proportional to V, V^m (m>2), and finally V^2 for increasing current (8). This I-V shape is preserved at any temperature as long as SCL I mechanisms dominate. The capacitance for the linear, resistive region is just its geometric value $\epsilon A/L$ independent of voltage. Here ϵ is the dielectric constant, A is the cross-sectional area and L is the width SCL I region. For the $I \propto V^2$ region, SCL I theory shows that this capacitance is increased by the factor 3/2 (8). The transition between these values occurs in the $I \propto V^m$ interval. Empirically this transistion has been observed to involve a sharp drop in capacitance for SCL I produced in thin film, polycrystalline CdS (9).

The quantitative relations between current and voltage with an arbitrary distribution of traps is obtained with numerical integration. Considering the simplest case of a highly compensated CdS layer (due to Cu acceptors) of width L with uniform concentrations of equilibrium conduction electrons n_o and electron traps N_{ti} with the traps located on an energy E_c-E_{ti} below the conduction band edge, allows Gauss's law for the region to be written as

$$\frac{d\xi(x)}{dx} = -\frac{e}{\epsilon}\left[n(x) - n_o - \sum_i \left\{p_{ti}(x) - p_{tio}\right\}\right] \quad (1)$$

where $\xi(x)$ is the electric field, x is the space variable, e is the electronic charge, n(x) is the non-equilibrium conduction electron concentration, and $p_{ti}(x)$ and p_{tio} are the non-equilibrium and equilibrium concentrations of holes in the ith trap respectively. It is implicitly assumed in this expression that the build-up of non-equilibrium space charge is so dominant that the presence or absence of a small initial, equilibrium space charge has negligible effect on the results. This is reasonable for the small equilibrium space charge present in a highly compensated and depleted CdS layer.

The second assumption, that is standard for SCL I (8), is that current is dominated by drift alone so the current density can be used to specify the carrier concentration by

$$n(x) = \frac{J}{e\mu\xi(x)} \quad (2)$$

where J is the current density and μ is the mobility. Substituting this back into Eq. 1 gives the primary differential equation as

*Work performed in part under the auspices of the U.S. Department of Energy by the Lawrence Livermore Laboratory under contract number W-7405-ENG-48.

**Present address: W. L. Gore and Assoc., Inc., Newark, Del. 19711

***Present address: Elect. Eng. Dept., Calif. Polytechnic State Univ., San Luis Obispo, Calif. 93401

$$\frac{d\xi(x)}{dx} = -\frac{J}{e\mu\xi(x)} + \frac{n_o e}{\epsilon} - \frac{e}{\epsilon}\sum_i N_{ti} \cdot \left[\frac{1}{\frac{2n_o}{N_i}+1} - \frac{1}{\frac{2J}{N_i e\mu\xi(x)}+1}\right] \quad (3)$$

since

$$p_{ti}(x) = N_{ti}\left(1 - \frac{1}{1+\frac{1}{2}e^{\frac{E_{ti}-E_{fn}(x)}{kT}}}\right)$$

$$= \frac{N_{ti}}{\frac{2n(x)}{N_i}+1}$$

$$= \frac{N_{ti}}{\frac{2}{N_i}\frac{J}{e\mu\xi(x)}+1} \quad (4)$$

with N_i defined by

$$N_i = N_c\, e^{-\frac{E_c - E_{ti}}{KT}} \quad (5)$$

so that

$$\frac{n(x)}{N_i} = e^{-\frac{E_{ti} - E_{fn(x)}}{KT}} \cdot \quad (6)$$

Here $E_{fn}(x)$ is the quasi-Fermi level for conduction electrons and N_c is the effective density of states (10). Similarly

$$p_{tio} = \frac{N_{ti}}{\frac{2n_o}{N_i}+1} \cdot \quad (7)$$

The required single boundary condition for finding $\xi(x)$ is (see Eq. 2)

$$\xi(o) = \frac{J}{e\mu n(o)} \quad (8)$$

The third assumption, also standard for SCL I (8), is that $n(0) >> 1$. This condition was found to be sufficiently satisfied for accurate numerical integration of Eq. 3 to give $\xi(x)$ when $n(o) = 10^5$ n_o. Again numerically integrating this $\xi(x)$ result finally gives the voltage V for a specified J as

$$V = -\int_0^L \xi(x)dx. \quad (9)$$

Note that this current-voltage relationship is totally specified by the concentrations n_o and N_{ti}, the energy spacings $E_c - E_{ti}$, the compensation width L, and the mobility μ.

In contrast, standard treatments of P-N junction transport indicate that current is exponentially related to voltage divided by temperature T (6,7). Tunneling models indicate that current is rather independent of T and the simplest treatments show that it is exponentially related to voltage (4,5). However quite varied relationships between I-V are seen in tunneling devices such as Zener and tunnel diodes so that a single required tunneling characteristic can not be specified.

RESULTS

Cu_xS/CdS samples A and B were fabricated at Lawrence Livermore onto a vacuum deposited CdS substrate with the Cu_xS layer formed by reactive sputtering. Sample C was constructed by the University of Delaware's Institute of Energy Conversion by wet-dip formation of the Cu_xS layer onto a vacuum deposited CdS layer. All samples were extensively heat treated.

Figure 1 shows the dark and light (simulated AM1) J-V characteristics measured on sample A. For convenience, the short circuit current density J_L has been added to the light data to make $J + J_L$ go to zero when V is zero. This allows plotting all the data on the same logarithmic scales. Note that both data sets exhibit the distinctive V and V^2 regions with the light data also showing the V^m regions of SCL I for current variations over 4 to 6 orders of magnitude. Measuring J in the light near zero voltage involved currents in the mA/cm^2 so that current changes less than 10^{-2} mA/cm^2 were not measureable for the light data.

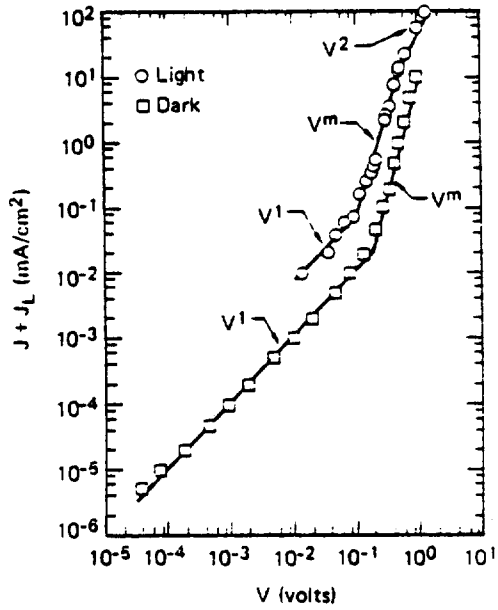

Fig. 1. The dark and light (AM1), current-voltage characteristics of sample A that demonstrate the distinctive SCL I behavior.

Similar measurements as a function of T were taken on sample B and plotted in Fig. 2. In addition to the V and V^m regions, the temperature independent slopes characteristic of SCL I are clearly shown. The curves definitely do not exhibit exponential dependence on V/T. All of the published data of temperature dependent J-V curves for Cu_xS/CdS cells have shown similar results with none demonstrating the exponential 1/T behavior (3-5, 11).

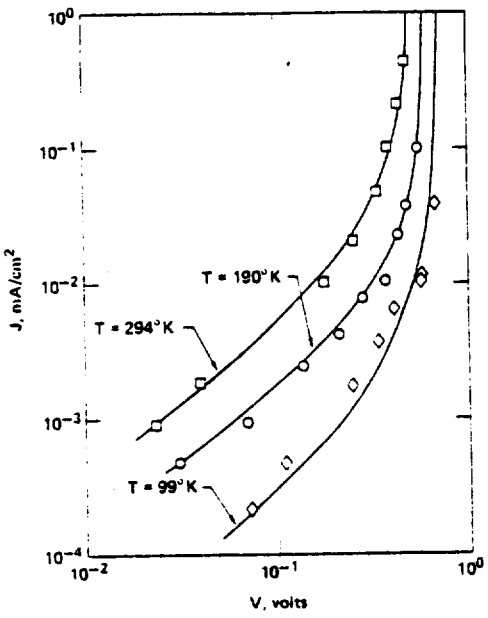

Fig. 2. The temperature dependent, current-voltage properties of sample B that show the T independent slope characteristic of SCL I.

The dark and light J-V properties measured on sample C are shown as the data points in Fig. 3 demonstrating the same properties as sample A. The theoretical fit of this data by the numerical integration, SCL I model is shown by the solid curves. For the theoretical curve, it was assumed that the short circuit current superimposes on the SCL I with light exposure. The parameters that gave this fit are $n_o = 2.7\ (10^{10})cm^{-3}$ (light) and $9(10^9)cm^{-3}$ (dark), $\mu = 20\ cm^2/V$ sec (light) and 7 cm^2/V sec (dark), $N_{t1} = 1.3(10^{14})\ cm^{-3}$ (light) and $7(10^{14})\ cm^{-3}$ (dark), $E_c - E_{t1} = 0.30$ eV, $N_{t2} = 5.1\ (10^{14})\ cm^{-3}$, $E_c - E_{t2} = 0.44$ eV, $L = 1.33(10^{-4})$ cm, $\epsilon/\epsilon_o = 10$, $m_n^*/m_o = 0.2$, and T = 294°K. The L was determined from zero bias, dark capacitance. The m^* and m_o are the conduction electron's effective and free masses respectively. These parameter values are typical of those reported for CdS. The trap levels and densities are close to those measured by Grill et al(12) on single crystal CdS using DLTS. The dark n_o and μ values and their change in light are approximately those found by Wu and Bube (13) on Cu compensated, polycrystalline CdS using thermoelectric techniques. Similar SCL I behavior was found in p-GaAs/n-ZnSe heterojunction solar cells as reported by Balch and Anderson(14).

When this sample C data and theory are plotted on linear scales the excellent agreement shown in Fig.4 is obtained. This graph shows that sample C has an efficiency of 6.1 percent, a J_L of 17 mA/cm^2, an open circuit voltage of 0.51 V, and a fill factor of 0.70. To the best of our knowledge this model provides the first quantitative fit of this dark-light crossover behavior that is characteristic of Cu_xS/Cds solar cells. This same crossover is seen when the Fig. 1 data is replotted on linear scales. The dark capacitance-voltage properties of sample C were obtained far into forward bias region using a transient technique similar to that of Dresner and Shallcross (9) with an accuracy that is undiminished by large current flow. The results are shown in Fig. 5 for various heat treatment times given the cell at 180°C in air. Note the sharp drop in capacitance at around 0.3 to 0.4 volts. From Fig. 3 this corresponds to the V^m region where an anomaly is theoretically indicated and where such behavior has been previously observed with SCL I(9).

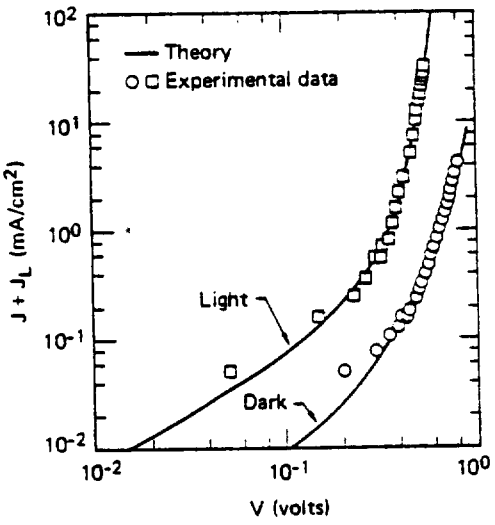

Fig. 3. Logarithmic plot of the current-voltage properties of sample C as shown by the data points for the dark and light. The solid curves are the SCL I theory fit obtained with numerical integration.

CONCLUSIONS

Measurements taken on Cu_xS/CdS solar cells of up to 6 percent efficiency fabricated by two different locations indicate that the I-V characteristics as a function of temperature and light and the C-V behavior demonstrate the highly distinctive properties of SCL I. The

current data definitely do not have the exponential V/T dependence of standard P-N junction models (6,7) or the exponential V variation of simple tunneling models (4,5). While tunneling current can exhibit a wide variety of behavior, it would be highly fortuitous if it had exactly the same properties as SCL I. Such I-V mimicing by tunneling has never been reported to the best of our knowledge. The fit that the SCL I model gives for the data is the first quantitative agreement that has been obtained for the dark and light properties. This was accomplished with parameter values well known to be characteristic of the involved materials and is in a form like that seen for another heterojunction solar cell.

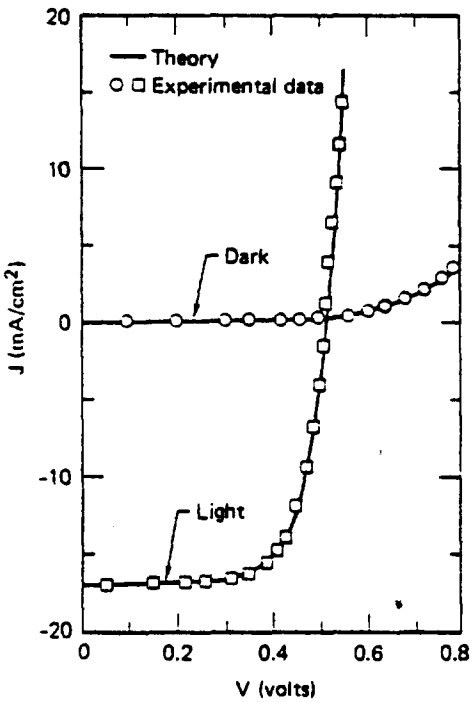

Fig. 4. Linear plot of sample C's measured data points and the numerical integration, SCL I theory given by the solid curves.

This indicates that the trap structure in the Cu compensated CdS layer controls the voltage dependence of current rather than the mechanisms of standard junction theory. Since these parameters have never been monitored in cells, they likely account for the non-repeatability often encountered. New calculations of ultimate device performance based on these results appear to be in order. This SCL I analysis is new so that only part of the cell behavior has been modeled so far. Continuing work is proceeding to use this approach to treat minority carrier collection, the energy band diagram, the reverse bias characteristics, and the photocapacitance.

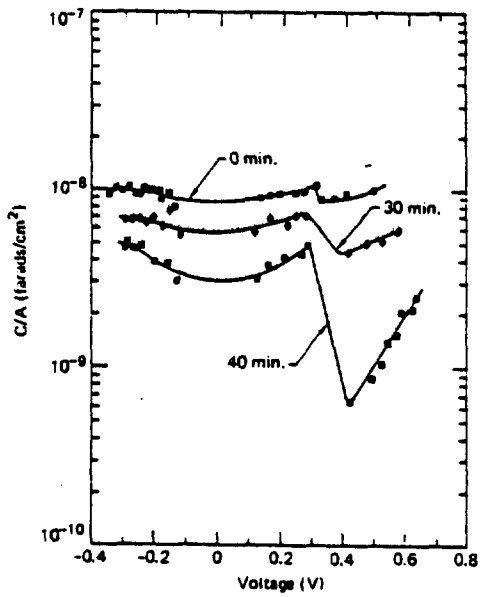

Fig. 5. The dc bias voltage dependence of sample C's small signal capacitance measured with a transient technique.

Valuable contributions to and assistance with all aspects of this work were provided by J. Leong, J. Yee, G. A. Armantrout, P. J. Warter, A. Rose, J. D. Meakin, A. Rothwarf, N. C. Wyeth, G. Storti, and W. W. Anderson. Appreciation is due to D. Rae for careful preparation of this manuscript.

REFERENCES

1. F. A. Shirland, Advanced Energy Conversion 6, 201 (1966).
2. A. Rothwarf and K. W. Boer, Progr. Solid-State Chem 10, Part 2, 71 (1975).
3. S. R. Das, A. Banerjee, and K. L. Chopra, Solid-State Electronics 22, 533 (1979).
4. A. Amith, J. Appl. Phys. 50, 1160 (1979).
5. S. Martinuzzi and O. Mallem, Phys. Stat. Sol. A16, 339 (1973).
6. N. C. Wyeth and A. Rothwarf, J. Vac. Sci. Tech 16, July/Aug. 1979.
7. K. W. Boer, J. Appl. Phys. 50, 5356 (1979).
8. M. A. Lampert and P. Mark, Current Injection in Solids (Academic Press, NY 1970).
9. J. Dresner and F. V. Shallcross, J. Appl. Phys. 34, 2390 (1963).
10. B. G. Streetman, Solid State Electronic Devices (Prentice-Hall, Englewood Cliffs, 1972) p. 75.
11. W. D. Gill and R. H. Bube, J. Appl. Phys. 41, 3731 (1970).
12. C. Grill, G. Bastide, G. Sagnes, and M. Rouzeyre, J. Appl. Phys. 50, 1375 (1979).
13. C. Wu and R. H. Bube, J. Appl. Phys. 45, 648 (1974).
14. J. W. Balch and W. W. Anderson, Phys. Stat. Sol. A9, 567 (1972).

B. EBIC STUDIES

Section III B.1

Obtaining Accurate Values of Diffusion Length With the Scanning Electron Microscope

Larry D. Partain and Stephen P. Shea

2nd E.C. Photovoltaic Solar
Energy Conference

West Berlin
April 23-26, 1979

D. Reidel Publ. Co., Dordrecht, Holland
pp. 639-646

OBTAINING ACCURATE VALUES OF DIFFUSION LENGTH WITH THE SCANNING ELECTRON MICROSCOPE*

Larry D. Partain
Electronics Engineering Department
Lawrence Livermore Laboratory
Livermore, California 94550, U.S.A.

Stephen P. Shea
Electrical Engineering Department
University of Delaware
Newark, Delaware 19711, U.S.A.

Summary

The slope of data plots of the logarithm of electron-beam-induced-current (EBIC) versus beam position directly specify the minority carrier diffusion length (L) for the special case where the beam-induced generation volume can be considered a point source many diffusion lengths away from external surfaces of a planar sample. Restricting the acceleration voltages (E_o) so that the Gruen range (R_G) is less than four times the diffusion length being measured allows the generation volume to be considered a point source as far as the influences of the surface parallel to the junction and the intersection of the junction with the generation volume are concerned if the thickness of the measured region is greater than or equal to 2L. Consideration of the surface perpendicular to the junction indicates that E_o should be further restricted so that $R_G \leq 0.84L$. This allows L values to be determined to within 15% simultaneously with recombination velocity values (V_R) normalized by the diffusion constant (D) to within 20% by curve fitting semilogarithmic EBIC data. This gave $L(Cu_2S) = 0.25\ \mu m$, $L(CdS) = 0.40\ \mu m$, $V_R/D\ (Cu_2S) = 4(10^4)/cm$ and $V_R/D(CdS) = 5(10^4)/cm$ for a Cu_2S/CdS heterojunction. Two tellurium doped GaAs Schottky barrier samples had L values of 3.0 and 6.0 microns with a single V_R/D value of $3.3\ (10^4)/cm$.

*Work performed under the auspices of the U.S. Department of Energy by the Lawrence Livermore Laboratory under contract number W-7405-ENG-48.

INTRODUCTION

Minority carrier diffusion length is a parameter that strongly influences the conversion efficiency of solar cells(1). In the ideal case with minority carrier generation by a point source at a distance x away from the planar boundary of a p-n or Schottky barrier junction space-charge-region (SCR), the induced short circuit current $I_{sc}(x)$ is given by

$$I_{sc}(x) = I(0)\ e^{-x/L} \qquad (1)$$

if the influences of all the exterior surfaces are negligible where L is the minority carrier diffusion length and I(0) is a constant directly proportional to the strength of the point source(2). The L value is simply obtained from the slope of log $I_{sc}(x)$ versus x data. The highly focused beam of a scanning electron microscope (SEM) can be used to provide the energy to generate minority carriers in localized regions of semiconductor samples that in some cases can approximate the ideal case above so that accurate values of L can be obtained from log current versus beam position data(3).

A typical experimental configuration is shown in the insert of Fig. 1 where the electron beam is scanned along an outer surface of a planar device in a direction perpendicular to the collecting junction SCR. In general the effect of this perpendicular beam-entry surface is not negligible and any other surfaces not located several diffusion lengths away from the generation volume also influence the experiment. In addition, the generation volume can not be considered a point source when its physical size is on the same order as the thickness of the sample region being measured or the diffusion length value being measured. The purpose of this paper is to define the conditions that allow the Fig. 1 configuration to be used to obtain data that can be analyzed by using Eq. 1 or by using simple modifications of it.

2. Background

The new information developed in this paper describes the effect of the perpendicular beam-entry surface. The influence of the surface parallel to the junction was treated by Oakes et al(4) using Hackett's analysis(5). These workers defined a distance t between the edge of the SCR and the parallel outer surface. For $t \geq 2L$, worst case errors no larger than + 15% and -15% were encountered for surface recombination

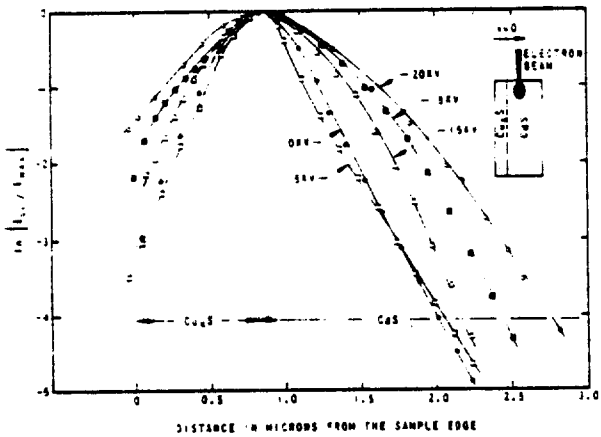

Fig. 1. Cu_2S/CdS data for various accelerating voltages.

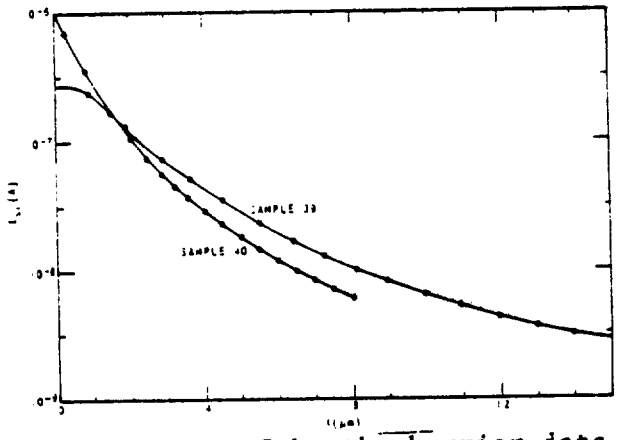

Fig. 2. GaAs Schottky barrier data of Sekela et al.

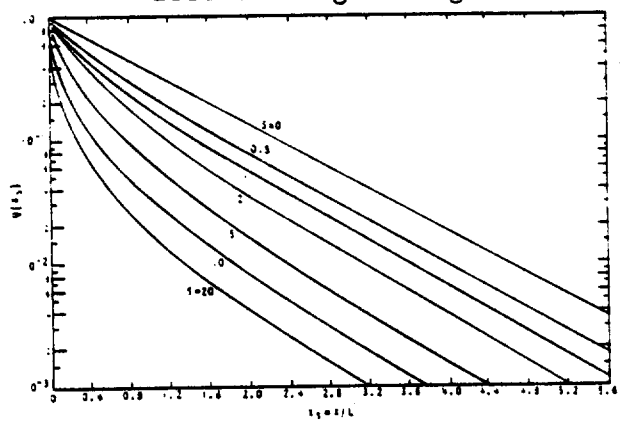

Fig. 3. Theoretical surface-point-source collection versus normalized position for various normalized surface recombination velocities.

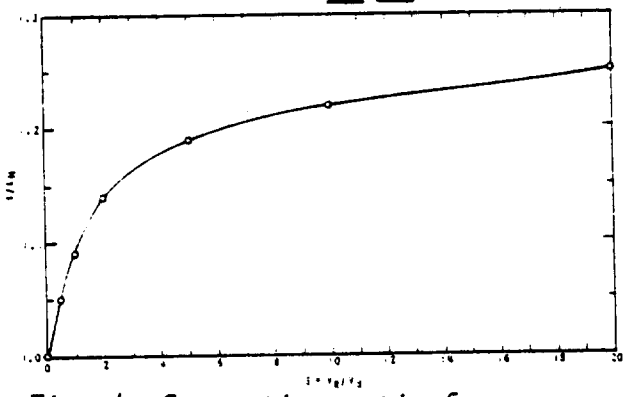

Fig. 4. Correction ratio for measured diffusion length versus normalized surface recombination velocity.

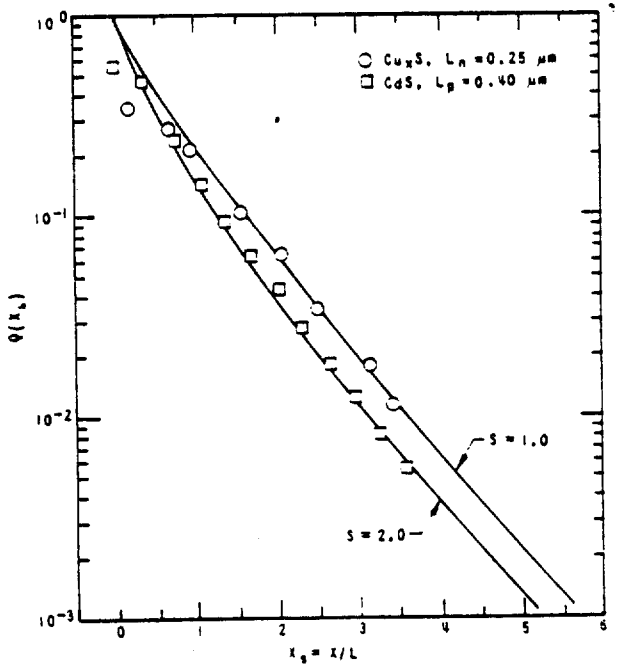

Fig. 5. Normalized Cu_2S/CdS data superimposed on van Roosbroeck's theory.

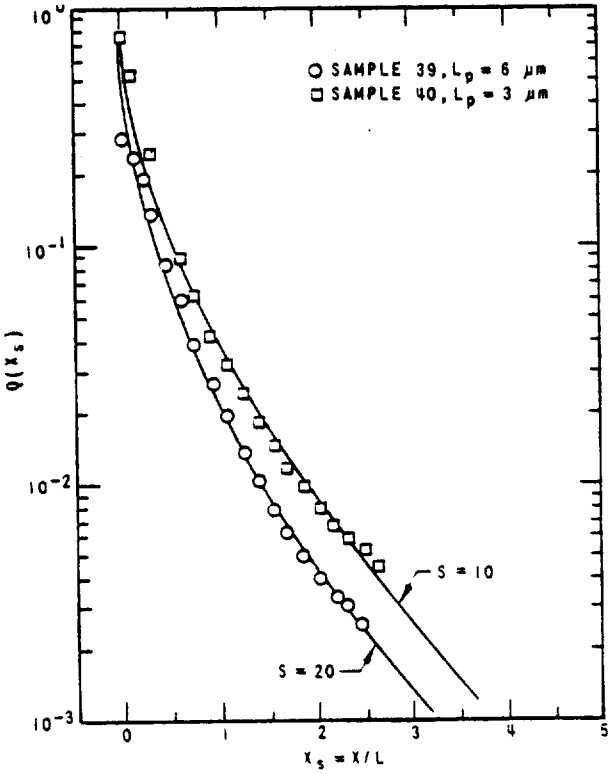

Fig. 6. Normalized GaAs data of Sekela et al superimposed on van Roosbroeck's theory.

velocities of zero and infinity respectively if the slope of log I versus x was measured at x = 0.75 L. When the surface recombination velocity V_R equaled the diffusion velocity V_d (V_d is equal to D/L where D is the minority carrier diffusion constant), this error reduced to zero.

The physical size of the generation volume is described by the Gruen range R_G(6). To be able to excite a single region of the sample and to still remain far enough away from the parallel surface at t, Oakes et al's arguement implies that R_G should remain something less than 4L if the effective width of the generation volume is estimated as $R_G/2$. Similar conditions on R_G are imposed by the results of Shea et al(3) whose experimental data for single crystal samples is given in Fig. 1. At higher electron beam accelerating voltages E_o, R_G which is proportional to E_o to some power, becomes too large. This gives log $I_{sc}(x)$ versus x data that has a curvature well fit by a Gaussian-shaped, universal, lateral- dose function(3) such as the 15, 18, and 20 kV data in Fig. 1. The slopes of the curves then bear no relationship to L but simply monotonically decrease with increasing R_G and E_o. To prevent this, they found that R_G should be kept less than 4L in value which, for the Fig. 1 data, occurs and E_o less than 13 kV and 15 kV in Cu_xS and CdS respectively. Unfortunately this brings the center of the beam-induced generation volume within a few L of the perpendicular, beam-entry surface. If this surface has a recombination velocity greater than zero, curvature is introduced as can be seen for the 5 kV data in Fig. 1. Such curvature, due to the influence of the beam-entry surface, is even more evident in the electron-beam-induced-current (EBIC) data on GaAs Schottky barriers obtained by Sekela et al(7) using a similar experimental technique. These data are given in Fig. 2.

3. Theory

The worst case of generation by a point source located right on the perpendicular beam-entry surface has been analytically described by van Roosbroeck using Green's functions(2). His results are shown in Fig. 3 as the logarithm of the fraction of collected minority carriers Q as a function as the normalized distance x_s = x/L of the surface point source from the planar boundary of the collecting SCR of the junction. Different curves result for different values of normalized surface

recombination velocity $S = V_R/V_d$. If $S = 0$, then a straight line curve exactly modeled by Eq. 1 is obtained. For higher S values, curvature similar to that seen in Fig. 2 is evident. For $x_s > 2$, the curves begin to approach a straight line but with a slope slightly greater than that specified by $-1/L$. If one uses the tangent of these curves at $x_s = 2$ to define an effective (measured) diffusion length L_m, then the ratio of the true diffusion length L to L_m is specified by van Roosbroeck's results(2). This ratio is plotted in Fig. 4 as a function of S. Note how the error rapidly rises to around 15% at S=2 but then appears to saturate at something above 25% for S greater than 20. An upper limit for $S=\infty$ was provided by Berz and Kuiken(8) who showed that a maximum error of 31% is obtained in the realistic case of generation at some small, finite depth h below the beam entry surface where $h << L$ and L_m is obtained for data where $L < x < 2L$(9).

If the accelerating voltage can be kept sufficiently low (so that R_G is low), then most minority carriers are generated near the beam-entry surface and the experimental data should begin to approximate the van Roosbroeck results. The relation of R_G to E_o can be obtained from the universalized, beam penetration and energy dissipation studies of Everhart and Hoff(10). Their results specify R_G in any material (solid, liquid, or gas) as

$$R_G = 1.03(10^{-11}) \frac{A}{Z\rho} CE^{*2} \left(\frac{E_o}{E^*}\right)^b \text{ (cm)} \tag{2}$$

where

$$E^* = [8.37(10^{-3}) + 5.04(10^{-2})Z^{-1.19}]Z \text{ (kV)} \tag{3}$$

for E_o in kV. Here Z is the atomic number; A, the atomic weight; and ρ, the density in g/cm^3 of the material struck by the electron beam. The constants C and b are determined by the range of E_o/E^* values used experimentally and are specified in Table I. Here the relationship of the Gruen range R_G to the Bethe range R_B used by Everhart and Hoff has been taken as $R_G/R_B = 0.81$ as found by Shea et al(3). The above is formulated for elemental materials. When compound material is used, average values of A and Z can be obtained by

$$\bar{Z} = \frac{1}{m} \sum_{i=1}^{m} Z_i \tag{4}$$

and

$$\bar{A} = A/m \tag{5}$$

where Z_i is the atomic number of each of the m atoms contained in a

basic unit of the material of total atomic weight A. This gives the specific values for Cu_2S, CdS and GaAs as shown in Table II. The overlapping ranges of Everhart and Hoff's expressions give R_G values that agree within about 20%. This is one indication of the expected accuracy of their model.

4. Results

The 5 kV results of Fig. 1 for Cu_xS/CdS were renormalized and replotted versus x/L for various trial L values. The best agreement between this data shown as circles and squares in Fig. 5 and the solid line theoretical curves of van Roosbroeck was obtained for L(Cu_xS) equal to 0.25 μm and L(CdS) equal to 0.40 μm. The corresponding R_G/L values of 0.84 for the Cu_2S and 0.70 for the CdS are certainly much less than 4. These L values are near the upper limit of the minus 20%, plus 40% error bounds for L values previously reported for Cu_xS/CdS fabricated on single crystal CdS (3,9). These earlier values had not been specifically corrected for the beam-entry surface effects but the errors bounds had been selected to include the possible uncertainties caused by this surface and other effects. Taking S equal to 1 and 2 as indicated in Fig. 5 respectively for the Cu_2S and the CdS specifies V_R/D values ($V_R/D = S/L$) of $4(10^4)$/cm for Cu_2S and $5(10^4)$/cm for CdS. These agree to within 20% with similar values measured by entirely different techniques of scanning the beam across an external surface which were reported earlier(9).

Sekela, et al's 25 kV data for n-GaAs Schottky barriers of Fig. 2 were also renormalized and replotted as circles and squares versus x/L for various L values as shown in Fig. 6. The best fit to van Roosbroeck's theory shown by the solid line curves for S equal 10 and 20 was obtained

Table I. The values of C and b as a function of E_o/E^*

E_o/E^* Range	C	b
5-50	0.95	1.51
10-100	0.68	1.62
50-500	0.34	1.78

Table II. The coefficients for Gruen range calculation following from Everhart and Hoff's studies(10).

Material	(g/cm^3)	$\bar{Z}$	$\bar{A}$ (g)	E^* (kV)
Cu_2S	5.60	24.7	53.0	0.234
CdS	4.82	32.0	72.2	0.294
GaAs	5.31	32.0	72.3	0.294

for L values of 3 and 6 microns. These correspond to R_G/L values of 0.80 and 0.40 respectively. The S and L values for both samples specify a single $V_R/D = S/L$ value of $3.3(10^4)$/cm for GaAs. The 3 micron L value for their sample 40 is 25% higher than the value they obtained from the slope of a tangent line drawn on their curve. Such an underestimation for S=10 is consistent with the predicitons of van Roosbroeck's theory as interpreted in Fig. 4.

9. Discussions and Conclusions

The curvature in data plots of the logarithm of EBIC current versus beam position introduced by the recombination velocity of the beam-entry surface perpendicular to the SCR junction of a planar sample can be modelled by van Roosbroeck's theory(2) of point generation right at this surface. Earlier studies dealing with the shape of the beam generation volume and the influence of an outer surface parallel to the junction (3,4) showed that a point source model accurately describes experimental results as long as $R_G/L < 4$ and the thickness t of the measured region is 2L or greater. R_G as a function of E_o is describable by Everhart and Hoff's universalized results(10). The present study showed that data on Cu_xS/CdS heterojunctions and n-GaAs Schottky barriers are well fit by van Roosbroeck's curves for $R_G/L \leq 0.84$ which enables normalized recombination velocities to be determined simultaneously with diffusion length with worst case uncertainties of 20 and 15% respectively that decrease significantly for thick samples ($t > 2L$) and appropriate recombination velocity values. Thus this study indicates that accurate parameter values are obtained by fitting van Roosbroeck's curves if E_o is restricted so that R_G is less than or equal to 0.84L.

Analysis of Cu_2S/CdS data gave $L(Cu_2S) = 0.25\ \mu m$ and $L(CdS) = 0.40\ \mu m \pm 10\%$ and $V_R/D\ (Cu_2S) = 4(10^4)$/cm and $V_R/D(CdS) = 5(10^4)$/cm $\pm$ 15%. Similar analysis of two tellurium doped GaAs samples gave L values of 3.0 and 6.0 microns $\pm$ 10% along with a single V_R/D value of $3.3(10^4)$ /cm $\pm$ 15%.

Acknowledgement

This study was a direct result of discussions with D. L. Feucht on SEM measurement accuracy. Valuable assistance with theoretical concepts and experimental details of this work were obtained by interactions with P. J. Warter, G. J. Sullivan, T. Hench, A. Rothwarf, and J. D. Meakin.

Appreciation is due D. Rae for the careful preparation of the manuscript.

References

1. A. G. Milnes and D. L. Feucht, Heterojunctions and Metal-Semiconductor Junctions, (Academic Press, New York, 1972).
2. W. van Roosbroeck, J. Appl. Phys. 26, 380 (1955).
3. S. P. Shea, L. D. Partain and P. J. Warter, Scanning Electron Microscopy, Vol. I (SEM Inc., AMF O'Hare, Illinois 60666, USA, 1978), p. 435.
4. J. J. Oakes. I. G. Greenfield, and L. D. Partain, J. Appl. Phys. 48, 2548 (1977).
5. W. H. Hackett, J. Appl. Phys. 43, 1649 (1972).
6. A. E. Gruen, Z. Naturforsch. A12, 89 (1957).
7. A. M. Sekela, D. L. Feucht and A. G. Milnes, Inst. of Phys. Conf. Series, No. 24, p. 245, 1975.
8. F. Berz and H. K. Kuiken, Solid State Electr. 19, 437 (1976).
9. S. P. Shea and L. D. Partain, 13th IEEE Photovoltaic Specialist Conf., Washington, DC, June 1978, p. 393.
10. T. E. Everhart and P. H. Hoff, J. Appl. Phys. 42, 5837 (1971).

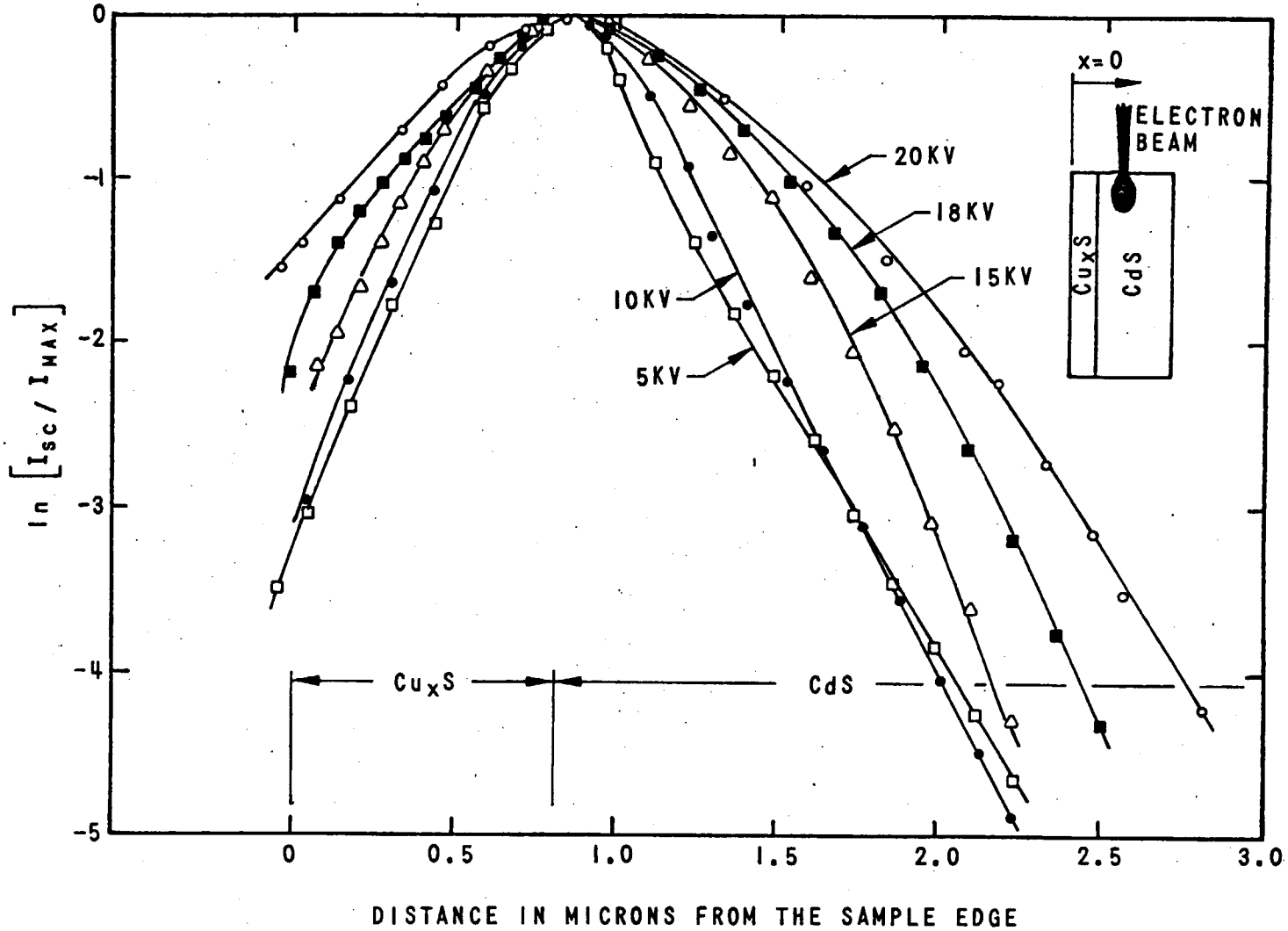

Fig. 1. Cu_2S/CdS data for various accelerating voltages.

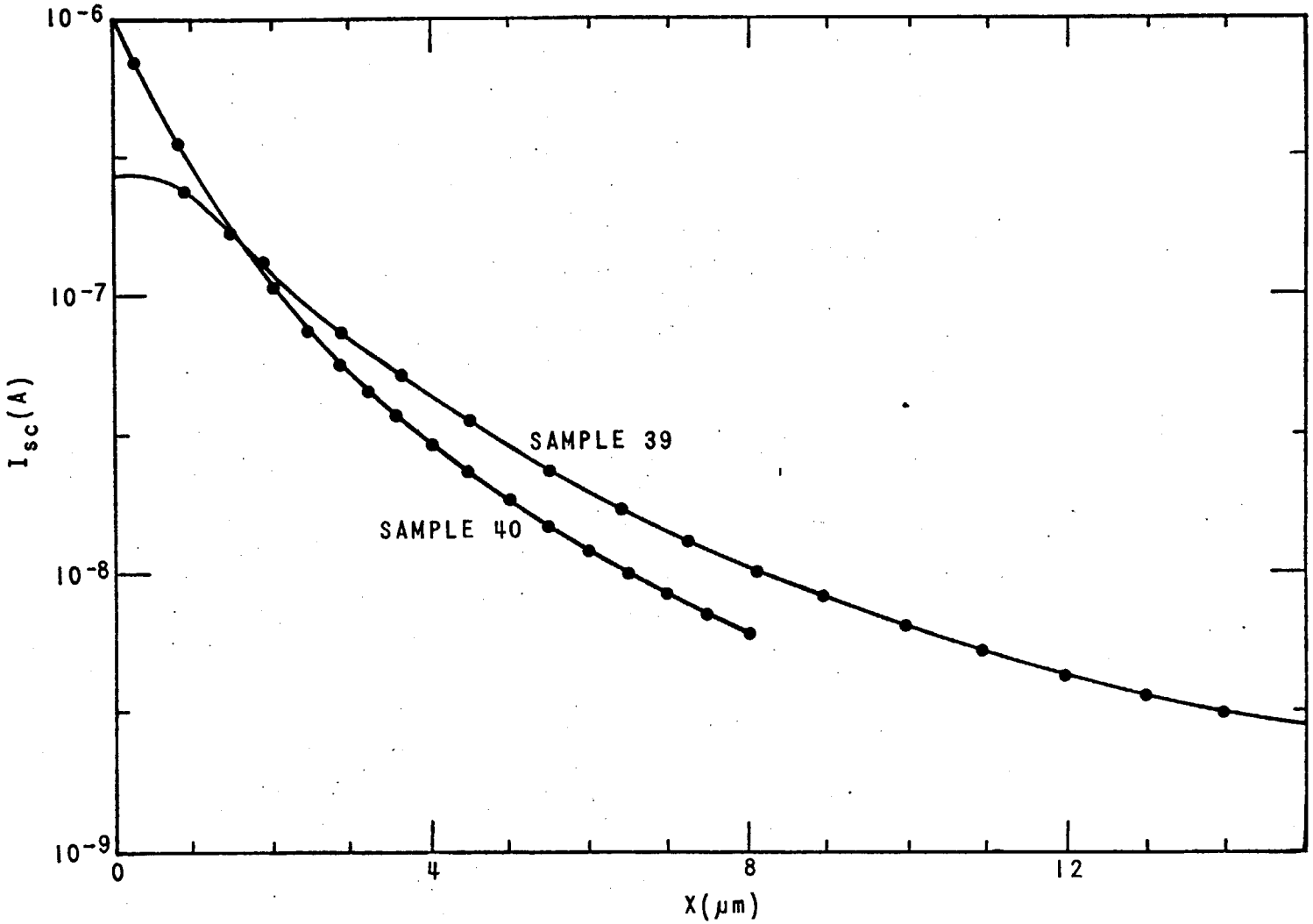

Fig. 2. GaAs Schottky barrier data of Sekela et al.

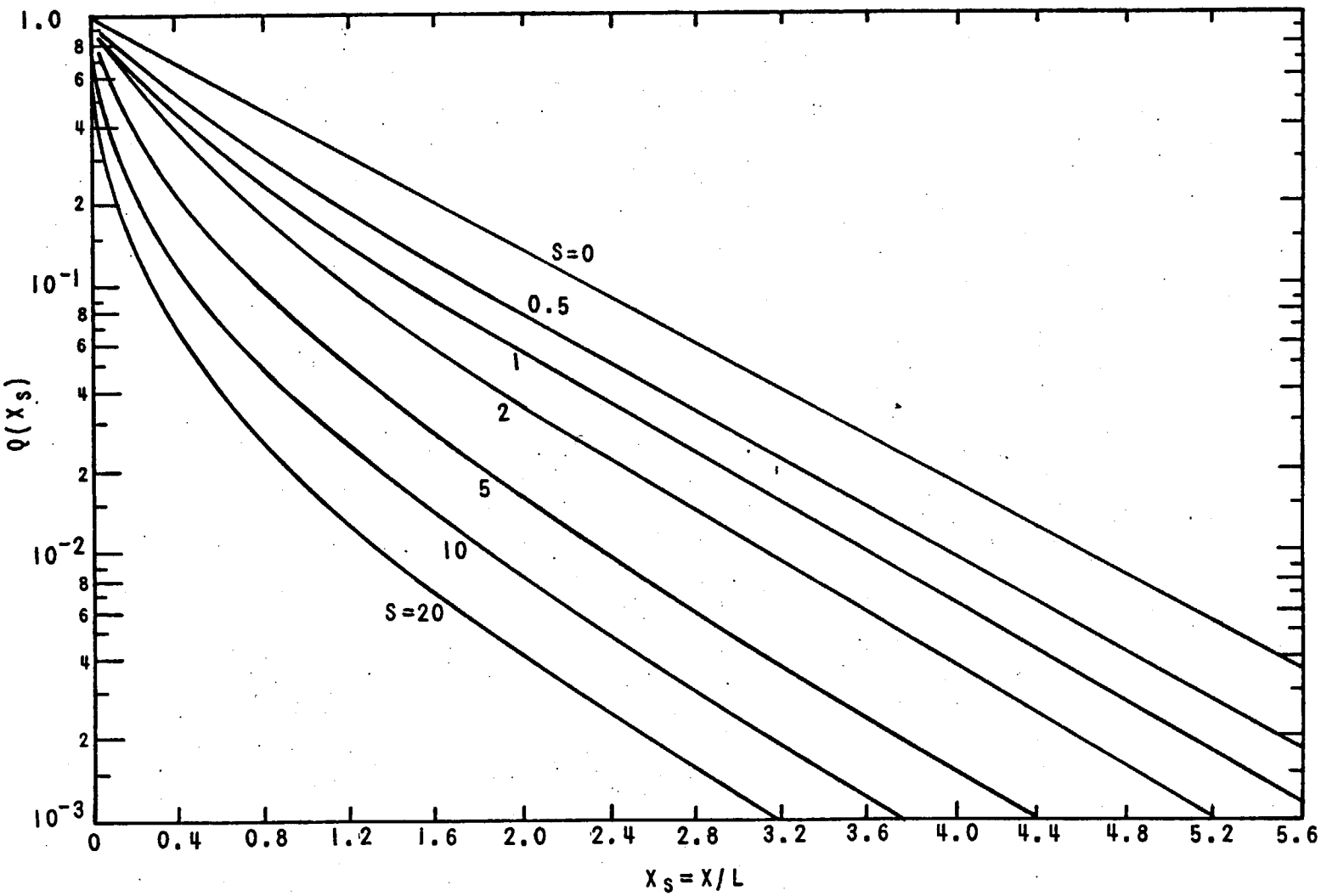

Fig. 3. Theoretical surface-point-source collection versus normalized position for various normalized surface recombination velocities.

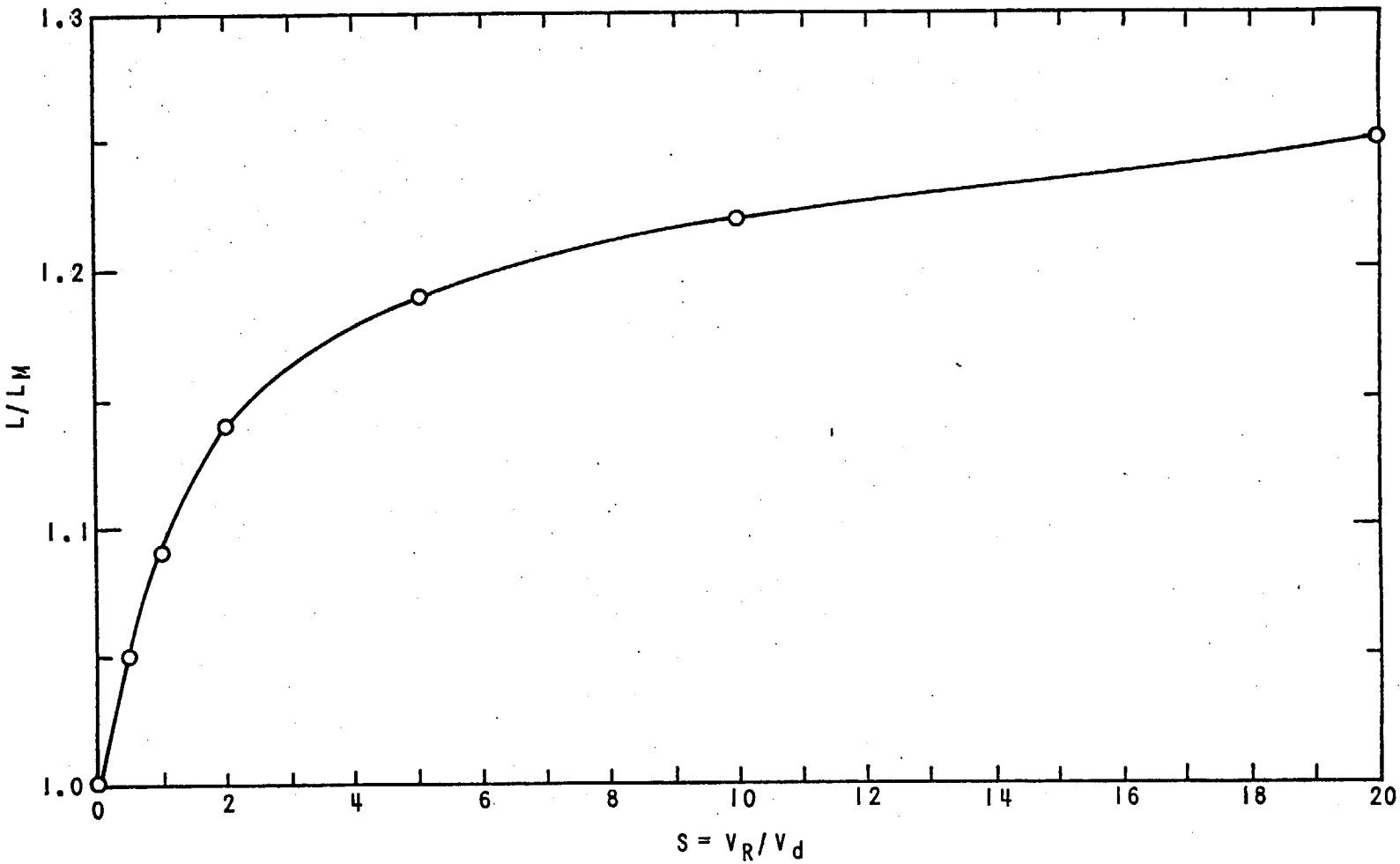

Fig. 4. Correction ratio for measured diffusion length versus normalized surface recombination velocity.

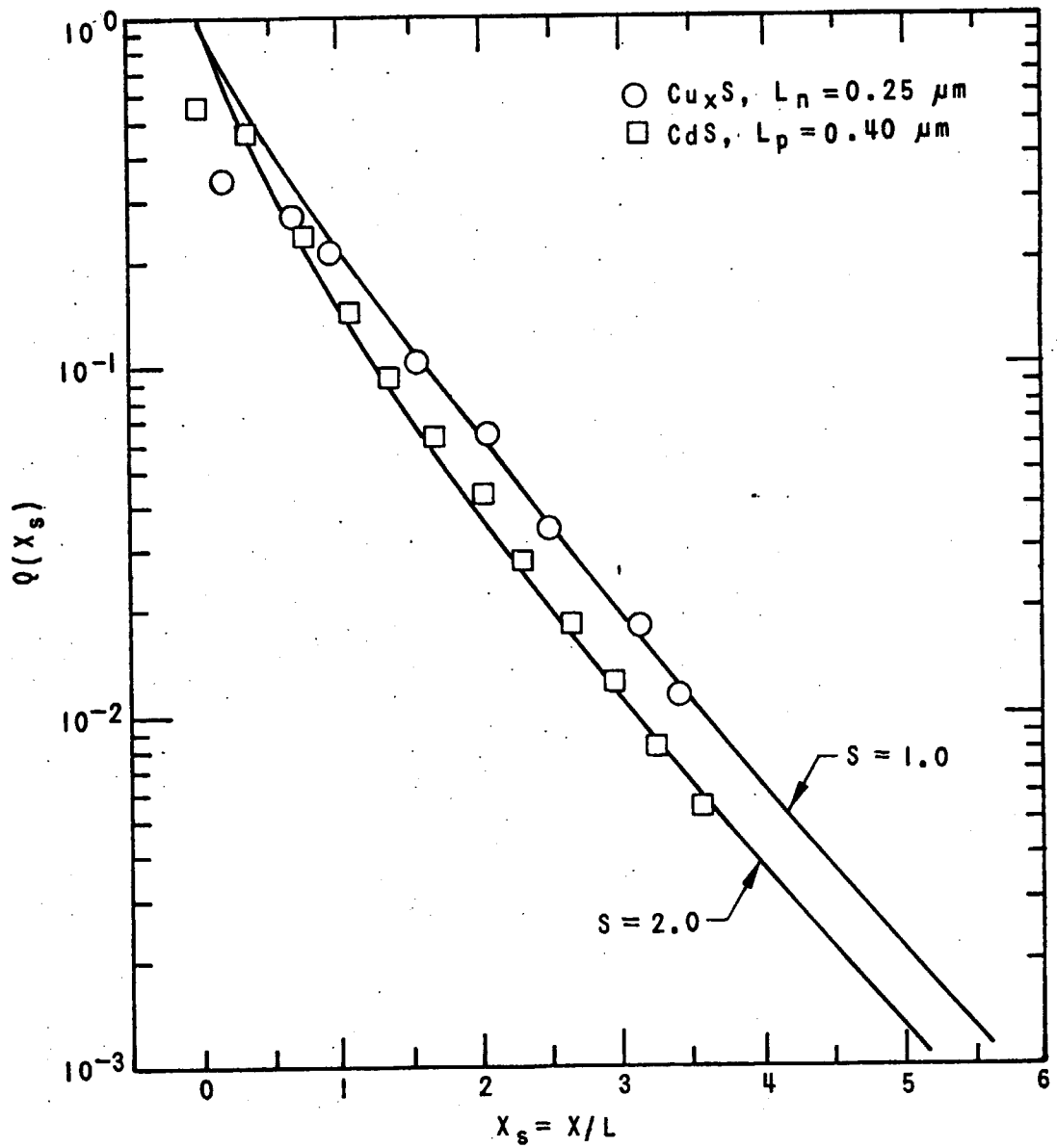

Fig. 5. Normalized Cu_2S/CdS data superimposed on van Roosbroeck's theory.

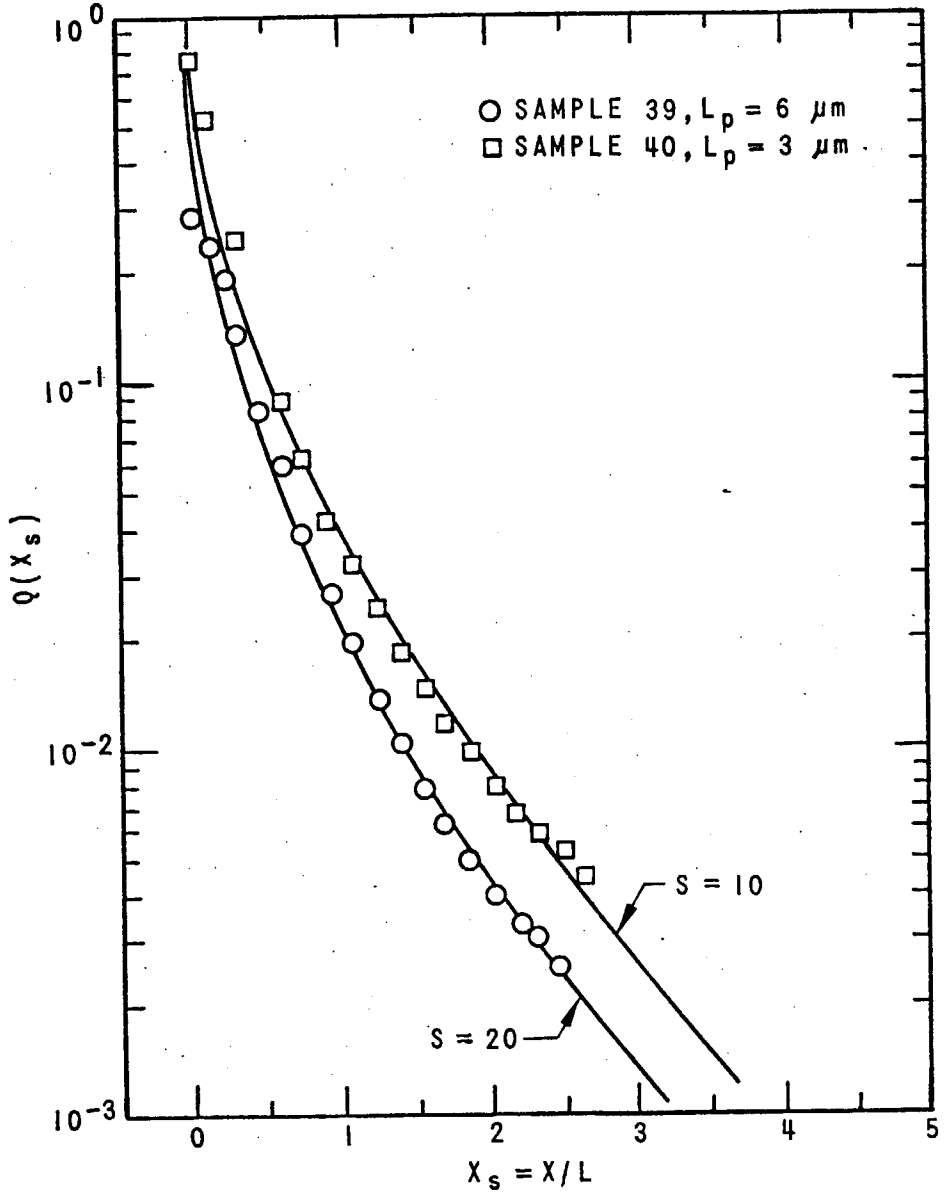

Fig. 6. Normalized GaAs data of Sekela et al superimposed on van Roosbroeck's theory.

Section III B.2

NON-DESTRUCTIVE SEM MEASUREMENT OF MINORITY CARRIER TRANSPORT PARAMETERS OF Cu_xS/CdS SOLAR CELLS AS A FUNCTION OF HEAT TREATMENT*

Larry Partain

Guy Armantrout

and

Dan Okubo

Lawrence Livermore Laboratory

Livermore, California 94550

This Paper was Prepared for Submittal to

IEEE Trans. Electron Devices,

Special Issue on Photovoltaics,

April, 1980**

---

*Work performed under the auspices of the U.S. Department of Energy by the Lawrence Livermore Laboratory under contract number W-7405-ENG-48.

ABSTRACT

Electron-beam-induced-current techniques of a scanning electron microscope have been extended to allow non-destructive measurements to be performed on P-N heterojunction devices consisting of thin layers sensitively influenced by surface effects and under conditions where junction collection efficiency is less than perfect. When applied to Cu_xS/CdS solar cells formed on polycrystalline CdS with an epitaxial Cu_xS layer that was heat treated at 180°C in a hydrogen-argon ambient, the dominant change was found to be the greater than two increases in junction collection efficiencies to a maximum and then a decrease for treatment times up to 120 minutes. No significant variations were found in the minority carrier diffusion lengths which remained in the 0.20 to 0.26 micron range for the Cu_xS and in the 0.41 to 0.46 micron range in the CdS. The Cu_xS surface recombination velocity retained a constant magnitude equal to its diffusion velocity. Optimization of the collection efficiency changes should lead to improved device performance.

I. INTRODUCTION

Heat treatment is a necessary step in the fabrication of high efficiency, polycrystalline Cu_xS/CdS heterojunction solar cells (1-9). However, the important changes that heating produces are only beginning to be understood. Of primary importance are the parameters that describe minority carrier behavior which essentially determines the current output of solar cells(10). The minority carrier diffusion lengths and surface recombination velocity are parameters important in homojunction as well as heterojunction devices(10). Losses in the space-charge-region (SCR) surrounding the junction interface that are described by the junction collection efficiency can become significantly large in heterojunctions due to recombination through the high density of defects associated with the junction mismatch of the two different materials at their interface (11-13). In homojunctions this junction collection efficiency is often considered to be perfect (100%).

Previously reported results (11), for destructive measurements with the scanning electron microscope (SEM) showed the dominant change occured in relative shifts in the junction collection efficiency with no significant variations observed in either the Cu_xS or the CdS diffusion lengths or in the Cu_xS surface

recombination velocity during air heat treatment. These data were obtained on samples fabricated on single crystal CdS with the Cu_xS layer formed topotaxially by a wet dip in a hot CuCl bath. The sample configurations required did not allow determination of the devices' I-V characteristics in the light and the analysis gave only relative values of junction collection efficiency. In the present work, the experimental studies have been extended to consider samples fabricated on polycrystalline, thin film CdS formed by vacuum evaporation with the Cu_xS layers formed epitaxially by reactive sputtering (14), and for reducing heat treatment ambients of hydrogen-argon. The SEM analysis was modified to use the non-destructive approach of Wu and Wittry(15) so that the light I-V characteristics were readily obtained. Prior analysis(15) was extended to allow studies of the thin device regions whose properties are sensitively affected by surface phenomena and so that absolute values of collection efficiency of the junction were obtained.

II. THEORY

In normal operation, photons absorbed in solar cells provide the energy required to break valence bonds and produce excess minority carriers of increased energy. Excess majority carriers are also produced in like numbers but cause such small relative changes in concentration as to result in negligible transport. Thus the current generated depends almost entirely on what fraction of the minority carriers

are collected and the voltage attained depends on what portion of the excitation energy remains after collection. In SEM measurements, the bond breaking energy is provided by the high energy electrons of the beam. Shorting of the cell results in an electron-beam-induced-current (EBIC) that is sensitive to the minority carrier collection and the parameters that influence it.

The experimental configuration is shown in Fig. 1 where the high energy electron beam of an SEM strikes the top surface of the P-type Cu_xS layer and dissipates its energy in a tear-drop-shaped region where the excess minority carriers are generated(16). As the beam acceleration voltage is increased, the generation volume grows in size proportionately so that excess minority carriers are produced deeper into the device including the N-type CdS region. The universalized shape of the rate at which energy is lost in the material to produce minority carriers as a function of distance below the beam entry surface has been well described in normalized form by Everhart and Hoff (17) as

$$\lambda(y) = \frac{d(F/fE_o)}{d(x/R)} = 0.600 + 6.21y - 12.40y^2 + 5.69y^3 \qquad (1)$$

where E is the energy of the beam electrons, E_o is the beam acceleration energy of the SEM, (1-f) E_o is the fraction

of the initial energy carried away by backscattered electrons, and x is the distance below the beam entry surface. The R is the Gruen range which is a measure of the distance a high energy electron travels in a material before it loses its excess energy and becomes thermalized and y = x/R.

The Gruen range can be specified in terms of the acceleration energy E_o in keV and simple materials properties using Everhart and Hoff's results that indicate (17)

$$R = B\left(E_o\right)^{1.62} \text{ (cm)}. \qquad (2)$$

The coefficient B is determined by the struct material's average atomic number $\overline{Z}$, average atomic weight $\overline{A}$, and mass density ρ in addition to the ratio of the Bethe range to the Gruen range used here. These details were given in an earlier paper (18). The B values resulting for Cu_2S and CdS are given in Table I.

If one has a three layered material such as shown in Fig. 1 with perfect collection for the layer between x_1 and x_2 and zero collection from all other regions, then the EBIC current is specified by Everhart and Hoff's treatment (17) as

$$\frac{I(EBIC)}{I(Beam)E_o} = \frac{f}{E_A(12)} \int_{y_1}^{y_2} \lambda(y)dy \qquad (3)$$

where I(EBIC) is the electron-beam-induced current flowing through the device, I(Beam) is the amplitude of the incident electron beam current, and $E_A(12)$ is the average energy required to generate an electron-hole pair in the material between x_1 and x_2. Here $y_1 = x_1/R(01)$ and $y_2 = (x_2 - x_1)/R(12) + y_1$, where the Gruen ranges of the materials are R(01) between 0 and x_1 and R(12) between x_1 and x_2 respectively. Since carrier multiplication processes such as avalanche breakdown are not believed to be operative, the gain factor discussed by Everhart and Hoff has been taken equal to one. In the present work the above is extended to apply to the Cu_xS/CdS device of Fig. 1 to give

$$\frac{I(EBIC)}{I(Beam)E_o} = \frac{f}{E_A(Cu_xS)} \int_0^{y_1} w_1(y)\lambda(y)dy + \frac{f}{E_A(CdS)} \int_{y_1}^{y_2} w_2(y)\lambda(y)dy + \frac{f}{E_A(CdS)} \int_{y_2}^{y_3} w_3(y)\,\lambda(y)dy \qquad (4)$$

where the $w_i(y)$'s describe the less than perfect collection of minority carriers from each region and $y_3 = (x_3-x_2)/R(CdS) + y_2 + y_1$. Here it has been assumed that there is a much higher carrier concetration in the Cu_xS than in the CdS which causes the SCR to exist primarily in the CdS (see Fig. 1).

Typically collection of minority carriers in a space charge region (SCR) has been taken to be 100%. However to allow for the possibility of recombination at the heterojunction at x_2, it will be taken as

$$w_2(y) = \eta \tag{5}$$

where $0 \leq \eta \leq 1.0$. Minority carrier collection in the low field regions outside the SCR is obtained from solutions to the one dimensional diffusion equation applicable to planar samples. If one considers the modified boundary conditions such non-perfect performance of the SCR implies, it has been shown that this equation leads to (19)

$$w_1(y) = e^{-\frac{y_1 - y}{L(Cu_xS)/R(Cu_xS)}} H_{SCR}(Cu_xS) \cdot \left[\frac{1 + \beta(Cu_xS)\, e^{\frac{-2y}{L(Cu_xS)/R(Cu_xS)}}}{1 - \beta(Cu_xS)\, e^{\frac{-2y_1}{L(Cu_xS)/R(Cu_xS)}}} \right] \tag{6}$$

where

$$\beta = \frac{1 - S/V_d}{1 + S/V_d} \tag{7}$$

$$H_{SCR} = \frac{V^*/V_d}{1 + \frac{V^*}{V_d}\left[\frac{1 + \beta e^{-\frac{2y_1}{L/R}}}{1 - \beta e^{-\frac{2y_1}{L/R}}}\right]} \tag{8}$$

$$V_d = D/L \tag{9}$$

and S is the recombination velocity of the surface of the low field region opposite the SCR and D and L are the minority carrier diffusion constant and diffusion length respectively. The V* is a velocity characteristic of carrier transport across the SCR whose magnitude is determined by an integral involving the degree of band bending in this region(19). Likewise

$$w_3(y) = e^{-\frac{(y - y_2^*)}{L(CdS)/R(CdS)}} H^*_{SCR}(CdS) \cdot \left[\frac{1 + \beta(CdS)\, e^{-\frac{2(y_3^* - y)}{L(CdS)/R(CdS)}}}{1 - \beta(CdS)\, e^{-\frac{2(y_3^* - y_2^*)}{L(CdS)/R(CdS)}}}\right] \tag{10}$$

where

$$H^*_{SCR} = \frac{V^*/V_d}{1 + \frac{V^*}{V_d}\left[\frac{1 + \beta e^{-\frac{2(y_3^* - y_2^*)}{L/R}}}{1 - \beta e^{-\frac{2(y_3^* - y_2^*}{L/R}}}\right]} \qquad (11)$$

and $y_2^* = x_2/R(CdS)$ and $y_3^* = x_3/R(CdS)$. In typical homojunctions, the band bending is sufficiently large compared to kT where k is Boltzmann's constant and T is absolute temperature, that $V^* >> V_d$ and $w_1(y)$ and $w_3(y)$ reduce to the expressions of Hackett(20) who treated minority carrier collection in thin layers when perfect SCR collection is present. The above dependence is similar to that discussed by Rhoderick (21) for Schottky barriers where the degree of SCR band bending determines the dominant transport mechanism involved. When the low field regions of the device have widths that are large compared to the minority carrier difffusion lengths, the limiting expressions for junction collection efficiency apply so that Eqs. 8 and 11 give

$$H^{\infty}_{SCR} = H^{*\infty}_{SCR} = \frac{V^*/V_d}{1 + V^*/V_d} \quad . \qquad (12)$$

This simplification also occurs for the special case where S = V_d (see Eqs. 7, 8, and 11). For these two special cases, the H^{∞}_{SCR} is similar to that also found by Crowell and

Sze (22) for metal-semiconductor junctions. These limiting H_{SCR}^{∞} values provide a useful estimate of the junction collection efficiency that take on a value of one for the perfect collection case where $V^* >> V_d$. A more detailed treatment of the V* expressions is contained in Shea's Masters Thesis(23).

This present treatment is an extension of Wu and Wittry's studies(15) in that imperfect junction collection is considered as described by V*, a three region device is treated with a thin top film strongly influenced by the top surface as modeled with S, and Everhart and Hoff's polynomial expression for the generation volume was used. This earlier work(15) considered geometries uninfluenced by surfaces, perfect junction collection, and beam generation shapes approximated by a displaced Gaussian.

III. RESULTS

The experimental samples were prepared on 1-10 ohm-cm, vacuum deposited N-CdS approximately 30 microns thick with carrier concentrations in the $10^{17}/cm^3$ range as indicated by $1/C^2$ measurements. After an HCl etch, approximately 2000 Å of P-Cu_xS was epitaxially grown on the CdS by reactive sputtering (14) followed by a vacuum deposited gold grid to give a cell of 1 cm^2 area. The whole structure was heat

treated at 180°C in hydrogen-argon gas for the time periods specified below. Monitor films obtained in parallel to the CdS and Cu_xS formation, allowed both film thicknesses to be measured with a profiliometer with 20 percent accuracy. Hall effect measurement performed on the Cu_xS monitor films indicated carrier concentrations of about $10^{19}/cm^3$ and hole mobilities around 5.0 cm^2/V-sec(24) that justify the assumption of SCR formation almost totally in the CdS. The EBIC data was obtained with a Keithley 610R Electrometer and a Coates and Welter Field Emission SEM using a beam current of about 0.1 nA monitored with a Faraday cup.

The measured current-voltage characteristics of sample A exposed to simulated air mass 1 white light of 100 mW/cm^2 is shown in Fig. 2. This sample had been heat treated for 3 hours. The open circuit voltage was 0.447V, the short circuit current was 13.1 mA/cm^2, the fill factor was 0.603, and the efficiency was 3.53 percent. The EBIC data measured on sample A as a function of accelerating voltage is shown by the data points in Fig. 3. For convenience the acceleration voltage has been plotted as 1/2 R (Cu_xS) using Eq. 2. This was earlier shown (16) to locate the approximate center of the generation volume and thus allow the change in response

versus the position of the generation volume in the sample to be monitored. As can be seen this gives data very similar in form to that produced by physically scanning the beam along a cleaved surface perpendicular to the junction as previously reported for the destructive SEM measurements on single crystal substrate samples(19). In the present work no data for accelerating voltages less than 2.5 kV were utilized since the beam generation volume's shape begins to differ significantly from Everhart and Hoff's universalized forms for E_o values less than those specified in their treatment and listed in Table I (25-27).

The least-mean-squared (LMS) error fit of these sample A measurements with Eq. 4 is shown by the solid line curve in Fig. 3. The fixed parameters input into this expression are given at the top of Table II. The Cu_xS and CdS thicknesses were determined from the monitor slides using the profiliometer. The SCR thickness (x_3-x_2) was obtained from the zero bias capacitance C(0) using

$$(x_3 - x_2) = \frac{\epsilon A}{C(0)} \qquad (13)$$

where ϵ is the CdS dielectric constant taken as $10\epsilon_o$ and A is the cell area uncorrected for surface roughness (that can make true area somewhat greater than the area specified by the sample's perimeter dimensions). The $E_A(CdS)$ was taken from published values(28). The $E_A(Cu_xS)$ was taken as half the CdS value assuming that such quantities are approximately proportional to the band gap of the material involved. The f value was taken from published results(17,29).

The six parameters varied to provide the LMS fit are shown at the bottom of Table II. These values were converged upon by an algorithm that numerically calculated the gradient of the mean-squared-error between the theory (Eq. 4) and the data so that the fastest descent to the minima was specified. Fortunately each of the fitting parameters affected different parts of the curve in characteristic ways. In Fig. 4, the solid theoretical curves show how $L(Cu_xS)$ variations affect the slope of the curve near the Cu_xS surface (corresponding to the lowest acceleration voltages). For reference, the sample A data is shown here and in the three following figures. The Cu_xS surface recombination velocity determines the curvature of the data near this surface as indicated in Fig. 5. The vertical shifts caused by changes in the junction collection efficiency for the minority carrier electrons

coming from the Cu_xS are shown in Fig. 6. For reference the corresponding $H^{\infty}_{SCR} = (V^*/V_d)/(1 + V^*/V_d)$ values are shown for each curve. With submicron diffusion lengths, the EBIC properties are totally insensitive to the CdS surface recombination velocity at the back niobium contact located some 30 microns from the SCR.

For comparison, the Table II values correlate quite well to the $L(Cu_xS) = 0.25\ \mu m$, $L(CdS) = 0.40\ \mu m$, reported for the highest accuracy, destructive measurements recently reported for Cu_xS/CdS samples topotaxially formed on single crystal CdS(18). Particularily note that the present S/V_d (Cu_xS) value is the forth independent technique that gives this same magnitude. Previous measurement of this quantity involved the Gatos slope-parallel-surface technique (19,30), and the van Roosbroeck curvature technique (18,31), and the Berz and Kuiken slope-perpendicular-surface technique (32,33) all of which gave the same results to within 20 percent. This present work is the first to specify absolute values for junction collection efficiency. Earlier studies gave only relative changes (19). The V^*/V_d collection-determining ratios of Table II correspond to junction collections efficiencies estimated by the limiting expressions of Eq. 12 as $H^{\infty}_{SCR}(Cu_xS) = 0.39$ and $H^{\infty}_{SCR}(CdS) = 0.50$ indicating

that about half of the minority carriers originating on either the Cu_xS or CdS sides of the device are lost in traversing the SCR. The effect that perfect collection ($V^* >> V_d$) should have on these data is shown by the vertical shift in the solid line curves in Fig. 7.

The evolution of such EBIC data with the 180°C, hydrogen-argon heat treatment is shown in Figs. 8 and 9 for sample B for treatment times between 30 and 120 minutes. While moderate changes could be occurring in several of the variables, the dominant effect is the vertical shift in the curves upward to a maximum followed by a decrease indicative of junction collection efficiency variations. The LMS error fits of these data were obtained for the parameters listed in Table III. The fixed parameter values were determined as with sample A. Within the accuracy of this data, the only significant changes during heat treatment were in those parameters determining junction collection efficiency. The approximations of this efficiency specified by $H^{\infty}_{SCR}(Cu_xS)$, $H^{\infty}_{SCR}(CdS)$, and the SCR parameter η are plotted in Fig. 10 versus heat treatment time. This result is analogous to that reported for heat treatment data in an air ambient measured on a sample formed on single crystal CdS with a wet dip, topotaxial Cu_xS layer. Thus the dominant change with heat treatment has again been shown to be with variations in junction collection efficiency with no significant variations

found in the minority carrier diffusion lengths or the Cu_xS surface recombination velocity. The present work was for polycrystalline CdS with an epitaxial, reactively sputtered Cu_xS layer heat treated in a hydrogen-argon ambient.

CONCLUSIONS

The non-destructive SEM techniques of Wu and Wittry (15) have been extended so that thin, multi-layer, polycrystalline films can be analyzed. This required theory modifications to account for the effects of surface recombination velocity and non-perfect collection by the space-charge-region. Such SCR behavior is related to similar effects analyzed by Rhoderick(21) and by Crowell and Sze(22). When applied to Cu_xS/CdS heterojunction solar cells heat treated at 180°C in hydrogen-argon, it showed that $L(Cu_xS)$ and L(CdS) had relatively constant values in the 0.20-0.26 and the 0.41-0.46 micron ranges respectively and that $S/V_d(Cu_xS)$ remained at the same 1.0 magnitude. However the junction collection efficiencies increased by more than a factor of two to a maximum and then decreased for treatment times of up to 120 minutes. When combined with earlier results (19), the SEM studies have shown that junction collection efficiency changes are the dominant effect of heat treatment in air and in hydrogen-

argon ambients for cells formed on polycrystalline and single crystal CdS upon which Cu_xS was formed topotaxially or epitaxially. Further study and optimization of this process could be expected to provide for improved device performance.

ACKNOWLEDGEMENTS

Appreciation is due to H. Brown for careful fabrication of the CdS substrates. Discussions of the results with J. Yee and J. Leong were most helpful. Thanks are due to D. Rae for patience and care in the manuscript preparation.

Table I. The coefficients for the Gruen range calculated from the Everhart and Hoff results

Material	ρ (g/cm^3)	$\bar{Z}$	$\bar{A}$ (g)	B	Allowed E_o Range(keV)
Cu_2S	5.60	24.7	53.0	$1.55(10^{-6})$	2.34-23.4
CdS	4.82	32.0	72.2	$2.06(10^{-6})$	2.94-29.4

Table II. Parameter values used to provide the least-mean-squared error fit of the data measured on sample A as shown in Fig. 3.

Fixed Parameters:

Cu_xS Thickness = 0.25 μm

CdS Thickness = 30 μm

SCR Thickness = 0.25 μm

$E_A(CdS)$ = 7.8 eV

$E_A(Cu_xS)$ = 3.9 eV

f = 0.9

Fitting Parameters:

$L(Cu_xS)$ = 0.26 μm

L(CdS) = 0.43 μm

$V^*/V_d(Cu_xS)$ = 0.65

$V^*/V_d(CdS)$ = 0.98

η = 0.52

$S/V_{d(Cu_{xS})}$ = 1.0

Table III. Parameter values used to provide the least-mean-squared error fit of the heat treatment data measured on sample B and presented in Figs. 8 and 9.

Fixed Parameters:

Cu_xS Thickness = 0.20 μm
CdS Thickness = 31 μm
SCR Thickness = 0.18 μm
$E_A(CdS)$ = 7.8 eV
$E_A(Cu_xS)$ = 3.9 eV
f = 0.9

Heat Treatment Time	Fitting Parameters					
			V^*/V_d			S/V_d
(min)	$L(Cu_xS)$ (μm)	L(CdS) (μm)	Cu_xS	CdS	η	(Cu_xS)
30	0.23	0.43	0.24	0.12	0.18	1.0
75	0.22	0.46	0.41	0.51	0.51	1.0
90	0.24	0.42	0.86	1.05	0.81	1.0
120	0.20	0.41	0.50	0.39	0.56	1.0

References

1. A. E. Middleton, D. A. Gorski, and F. A. Shirland, "Evaporated CdS Film Photovoltaic Cells for Solar Energy Conversion," in Energy Conversion for Space Power, Progress in Astronautics and Rocketry, N. W. Snyder Ed. (Academic Press, NY, 1961), p. 275.
2. F. A. Shirland, "The History, Design, Fabrication and Performance of CdS Thin Film Solar Cells," Advanced Energy Conversion 6, 201 (1966).
3. L. R. Shiozawa, G. A. Sullivan, and F. Augustine, "The Mechanism of the Photovoltaic Effect in High Efficiency CdS Thin-Film Solar Cells," 7th IEEE Photovoltaic Specialists Conf. Record, Nov. 1968, p. 39, also available in Solar Cells, C. E. Backus, Ed. (IEEE Press, NY, 1976) p. 231.
4. L. R. Shiozawa, F. Augustine, G. A. Sullivan, J. M. Smith III and W. R. Cook, "Research on the Mechanism of the Photovoltaic Effect in High Efficiency CdS Thin-Film Solar Cells," Aerospace Research Laboratories Rept. No. ARL 69-0155, Clevite Corp, Oct. 1969.
5. S. Martinuzzi and O. Mallem, "Dark-Current Conduction Processes in CdS-Cu_2S Thin-Film Photocells," Phys. Stat. Sol. (A) 16, 339 (1973).
6. A. Rothwarf, "Theoretical Prospects of the CdS-Cu_2S Solar Cell," Intern. Conf. on Solar Energy, Toulouse, France, Mar. 1976.
7. A. Rothwarf and A. M. Barnett, "Design Analysis of the Thin-Film CdS-Cu_2S Solar Cell," IEEE Trans. Electron Devices, ED-24, 381 (1977).

8. A. Amith, "Thin-Film CdS/Cu_2S Heterojunctions: Dark I-V Characteristics and Heat Treatment," J. Appl. Phys. 50, 1160 (1979).

9. J. J. Loferski, J. Shewchun, S. D. Mittleman, E. A. DeMeo, R. Arnott, H. L. Hwang, and R. Beaulieu, "Cathodoluminescence Characteristics of Cu_xS Films Produced by Different Methods," Solar Energy Materials 1, 157 (1979).

10. A. G. Milnes and D. L. Feucht, Heterojunction and Metal-Semiconductor Junctions (Academic Press, NY, 1972).

11. S. P. Shea and L. D. Partain, "Heat Treatment Effects on the Minority Carrier Diffusion Lengths, Surface Recombination Velocity and Junction Collection Factor of Cu_xS/CdS Solar Cells," 13th IEEE Photovoltaic Specialists Conf., Washington, DC, June 1978, p. 393.

12. L. D. Partain and S. P. Shea, "SEM Measurement of Diffusion Lengths, Recombination Velocity, and Junction Collection Efficiency in Heterojunction Solar Cells: Application to Cu_xS/CdS," IEEE Intern. Electron Devices Meeting Techn. Digest, Washington, DC, Dec. 1978, p. 239.

13. A. Rothwarf, J. Phillips, and N. Convers Wyeth, "Junction Field and Recombination Phenomena in the CdS/Cu_2S Solar Cell: Theory and Experiment," 13th IEEE Photovoltaic Specialists Conf. Record, Washington, DC, June 1978, p. 399.

14. G. A. Armantrout, D. E. Miller, K. E. Vindelov, and T. G. Brown, "Formation of Thin Cu_2S (Chalcocite) Films Using Reactive Sputtering Techniques," J. Vacuum Science and Technology 16, 212 (1979).

15. C. J. Wu and D. B. Wittry, "Investigation of Minority-Carrier Diffusion Lengths by Electron Bombardment of Schottky Barriers," J. Appl. Phys. 49, 2877 (1978).

16. S. P. Shea, L. D. Partain, and P. J. Warter, "Resolution Limits of the EBIC Technique in the Determination of Diffusion Lengths in Semiconductors," in Scanning Electron Microscopy 1978, Vol. I (SEM Inc., AMF O'Hare, IL, 1973), p. 435.

17. T. E. Everhart and P. H. Hoff, "Determination of Kilovolt Electron Energy Dissipation vs Penetration Distance in Solid Materials," J. Appl. Phys. 42, 5837 (1971).

18. L. D. Partain and S. P. Shea, "Obtaining Accurate Values of Diffusion Length with the Scanning Electron Microscope," 2nd European Communities Photovoltaic Solar Energy Conf., West Berlin, April 1979 (D. Reidel Publ. Co., Dordrecht, Holland, 1979), p. 639.

19. L. D. Partain and S. P. Shea, "SEM Measurement of Diffusion Lengths, Recombination Velocity, and Junction Collection Efficiency in Heterojunction Solar Cells: Application to Cu_xS/CdS," Intern. Electron Devices Meeting Techn. Digest, Washington, DC, Dec. 1978, p. 239.

20. W. H. Hackett, Jr., "Electron-Beam Excited Minority-Carrier Diffusion Profiles in Semiconductors," J. Appl. Phys. 43, 1649 (1972).

21. E. H. Rhoderick, "Comments on the Conduction Mechanism in Schottky Diodes," J. Phys. D, 5, 1920 (1972).

22. C. R. Crowell and S. M. Sze, "Current Transport in Metal-Semiconductor Barriers," Solid-State Electronics 9, 1035 (1966).

23. S. P. Shea, Masters Thesis, Electrical Engineering Dept., Univ. Delaware, June 1978 (also available as Institute of Energy Conversion Techn. Rept. IEC/PV/TR/77/4, Univ. Delaware, Dec. 1977).

24. J. Y. Leong and J. H. Yee, "Hall Effect in Reactively Sputtered Cu_xS," Applied Physics Letters (in press).

25. S. P. Shea, Private communication, Mar. 1979.
26. R. F. Herzog, J. S. Greeneich, T. E. Everhart, and T. Van Duzer, "Computer-Controlled Resist Exposure in the Scanning Electron Microscope," IEEE Trans. Electron Devices, ED-19, 635, (1972).
27. W. Ehrenberg and D. E. N. King, "The Penetration of Electrons into Luminescent Materials," Proc. Phys. Soc. (London) 81, 751 (1963).
28. H. J. Leamy, L. C. Kimerling and S. D. Ferris, "Electron Beam Induced Current" in Scanning Electron Microscopy/1978, Vol. I, (SEM Inc., AMF O'Hare, IL, 1978). p. 717.
29. H. E. Bishop,"Electron Scattering in Thick Targets," Brit. J. Appl. Phys. 18, 703 (1967).
30. M. Watanabe, G. Actor, and H. C. Gatos, "Determination of Minority-Carrier Lifetime and Surface Recombination Velocity with High Spacial Resolution," IEEE Trans. Electron Devices, ED-24, 1172 (1977).
31. W. van Roosbroeck, "Injected Current Carrier Transport in a Semi-Infinite Semiconductor and the Determination of Lifetimes and Surface Recombination Velocities," J. Appl. Phys. 26, 380 (1955).
32. S. P. Shea and L. D. Partain, "Effect of Heat Treatments on the Minority Carrier Diffusion Lengths and Junction Collection Factor in Cu_xS/CdS Solar Cells," World Electrotechnical Congress, Moscow, June 1977.
33. F. Berz and H. K. Kuiken, "Theory of Life Time Measurements with the Scanning Electron Microscope: Steady State," Solid St. Electron 19, 437 (1976).

List of Figure Captions

Fig. 1 Sample and electron beam arrangement that allows non-destructive EBIC measurements of minority carrier transport parameters on thin film, polycrystalline, heterojunction devices.

Fig. 2. The current density-voltage properties of sample A exposed to simulated AM1, 100 mW/cm^2 white light.

Fig. 3. The sample A variation of EBIC data with acceleration voltage displayed as an "effective" depth of penetration into the Cu_xS. Data points were experimentally measured. The solid curve is the theoretical least-mean-squared error fit of the data for the parameter values of Table III.

Fig. 4. Variation of the theoretical results with changes in the Cu_xS minority carrier diffusion length. Sample A data points are shown for reference.

Fig. 5. Variation of the theoretical results with changes in the Cu_xS surface recombination velocity. Sample A data point are shown for reference.

Fig. 6. Variation of the theoretical results with changes in the efficiency with which the SCR collects minority carriers arriving from the Cu_xS. This efficiency is approximated here by $H_{SCR}^{\infty} = (V^*/V_d)/(1 + V^*/V_d)$. Sample A data are shown for reference.

Fig. 7. Improvement in the theoretical results that would be achieved with perfect collection of minority carriers as modeled when $V^* >> V_d$ for both the Cu_xS and CdS and when $\eta = 1.0$. Sample A data are shown for reference.

Fig. 8 The effects of 180° C, hydrogen-argon ambient heat treatment of sample B shown by the data points for 30, 75, and 90 minute treatment times. The solid curves are the least-mean-squared error fits of the data obtained with the parameter values listed in Table IV.

Fig. 9 The effects of 180°C, hydrogen-argon ambient heat treatment of sample B shown by the data points for 90 and 120 minute treatment times. The solid curves are the least-mean-squared error fits of the data obtained with the parameter value listed in Table IV.

Fig. 10 The variations in junction collection efficiencies of sample B as a function of hydrogen-argon heat treatment time at 180°C. The Cu_xS and CdS efficiencies are approximated by H^{∞}_{SCR} and $H^{*\infty}_{SCR}$ respectively and the SCR itself is described by η .

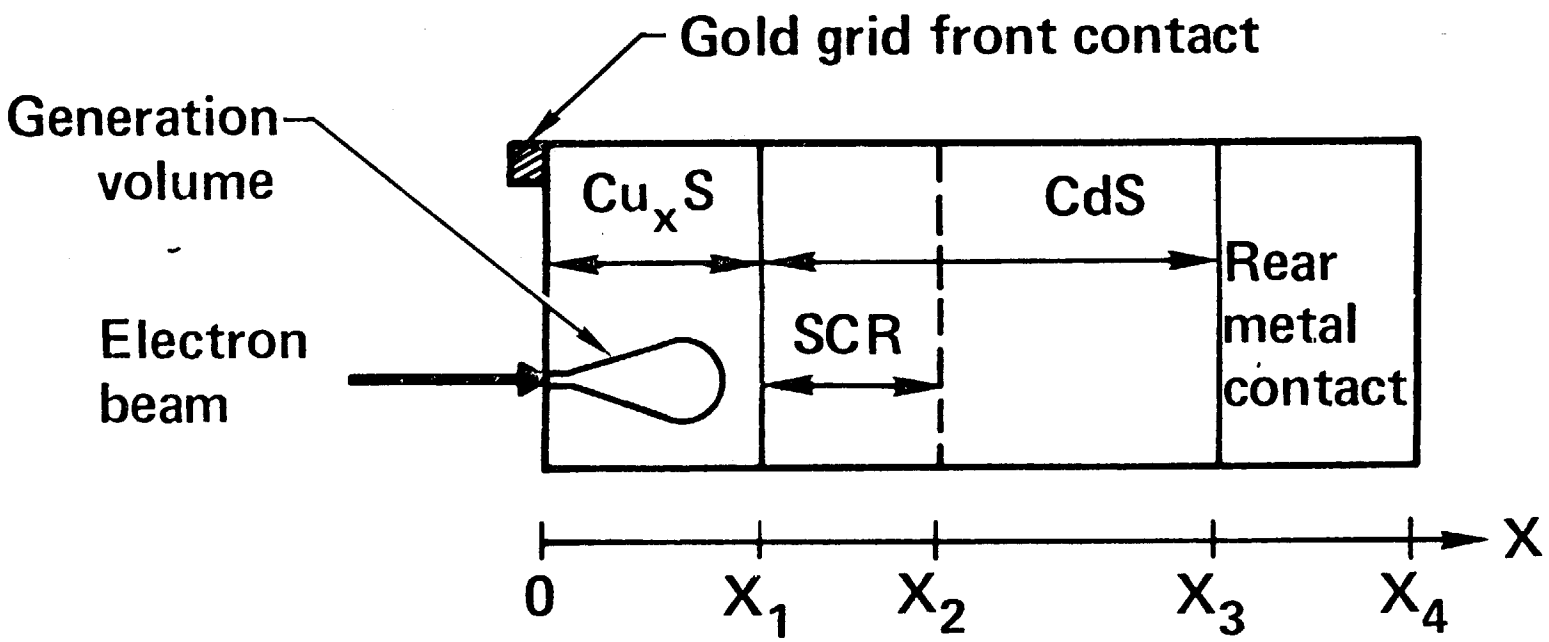

Fig. 1 Sample and electron beam arrangement that allows non-destructive EBIC measurements of minority carrier transport parameters on thin film, polycrystalline, heterojunction devices.

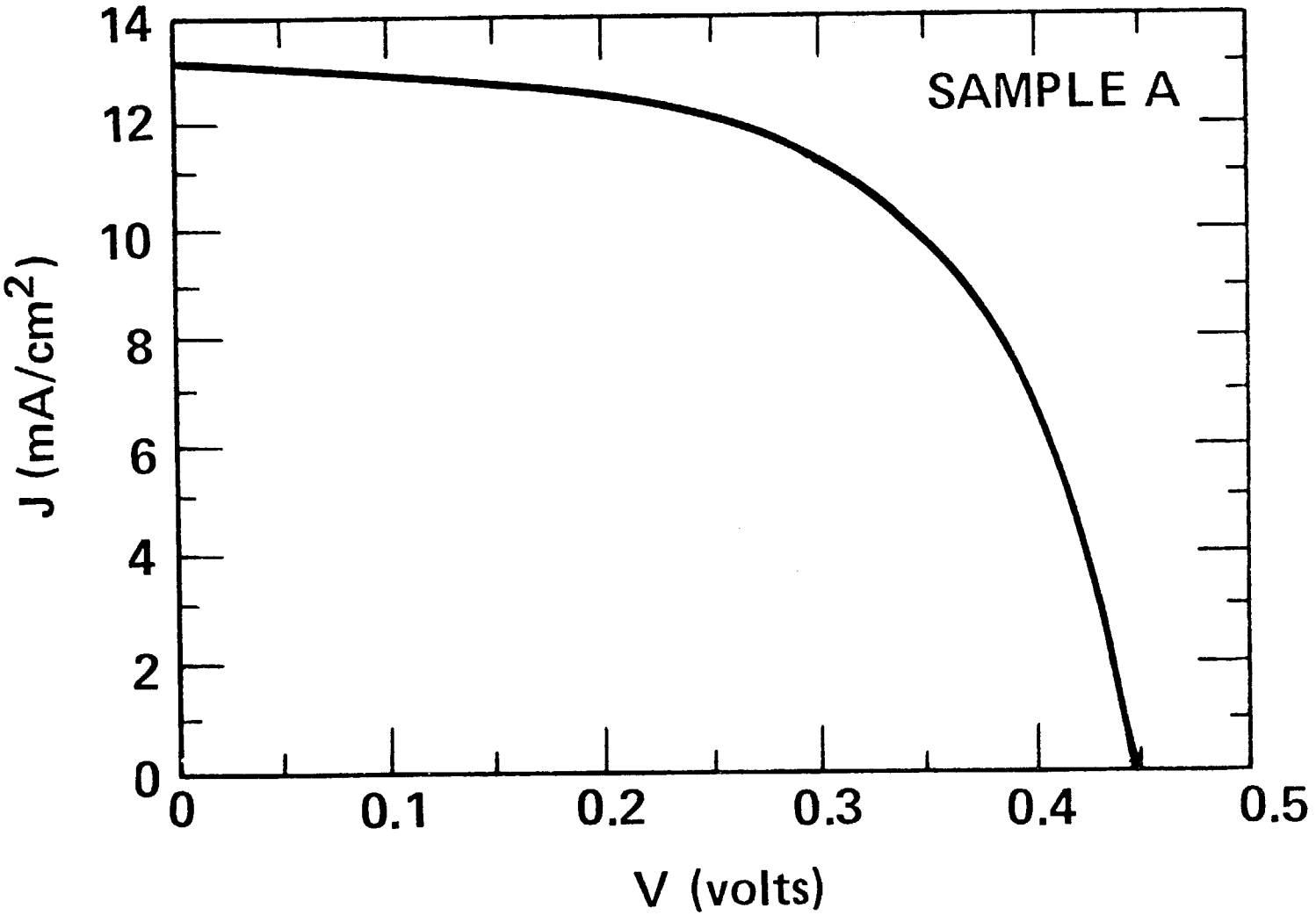

Fig. 2. The current density-voltage properties of sample A exposed to simulated AM1, 100 mW/cm^2 white light.

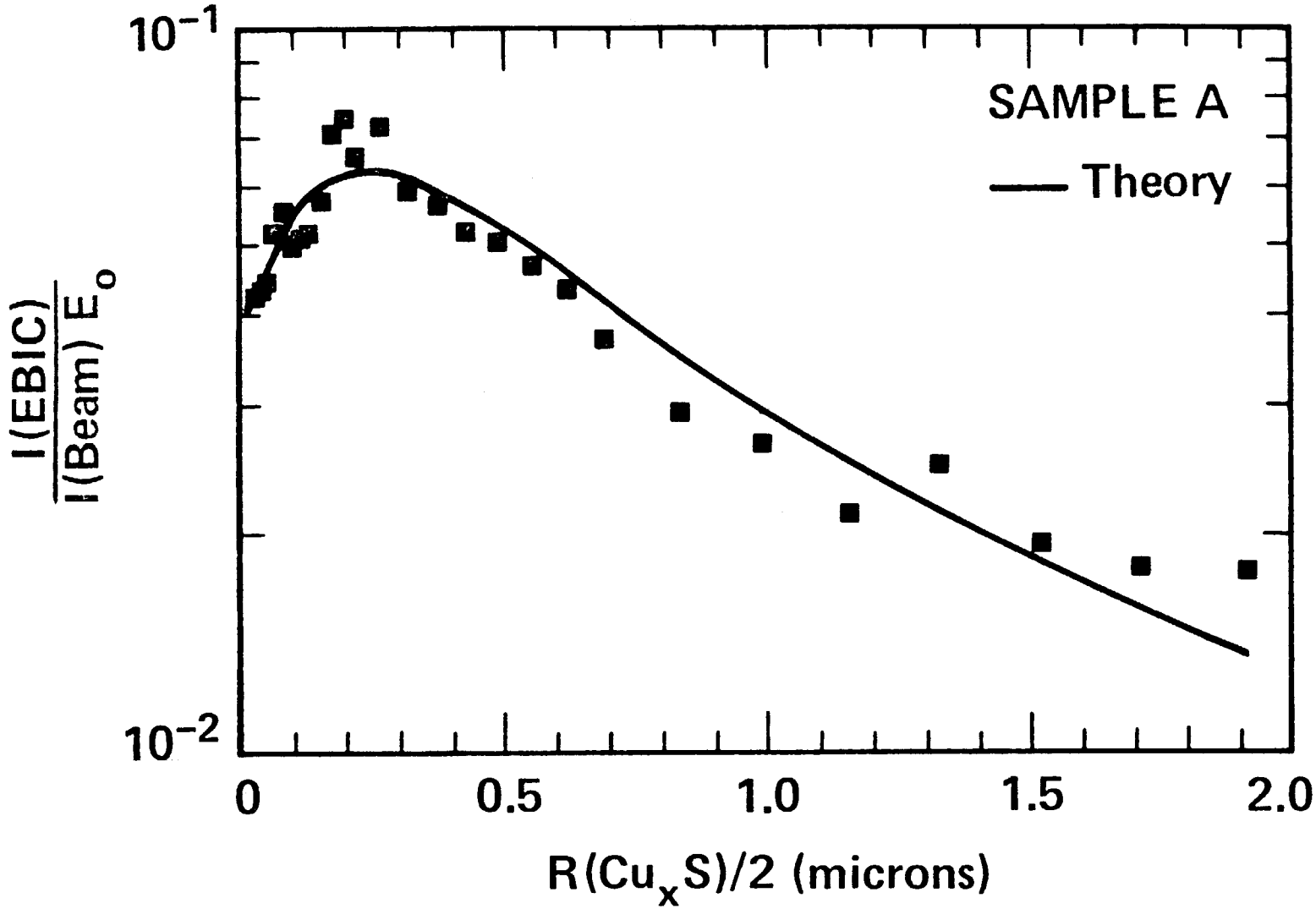

Fig. 3. The sample A variation of EBIC data with acceleration voltage displayed as an "effective" depth of penetration into the Cu_xS. Data points were experimentally measured. The solid curve is the theoretical least-mean-squared error fit of the data for the parameter values of Table III.

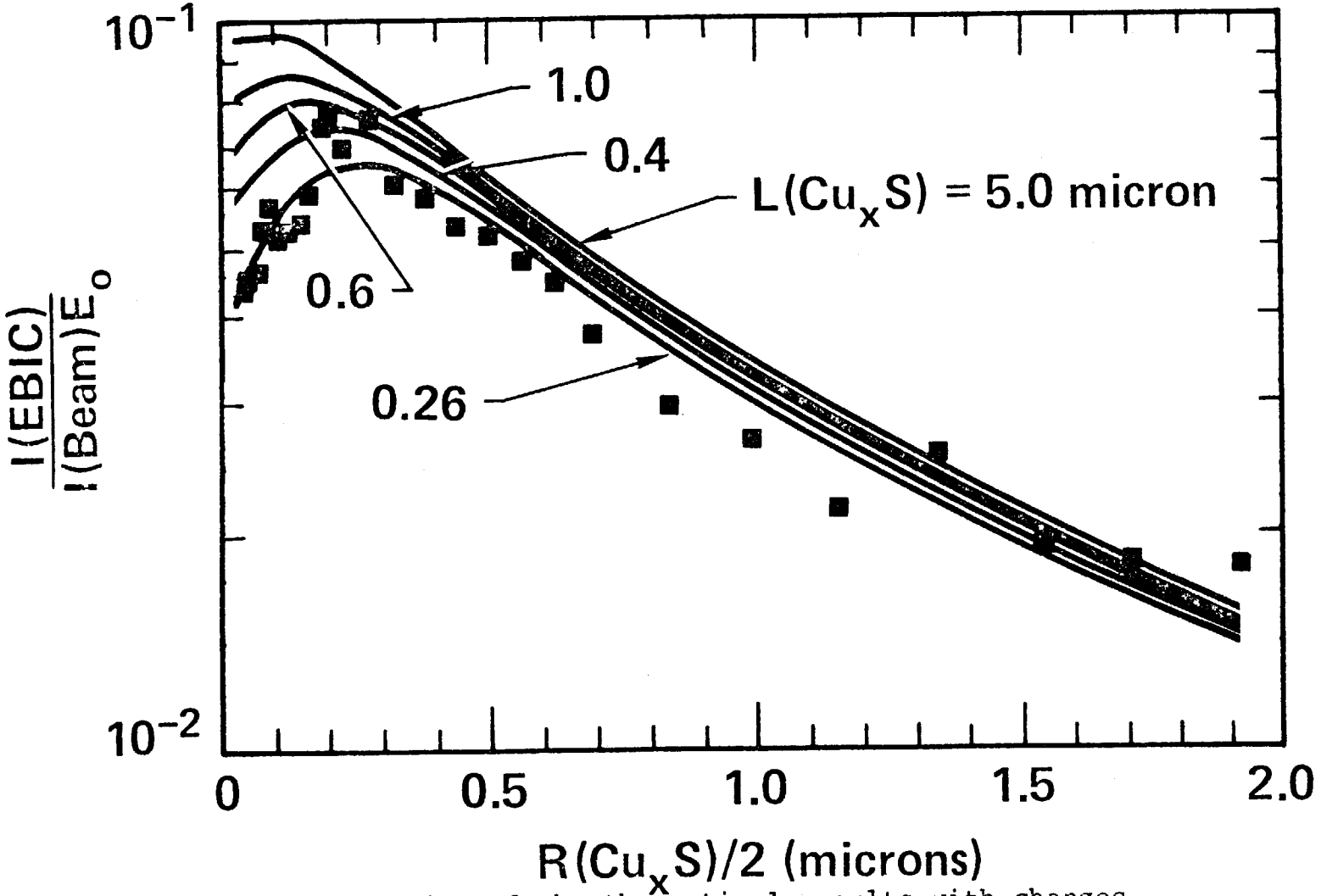

Fig. 4. Variation of the theoretical results with changes in the Cu_xS minority carrier diffusion length. Sample A data points are shown for reference.

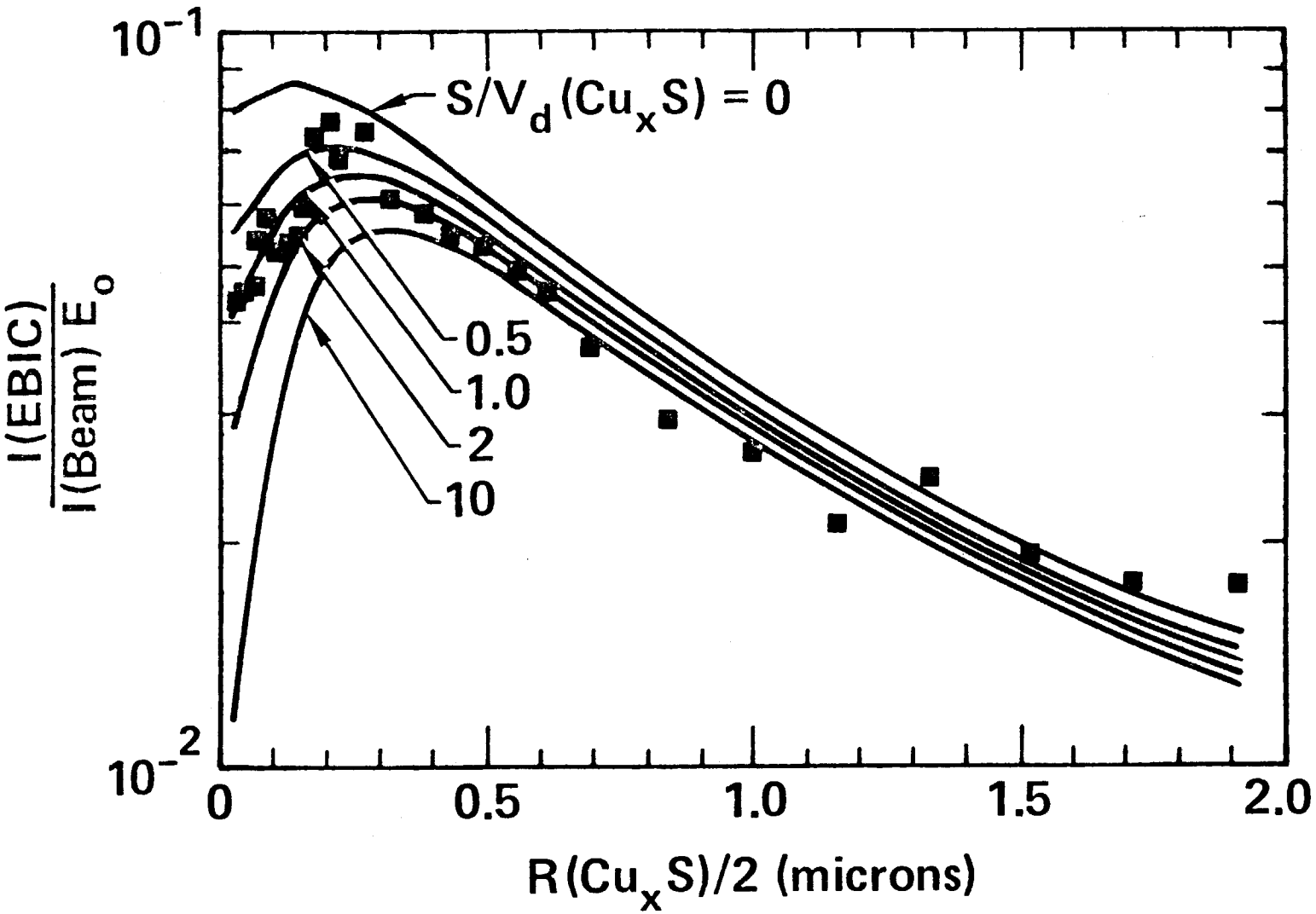

Fig. 5. Variation of the theoretical results with changes in the Cu_xS surface recombination velocity. Sample A data point are shown for reference.

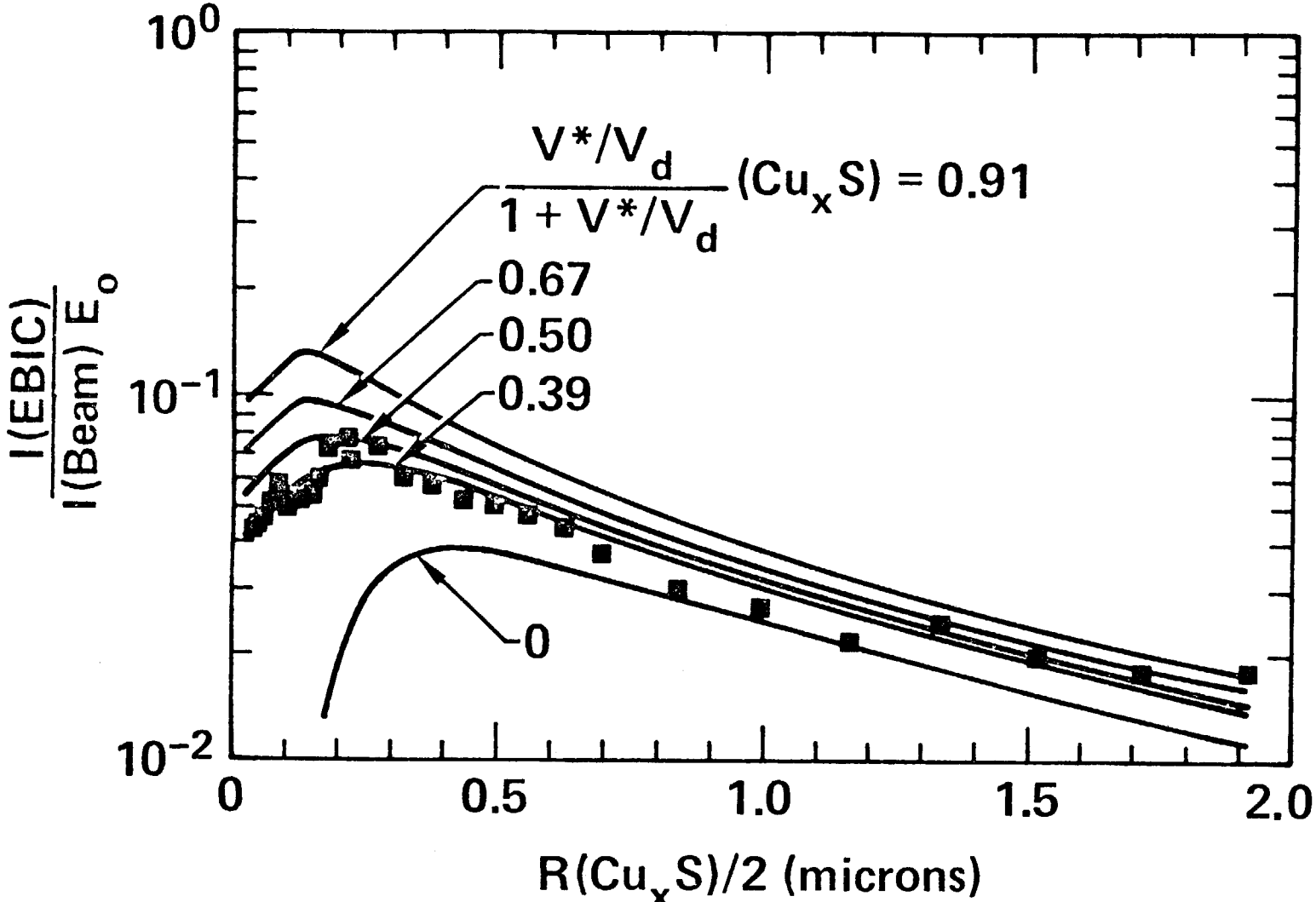

Fig. 6. Variation of the theoretical results with changes in the efficiency with which the SCR collects minority carriers arriving from the Cu_xS. This efficiency is approximated here by $H^{\infty}_{SCR} = (V^*/Vd)/1 + V^*/Vd)$. Sample A data are shown for reference.

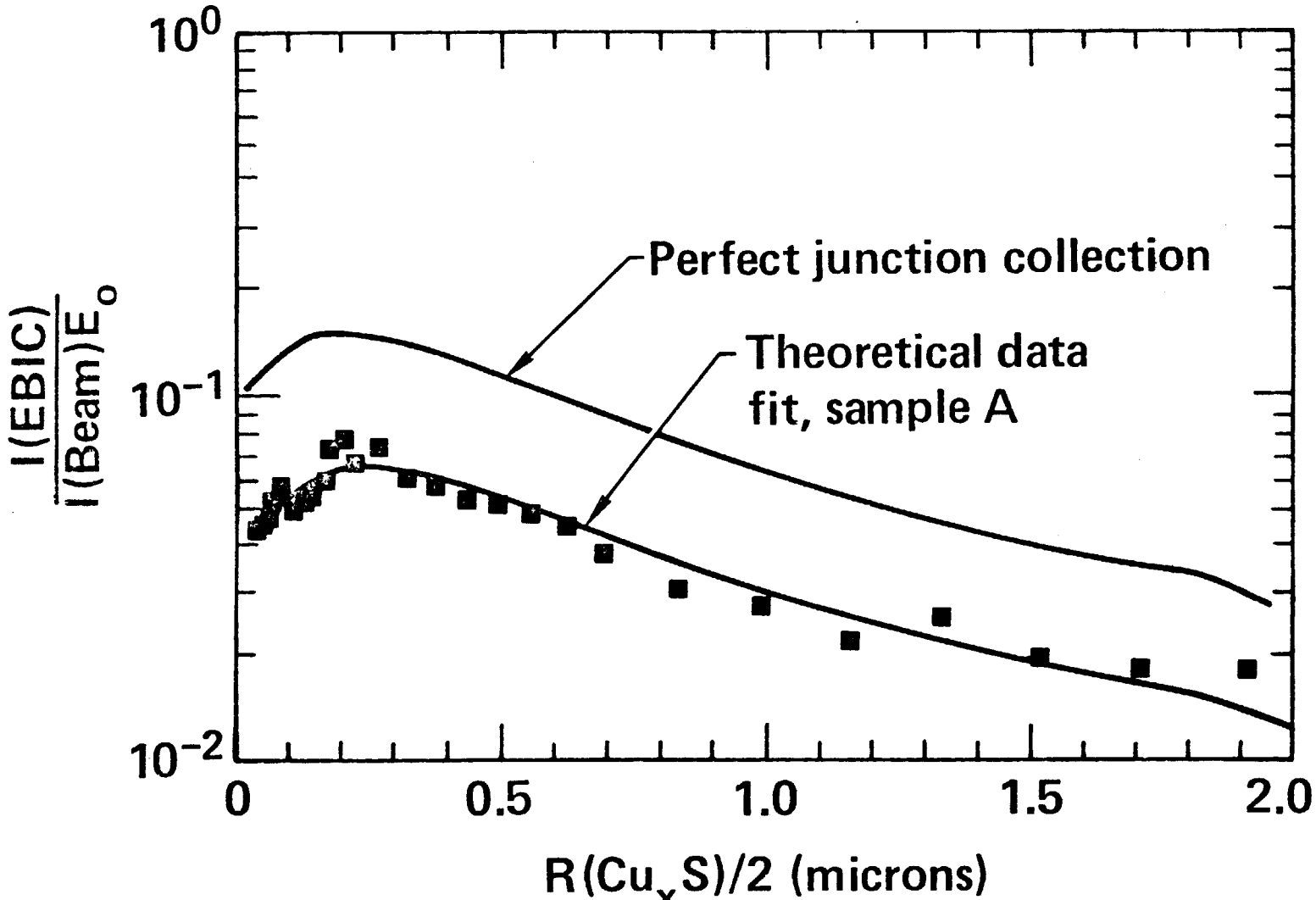

Fig. 7. Improvement in the theoretical results that would be achieved with perfect collection of minority carriers as modeled when $V^* >> V_d$ for both the Cu_xS and CdS and when $\eta = 1.0$. Sample A data are shown for reference.

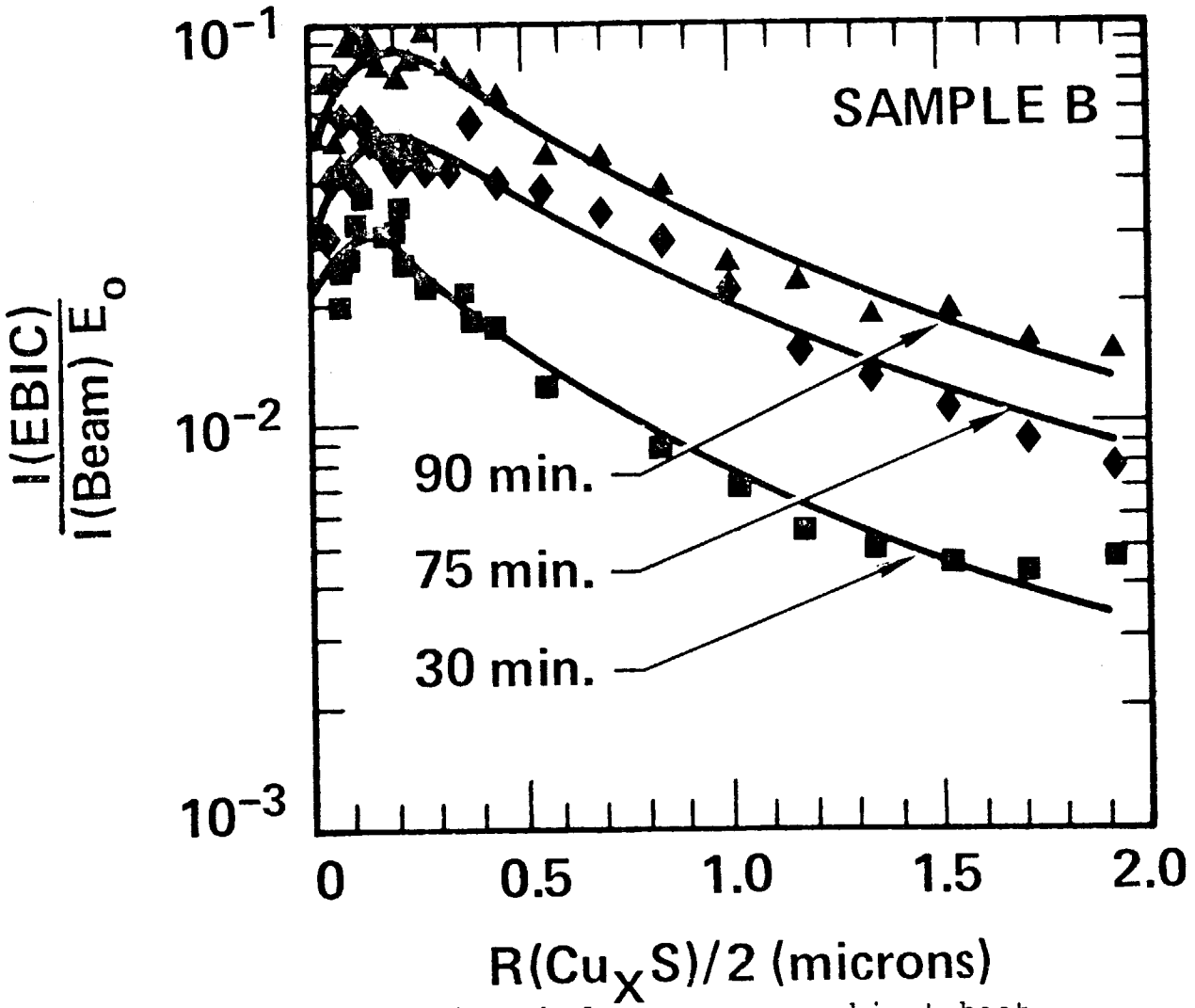

Fig. 8 The effects of 180° C, hydrogen-argon ambient heat treatment of sample B shown by the data points for 30, 75, and 90 minute treatment times. The solid curves are the least-mean-squared error fits of the data obtained with the parameter values listed in Table IV.

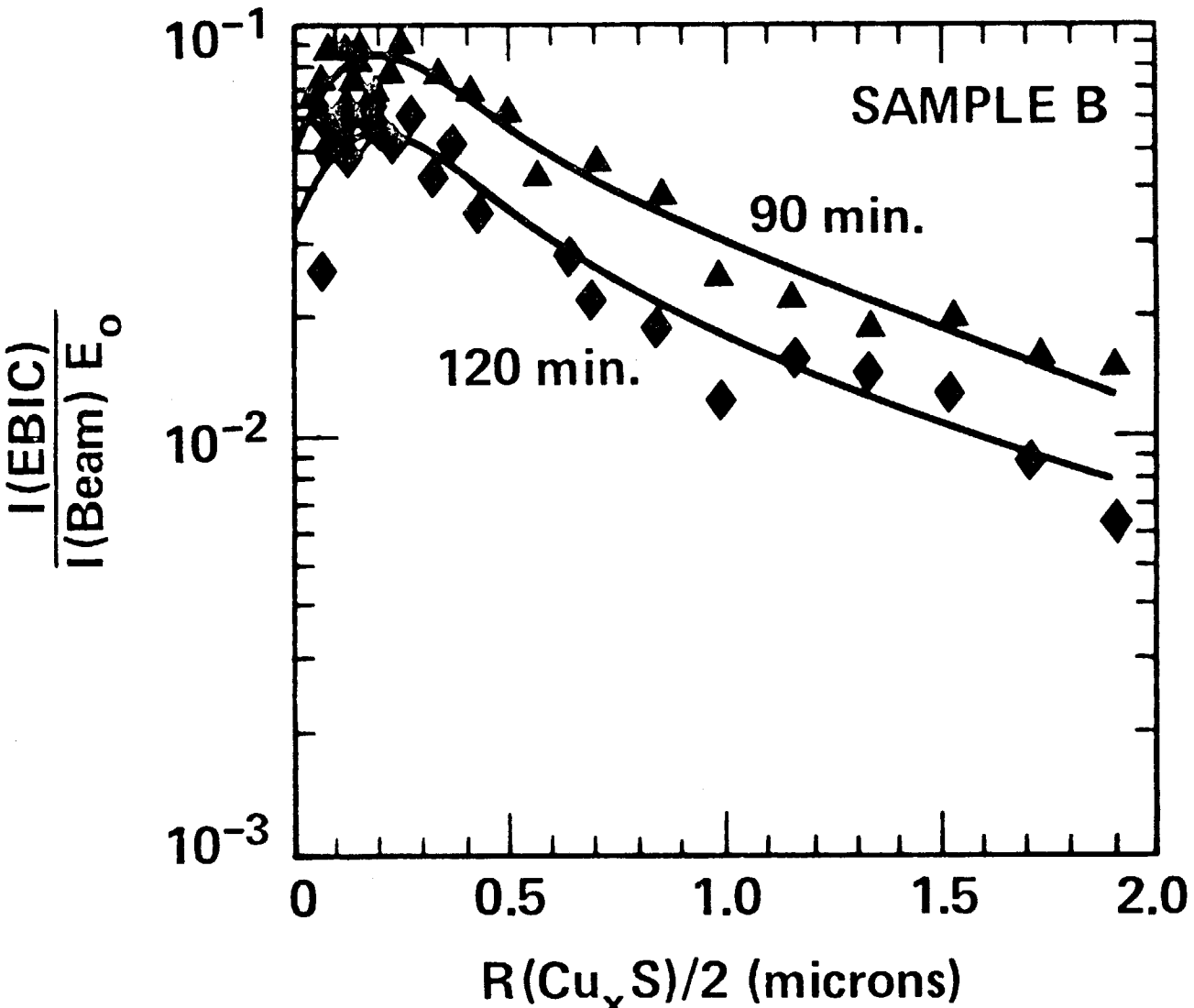

Fig. 9 The effects of 180°C, hydrogen-argon ambient heat treatment of sample B shown by the data points for 90 and 120 minute treatment times. The solid curves are the least-mean-squared error fits of the data obtained with the parameter value listed in Table IV.

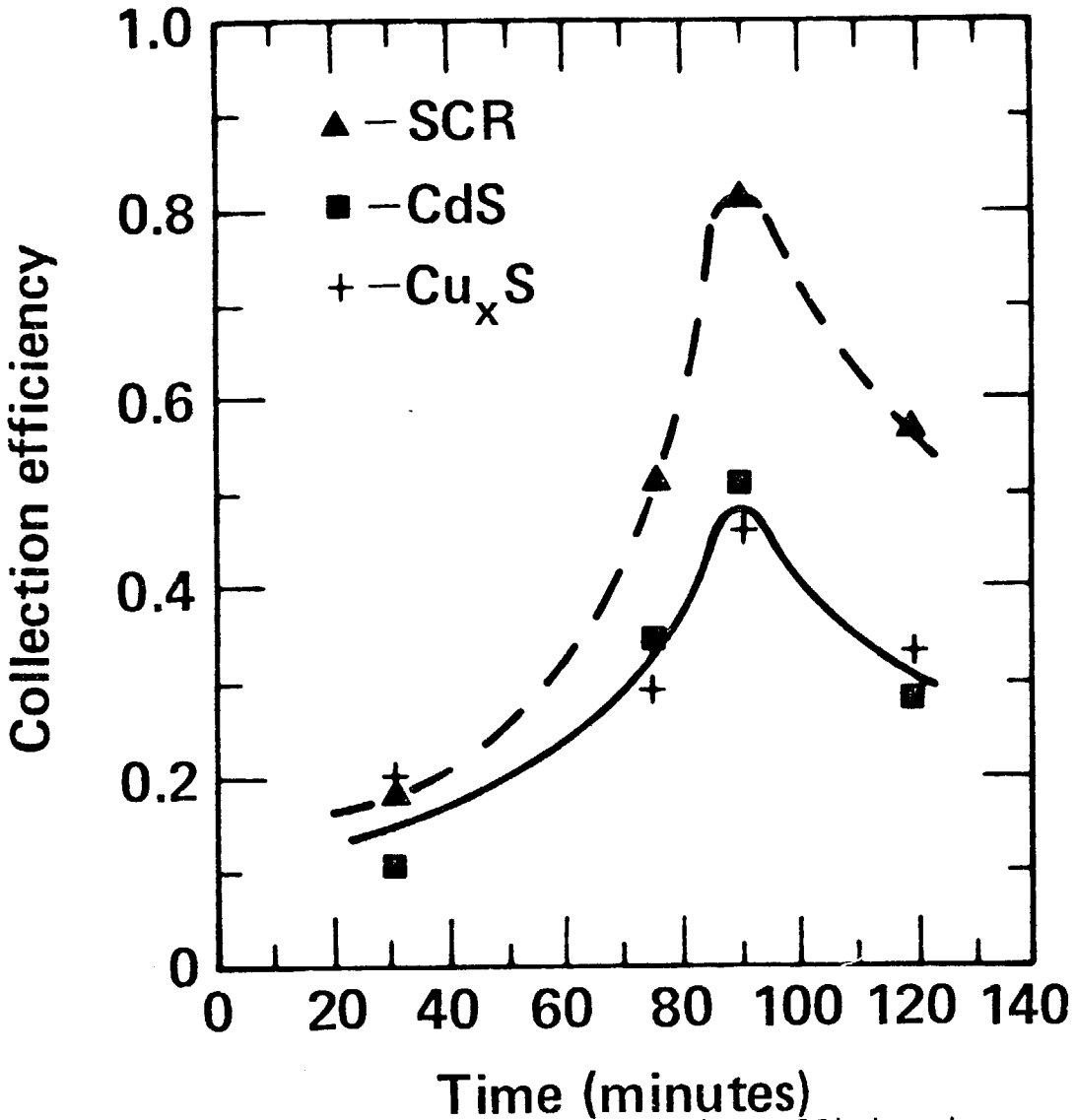

Fig. 10 The variations in junction collection efficiencies of sample B as a function of hydrogen-argon heat treatment time at 180°C. The Cu_xS and CdS efficiencies are approximated by H^{∞}_{SCR} and $H^{*\infty}_{SCR}$ respectively and the SCR itself is described by η.

Hall effect in reactively sputtered Cu_2S

John Y. Leong and Jick H. Yee
Lawrence Livermore Laboratory, University of California, Livermore, California 94550

(Received 16 April 1979; accepted for publication 6 August 1979)

The Hall effect in thin films of reactively sputtered Cu_2S was measured at temperatures from 90 to 300°K. The hole concentration ranged from 10^{18} to 2×10^{19} cm^{-3}. The hole mobility ranged from 5.5 to 9 cm^2/V s. The predominant scattering mechanisms are ionized impurity scattering at $T < 100$°K and optical phonon scattering at $T > 100$°K.

PACS numbers: 72.20.Fr, 71.55. – i

Cu_2S is a semiconductor of considerable interest for solar cell application, but many basic properties such as dominant scattering mechanisms are still not well understood. Findings of a study of the Hall effect in thin-film Cu_2S are presented in this letter.

Similar studies have been made, but the results are inconclusive. The first such study was conducted by Hirahara[1] in 1951. His measurements were made on polycrystalline bulk material at temperatures of – 20 to 250 °C. He reported a room-temperature hole mobility μ_h of 12 cm^2/V·s. Nonstoichiometric samples with excess sulphur had lower μ_h and higher hole concentration p than the stoichiometric ones. He therefore concluded that impurity scattering played a dominant role in free-carrier transport in Cu_2S. Abdullaev *et al.*[2] measured μ_h in single crystals of Cu_2S from 20 to 600 °C. The hole mobility was 25 cm^2/V·s at room temperature and decreased with increasing temperature, with a $T^{-3/2}$ dependence, up to 250 °C. Consequently, acoustic phonon scattering was believed to be dominant in this temperature range. Sorokin and Paradenko[3] observed the same temperature dependence in polycrystalline thick layers and thin films of Cu_2S. The mobility in thin films was about 5 cm^2/V·s, while that of bulk material was an order of magnitude larger. The great difference in mobility was explained by grain boundary scattering, which was much more prevalent in thin films. Later, Sorokin *et al.*[4] reported μ_h as high as 90 cm^2/V·s in single-crystal Cu_2S that deviated by less than 3% from stoichiometric. More recently, Bougnot *et al.*[5] reported hole mobilities of 4 cm^2/V·s in bulk Cu_2S. The μ_h is almost independent of temperature from 77 to 200 K, then decreases with increasing temperature according to $T^{-3/2}$.

The samples used in the present study were obtained by rf reactive sputtering of copper onto glass slides in an H_2S/Ar atmosphere. The photovoltaic research group at Lawrence Livermore Laboratory has demonstrated that nearly stoichiometric Cu_2S can be obtained by using this process.[6] The samples were $1\times1\times10^{-4}$-cm films with gold contacts evaporated onto the four corners. The magnetic field strength used was 8.6 kG. The voltage measuring system was capable of detecting signals as low as 1.0 μV. The temperature ranged from 90 to 300 °K and could be controlled to within 1 °K.

Raw data were reduced by the van der Pauw method to obtain the resistivity ρ and Hall mobility μ_H.[7] The hole concentration was then calculated from

$$p = 1/q\rho\mu_H\,, \tag{1}$$

where q is the electronic charge.

The Hall mobility was used in place of the drift mobility in the calculations, because for the common scattering mechanisms (ionized and neutral impurity, acoustic and optical phonon, and piezoelectric scattering) the Hall scattering factor is nearly unity. In particular, for optical phonon scattering, which dominates over most of the measured temperature range, the scattering factor is between 1.00 and 1.06.[8]

Data from a typical sample are presented in Figs. 1–3. Figure 1 is a semilog plot of hole concentration versus reciprocal temperature. The hole concentration p is related to temperature by

$$p \propto \exp[-(E_A - E_V)/2kT]\,, \tag{2}$$

where E_A is the energy of acceptors (eV), E_V is the valance band edge (eV), k is Boltzmann's constant, and T is temperature (°K). From the slopes of the plot there appears to be a series of close-lying states with $(E_A - E_V) = 0.013$, 0.053, 0.073, and 0.17 eV. This is consistent with the high defect concentrations present in Cu_2S.

A log-log plot of μ_h versus T is presented in Fig. 2. As a

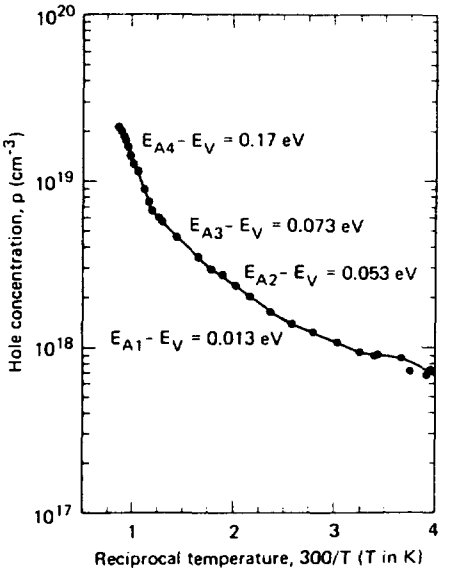

FIG. 1. Hole concentration versus reciprocal temperature.

 0003-6951/79/200601-02$00.50

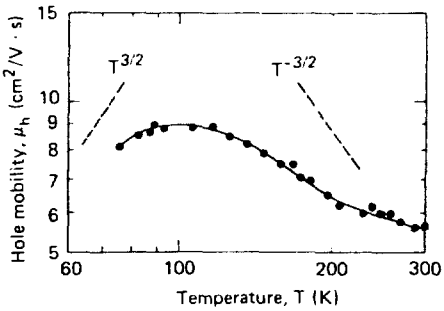

FIG. 2. Log-log plot of hole mobility versus temperature.

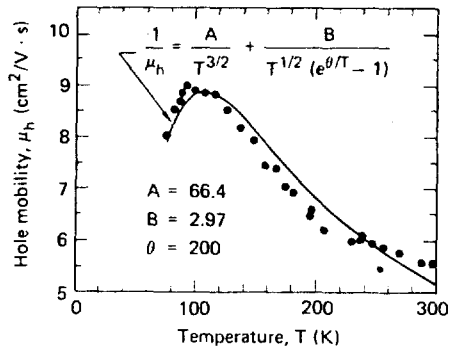

FIG. 3. Linear plot of hole mobility versus temperature, showing data and best fit.

first approximation, it would appear that ionized impurity scattering, which has a characteristic $T^{3/2}$ dependence, dominates for $T < 90$ °K. There is some doubt as to the importance of acoustic phonon scattering at higher temperatures, contrary to the results of previous investigators.[2,3,5] The slope for temperatures greater than 100 °K is too shallow for the $T^{-3/2}$ dependence of acoustic phonon scattering. The shallow slope may be due to the influence of impurity scattering, but the fact that the data deviate from the $T^{3/2}$ dependence even more as the temperature increases suggests that another scattering mechanism is prevalent at the higher temperatures.

Least-squares fits of the data to other functional forms of μ_h were attempted. In all cases it was assumed that the various mechanisms were independent so that the general form could be expressed as

$$\frac{1}{\mu_h} = \sum_i^N \frac{1}{\mu_i}. \tag{3}$$

The maximum number of mechanisms attempted in the analysis was $N = 5$, which included ionized and neutral impurity, acoustic and optical phonon, and piezoelectric scattering. The best fit, presented in Fig. 3, is

$$\frac{1}{\mu_h} = \frac{A}{T^{3/2}} + \frac{B}{T^{1/2}[\exp(\theta/T) - 1]}, \tag{4}$$

where $A = 66.4$ V s °K$^{3/2}$ cm^{-2}, $B = 2.97$ V s °K$^{3/2}$ cm^{-2}, and $\theta = 200$ °K.

The first term of Eq. (4) corresponds to ionized impurity scattering. Conwell and Weisskopf[9] obtain this form by using a classical Rutherford scattering model. The same temperature dependence was obtained by Dingle[10] and Brooks[11] using a screened potential model. The second term corresponds to optical phonon scattering. The original formulation is due to Howarth and Sondheimer,[12] who solved the Boltzmann transport equation with a relaxation time as defined by Frohlich and Mott.[13] It was later corrected to its present form by Petritz and Scanlon.[14]

This letter presents preliminary findings of an in-depth study of the properties of reactively sputtered Cu_2S. Hall measurements at temperatures down to that of liquid helium are in progress; a more definitive statement on the low-temperature scattering mechanism and the energy levels of defects is forthcoming.

We wish to thank Dr. Larry Partain for helpful discussions and Harry Fiedler for his assistance in some of the computations. Both are members of the Electronics Materials and Effects Group at the Lawrence Livermore Laboratory. This work was performed under the auspices of the U.S. Department of Energy by the Lawrence Livermore Laboratory under contract number W-7405-ENG-48.

[1]Hirahara, J. Phys. Soc. Jpn. **6**, 428 (1951).
[2]G.B. Abdullaev, Z.A. Aliyarova, E.H. Zamonova, and G.A. Asadov, Phys. Status Solidi **26**, 65 (1968).
[3]G.P. Sorokin and A.P. Paradenko, Izv. Vyssh. Uchebn. Zaved. Fiz. **5**, 91 (1966) [Sov. Phys. J. **9**, 59 (1966)].
[4]G.P. Sorokin, I. Ya. Andronik, and E.V. Kovtun, Izv. Akad. Nauk SSSR Neorg. Mater. **11**, 2129 (1975) [Inorg. Mater. USSR **11**, 1828 (1975)].
[5]J. Bougnot, F. Gustavino, G.M. Moussalli, and M. Savelli, in *International Workshop on Cadmium Sulfide Solar Cells and Other Abrupt Heterojunctions, April* 30–*May* 2, 1975, *Newark, Delaware*, edited by K.W. Boer and J.D. Meakin (Institute of Energy Conversion, University of Delaware, Newark, 1975), p. 337.
[6]G. Armantrout, J. Yee, E. Fischer-Colbrie, D. Miller, E. Hsieh, J. Leong, K. Vindelov, and T. Bron, in *Thirteenth IEEE Photovoltaic Specialists Conference, Washington, D.C.*, 1978, (IEEE, New York, 1978), p. 383.
[7]L.J. van der Pauw, Philips Res. Rep. **13**, 1 (1958).
[8]S.S. Devlin, Ph.D. thesis, Case Institute of Technology, 1964.
[9]E.M. Conwell and V.F. Weisskopf, Phys. Rev. **77**, 388 (1950).
[10]R.B. Dingle, Philos. Mag. **46**, 831 (1955).
[11]H. Brooks, Adv. Electron. Electron Phys. **8**, 85 (1955).
[12]D. Howarth and E. Sondheimer, Proc. R. Soc. London Ser. A **219**, 53 (1953).
[13]H. Frohlich and N.F. Mott, Proc. R. Soc. London Ser. A **171**, 496 (1939).
[14]R.L. Petritz and W.W. Scanlon, Phys. Rev. **97**, 1620 (1955).

IV CONCLUSIONS

There is strong experimental and theoretical evidence that the behavior of Cu_xS/CdS solar cells formed by sputtering and by other techniques is dominated by space-charge-limited current mechanisms that are controlled by trapping phenomena that are different from the parameters that specify standard p-n junction behavior. Direct measurement of the minority carrier transport properties in ordinary thin-film devices without destructive preparations was accomplished by extensions of the SEM EBIC method for a sputtered sample. The measurement of the majority carrier and optical properties of polycrystalline Cu_xS films was made possible by the reactive sputtering process which provided the necessary free standing films. The transport and optical constants were found to have values among the highest reported for polycrystalline material and were observed to not change significantly with air or reducing heat treatments with the exception of the Cu_xS hole concentration and the Cu_xS optical absorption. A dominant effect of heating of sputtered devices was shown to be in changes induced in the junction collection efficiency of the cells in agreement with increasing evidence from other studies that used devices fabricated by the other methods. Comparisons among films formed by topotaxy and by sputtering onto poly and single crystal substrates indicated that the optical and minority carrier properties obtained with sputtered films should be representative of the characteristics of topotaxial films. The majority carrier transport properties of sputtered and topotaxial polycrystalline films should also be well correlated. The reactive sputtering process provides the unique ability to provide polycrystalline samples in the forms required for

unambiguous determinations of the mechanisms that control Cu_xS/CdS device behavior which should be understood for the cells to reach their full potential. The indications are that the greatest improvements in device behavior will be achieved by future studies which monitor, control and optimize the trap structure of the Cu_xS/CdS devices. The potential payoff is in greatly improved fabrication repeatability, in meaningful characterizations and definitions of the device stability requirements, in enhanced device performance, and in better evaluations of the device's ultimate performance potential.

According to the new results of this study the most pressing problems for future study should involve answers to the following three questions:

1. How can the trapping structures in Cu_xS/CdS devices be measured and how can they be controlled?

2. What are the specific mechanism or mechanisms involved in the strong variations observed in junction collection efficiency and how can they be controlled?

3. What heat treatment steps will allow the Cu_xS layer to achieve its optimal optical properties simultaneously with the values desired for the other parameters influenced by heat treatment?

V. REFERENCES

1. G. A. Marlor and J. Woods, "Space-Charge Limited Currents and Electron Traps in CdS Crystals," Brit. J. Appl. Phys. 16, 1449 (1965).
2. H. B. Im, H. E. Matthews, and R. H. Bube, "Evidence for Photochemical Changes in Traps in CdS Crystals," J. Appl. Phys. 41, 2581 (1970).
3. E. Tscholl, "The Photochemical Interpretation of Slow Phenomena in Cadmium Sulfide," Philips Res. Rep. Suppl. 6, 1 (1968).
4. J. Woods and K. H. Nicholas, "Photochemical Effects in Cadmium Sulfide Crystals," Brit. J. Appl. Phys. 15, 1361 (1964).
5. G. South and D. M. Hughes, "The Effects of Absorbed Oxygen and Hydrogen on the Electrical Properties of High Purity Cadmium Sulfide Films," Thin Folid Films 20, 135 (1974).
6. J. R. Szedon, F. A. Shirland, W. J. Biter, T. W. O'Keeffe, J. A. Stoll, and S. J. Fonash, "Cadmium Sulfide/Copper Sulfide Heterojunction Cell Research," Final Report, Sept. 30, 1977 to July 31, 1979, Contr. No. DE-AC03-77ET20429, July 1979, pp. 91, 99.
7. S. P. Shea and L. D. Partain, "Heat Treatment Effects on the Minority Carrier Diffusion Lengths, Surface Recombination Velocity and Junction Collection Factor of Cu_xS/CdS Solar Cells," 13th IEEE Photovoltaic Specialists Conf. Record, Washington, DC, June 1978, p. 393.
8. G. A. Armantrout, D. E. Miller, K. E. Vindelov, and T. G. Brown, "Formation of Thin Cu_2S (Chalcocite) Films Using Reactive Sputtering Techniques," Journal of Vacuum Science and Technology 16, 212 (1979).

9. A. Rothwarf, "Optimal Material Properties for CdS/Cd_2S Solar Cells," 2nd E.C. Photovoltaic Energy Conf., West Berlin, April 1979 (D. Reidel Publ. Co., Dordrecht, Holland, 1979), p. 370.

10. N. C. Wyeth and A. W. Catalano," Variation of Short-Circuit Current Spectral Response with $Cu_{2-x}S$ Composition in Thin Film Cu_{2-x}/CdS Photovoltaic Cells," 12th IEEE Photovoltaic Specialist Conf. Record, Baton Rouge, Nov. 1976, p. 471.

11. G. Z. Idrichan and G. P. Sorokin, "Chalcogenides of Cu(I) as p-Components of Heterojunctions," Inorganic Materials 11, 1449 (1975).

12. G. P. Sorokin and A. P. Paradenko, "Electrical Properties of Cu_2S," Sov. Phys. J 9, 59 (1966).

13. E. Hirahara, "The Electrical Conductivity and Isothermal Hall Effect in Cuprous Sulfide, Semi-Conductor," J. Phys. Soc. Japan 6, 428 (1951).

14. J. Bougnot, F. Gustavino, G. M. Moussalli, and M. Savelli, "On the Electrical and Optical Properties of Bulk Cu_2S," in International Workshop on Cadmium Sulfide Solar Cells and Other Abrupt Heterojunction, April 1975, Newark, DE, p. 337.

15. G. B. Abdullaev, Z. A. Aliyaroua, E. H. Zamanoua, and G. A. Asadov, "Investigation of the Electric Properties of Cu_2S Single Crystals," Phys. Stat. Sol. 26, 65 (1968).

16. W. G. Oldham and A. G. Milnes, "Interface States in Abrupt Semiconductor Heterojunction," Solid-State Electr. 7, 153 (1964).

17. N. C. Wyeth and A. Rothwarf, "Measurements of Interface Recombination Velocity by Capacitance/Collection Efficiency Variation in Cu_2S/CdS Heterojunctions," Journal of Vacuum Science and Technology 16, July/Aug. 1979.

18. S. R. Das, A. Banerjee and K. L. Chopra, "$Zn_xCd_{1-x}S/Cd_2S$ Heterojunction Solar Cells-II: Junction Analysis," Solid-State Electronics 22, 533 (1979).

19. A. Rothwarf, J. Phillips, and N. C. Wyeth, "Junction Field and Recombination Phenomena in the CdS/Cu_2S Solar Cell: Theory and Experiment," 13th IEEE Photovoltaic Specialists Conf. Record, Washington, DC, June 1978, P. 399.

20. E. H. Rhoderick, "Comments on Conduction Mechanims in Schottky Diodes," J. Phys. D. 5, 1920 (1972).

21. C. R. Crowell and M. Beguwala, "Recombination Velocity Effects on Current Diffusion and Imref in Schottky Barriers," Solid-State Electron, 14, 1149 (1971).

22. C. R. Crowell and S. M. Sze, "Current Transport in Metal-Semiconductor Barriers," Solid-State Electron, 9, 1035 (1966).

23. L. D. Partain and S. P. Shea, "SEM Measurement of Diffusion Lengths, Recombination Velocity, and Junction Collection Efficiency in Heterojunction Solar Cells," Application to Cu_xS/CdS," Intern. Electron Devices Meeting Tech. Digest, Washington, DC, Dec. 1978, p. 239.

24. A. D. Jonath, W. W. Anderson, J. A. Thornton, and D. G. Cornog, "Copper Sulfide Films Deposited by Cylindrical Magnetron Reactive Sputtering," Journal of Vacuum Science and Technology 16, 200 (1979).

25. L. C. Burton and H. M. Windawi, "Thermally Induced Changes of Cu_xS Films and Effect on $CdS-Cu_xS$ Solar Cell Response," J. Appl. Phys. 47, 4621 (1976).

26. J. J. Kramer, Electrical Engineering Dept., Univ. of Delaware, 1976, Private Communication.

27. K. Okamoto and S. Kawai, "Electrical Conduction and Phase Transition of Copper Sulfides," Jap. J. Appl. Phys. 12, 1130 (1973).

28. F. A. Shirland, "The Structure of the Cu_2S Layer of Cu_2S/CDS Thin-Film Solar Cells," J. Appl. Phys. 50, 4717 (1979).

29. "Cadmium Sulfide-Copper Sulfide Heterojunction Cell Research," Quarterly Progress Rept., Dec. 1, 1978-Mar. 1, 1979, Institute of Energy Conversion, Univ. of Delaware, Contr. No. XR-9-8063-1, Aug. 1979.

30. J. A. Bragagnolo, "Photon Loss Analysis and Design of Thin-Film Planar Junction Cu_2S/CdS Devices," 2nd E. C. Photovoltaic Solar Energy Conf. Proc., Berlin, April 1979, (D. Reidel Publ. Co., Dordrech, Holland, 1979) p. 882.

31. A. M. Barnett, J. A. Bragagnolo, R. B. Hall, J. E. Phillips and J. D. Meakin, "Achievement of 9.15% Efficiency in Thin-Film CdS/Cu_xS Solar Cells," 13th IEEE Photovoltaic Specialists Conf. Record, Washington, DC, June 1978, p. 419.